Investigating the Redispersibility of Calcium Carbonate

by

Ardeep Dosanjh

A thesis submitted to
The University of Birmingham
for the degree of
MASTER OF RESEARCH
in Chemical Engineering Science

School of Chemical Engineering
The University of Birmingham
October 2009

Abstract

The primary aim of this research was to investigate the redispersibility of the commercial calcite slurry product, Carbilux, after drying. Various dispersants and pH changes were made to improve the colloidal stability. The commercial product contained an unknown organic dispersant which was removed by washing and zeta potential results were measured. The rheological properties of the various samples were investigated and a sample selection was made to obtain powders from conventional oven drying, freeze drying and spray drying for redispersibility analysis.

The powder properties were compared using laser diffraction for particle size analysis and zeta potentials, scanning electron microscopy, gas adsorption for surface area analysis, shear rate controlled rheology tests and compressive load tests to obtain agglomerate strengths.

The particle size distributions and rheological properties are strongly correlated as an increased number of free fine particles increased the viscosity due to more interparticulate interactions. The removal of the organic dispersant produced unstable systems supported by rheological evidence of shear thickening at high shear rates.

The agglomerate strengths weakened with the removal of the organic. The particle size distribution analysis supports this but the rheological evidence tends to be less conclusive due to changes of the colloidal chemistry in the washing and drying processes.

Acknowledgement

I would like to express my most sincere gratitude to my supervisor, Professor Stuart Blackburn, for all of his support and guidance throughout the entire research project. His time, expertise and perspectives were invaluable. I would also like to express my appreciation towards Dr Richard Greenwood and the School of Engineering for this research opportunity.

In addition, I would also like to thank Imerys Minerals for providing the sample for this research and the IRC and Loughborough University for allowing me to use their facilities.

Finally I would like to thank all my dear friends and family for their support and in particular my mother, Rajwant Dosanjh, and my father, Joginder Dosanjh.

Content

List of Figures

List of Tables

1 Introduction

The three natural polymorphs of calcium carbonate ($CaCO_3$) are calcite, aragonite and vaterite [1]. Calcite is the most common and occurs naturally in the form of chalk, limestone or marble.

Imerys Minerals converts calcium carbonate into products for the paint, plastics, film, adhesives and rubber industries. In the paint industry, the grade is of great importance in its application, as coarser grades act as simple fillers and can control gloss, whereas finer grades can be used as extenders. For plastics, the addition of calcium carbonate increases rigidity and also has a positive impact on other mechanical properties such as tensile strength and impact strength. The film industry uses it to reduce the formulation cost and to increase the processing speeds as an alternative to polymers. Its use in adhesives and sealants is to adjust the rheological properties [2, 3].

In addition to Kaolin, calcium carbonate is also one of the most widely used pigments in the paper coating industry, due to its optical properties and its white appearance. It can also be used in health and dietary applications as a calcium supplement and as an environmental application to neutralise rivers which have been adversely affected by acid rain or in waste water treatment [4, 5, 6].

1.1 Problem Statement

Imerys Minerals provided a ground calcium carbonate sample, primarily calcite (99.9%), dispersed in water under the trade name Carbilux. The remainder of the sample is made up of an unknown organic dispersant. This product is a slurry of approximately 75 wt% by solids (51.7 vol%) and is Imerys Minerals most finely ground calcium carbonate with a relatively steep, narrow particle size distribution of 0.3-4 µm. These characteristics provide this product with an exceptional gloss and brightness [7]. The structure of calcite is shown in Figure 1.1.

The current key applications of Carbilux are dextrine adhesives, polyvinyl acetate adhesives and starch adhesives. Imerys Minerals would like to broaden its application by investigating the redispersibility of this product after drying.

The primary objective in this research is to explore alternative ways to produce an aggregate-free dry powder of Carbilux from solutions and colloidal suspensions. It is desirable to achieve this in the micron-domain. However, the already existing techniques in producing well dispersed particles on such a small scale are often impractical or fail. This is due to the high surface area to volume ratio which dominates the bulk properties of the colloidal system, thus an understanding of surface chemistry is of great importance.

A combination of correct surface chemistry and mechanical action both help to provide a well dispersed colloidal system, but aggregates require great amounts of energy in order to break particles apart and to do this on the micron scale is highly energy intensive and thus economically unviable. This makes it preferable to explore ways to prevent aggregation from the start of the process by stabilising the colloidal system.

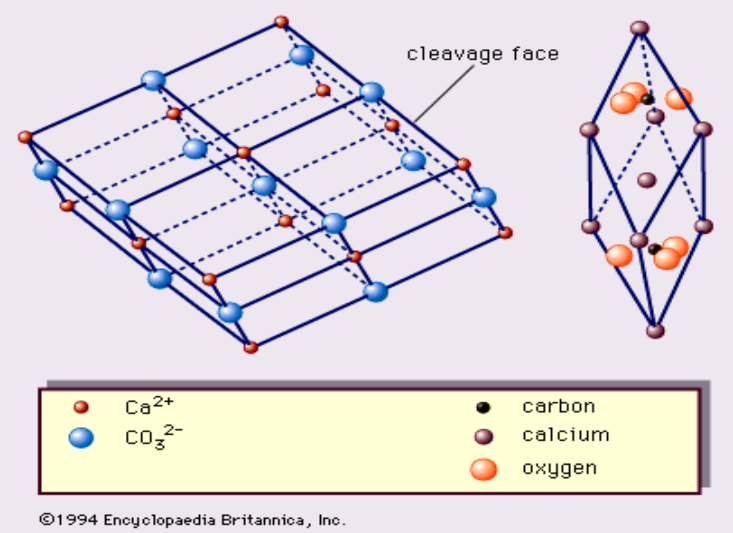

Figure 1.1- The crystal structure of calcite. This schematic diagram shows both (left) the true unit cell (the acute rhombohedron, which contains 2[$CaCO_3$]) and (right) an alternative cell based on the cleavage rhombohedron [8]

1.2 Thesis Layout

This thesis is divided into 6 main sections. Following the introduction, chapter 2 is a literature review into the background theory of colloidal stability, rheology, agglomerate strengths and drying processes. Chapter 3 explains the experimental and analytical methods used in this research and the results obtained from these methods are discussed in chapter 4. This is followed by a conclusion and recommendations for future work.

2 Literature Review

2.1 Colloidal Stability

2.1.1 Introduction

Colloidal systems consisting of particles in the micro and nano meter scale domain have a high surface area to volume ratio. As the particles approach the nano scale, the number of molecules at the surface increases from 1 in 500 for a 1µm particle to 1 in 4 for a 1nm particle. The properties of surface molecules, such as energy, differ from the bulk phase properties, thus the increase in surface molecules will dominate the properties of a colloidal system [9].

Agglomeration or aggregation is often a result of the instability of a colloidal system because of the high surface free energy. Agglomeration and aggregation are similar occurrences in which particles gather together into a cluster or mass in agglomerated form but the particles in aggregates are brought together by collisions and are held in contact by surface forces. Agglomerates tend not be as strong as aggregates and are more readily reversible to break down to smaller agglomerates or individual particles. When particles aggregate the clusters formed may take on a variety of structures. An open formed aggregate is called a floc and as the number of flocs increase, there is an increase in the number of possible structures.

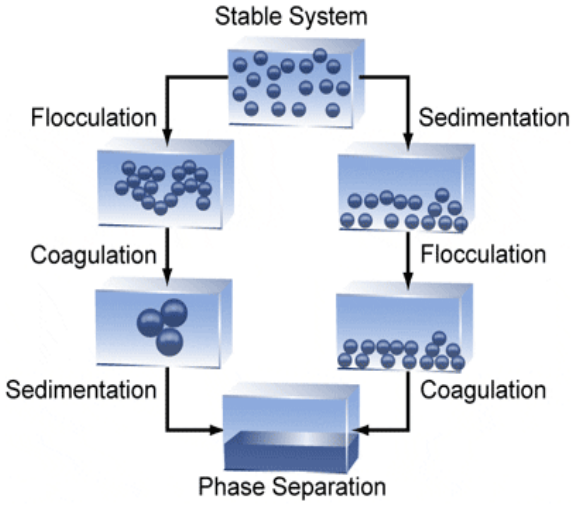

Figure 2.1- The process of phase separation of an unstable system [10]

Figure 2.1 shows how flocculation can lead to phase separation as it rearranges to a denser form resulting in coagulation and finally sedimentation if the particles are denser than the dispersion medium. Phase separation also occurs when particles held in suspensions are settling out due to gravity or applied forces before flocculating and coagulating.

The interactions of surface molecules leads to adhesion between particles and thus aggregation and agglomeration as previously mentioned. The following adhesive forces between 1µm diameter particles are given for [11]:

a) van der Waals- present on all particles, $F_{vdW} = 4 \times 10^{-6}$ N
b) Electrostatic surfaces- usually associated with dry powders, $F_{Electrostatic} = 5.2 \times 10^{-8}$ N
c) Capillary- where a liquid film is present, e.g. RH>70%, $F_{Capillary} = 4.5 \times 10^{-6}$ N
d) Gravity- present on all particles, $F_{Gravity} = 5.1 \times 10^{-15}$ N

It is clear that van der Waals forces and capillary forces dominate on this scale, although this can vary for different materials.

2.1.2 Particle Interactions

2.1.2.1 Brownian Motion

In 1827 the botanist Robert Brown observed a phenomenon of the random motion of microscopic particles when suspended in a fluid during experiments of pollen grains suspended in water. This motion is referred to as Brownian motion and is when particles are continually changing path in an irregular form due to interactions and random collisions with other similar particles and those of the suspended medium [12]. Brownian motion can be described as translational motion or rotational motion in which an axis is bound to the particle [13].

Einstein noticed that Brownian motion met the requirements of the kinetic theory model and began to investigate this further to conclude this motion as a thermal agitation caused by the thermal energies in the continuous phase [14, 15]. Thus Brownian motion is the form of thermal motion at the microscopic level, whereas diffusion and osmosis are forms at the macroscopic level [12].

2.1.2.2 van der Waals Forces

Van der Waals forces are the attractive forces between atoms and molecules and have three contributions:

a) Keesom (orientation) interactions- these occur between polar molecules in which a permanent dipole occurs in asymmetric molecules only.

b) Debye (induction) interactions- these occur between a polar and a non-polar molecule where the electron cloud of the non-polar molecule is polarised by the dipole of the polar molecule.

c) London (dispersion) forces- these occur in all atoms and molecules, polar and non-polar, as a result of the fluctuating dipoles caused by the motion of electron clouds [9,16].

London forces are long ranged and the most important of the three contributions to the van der Waals forces, as they are larger than the Keesom and Debye interactions.

2.1.3 Electrical Double Layer and DVLO theory

2.1.3.1 Electrical Double Layer

The Electrical Double Layer can be explained by Figure 2.2 where a highly negative charged colloid is attracting some of the positive ions of the surrounding liquid. These are referred to as the counter-ions, as they have the opposite charge to the colloid and form a firmly attached layer around the surface of the colloid, known as the Stern Layer. Additional positive ions are still attracted to the negative colloid, but repulsion starts to occur from the Stern layer as well as by other positive ions that are also trying to approach the colloid. This dynamic equilibrium results in the formation of a diffuse layer of counter-ions. These two layers are known as the Electrical Double Layer [12].

The concentration of counter ions is high near the surface and gradually decreases with distance until it reaches equilibrium with the counter-ion concentration in the solution. There is a lack of negative ions in the neighbourhood of the surface due to repulsion of the negative colloid. Negative ions in this case are called *co-ions* as they have the same charge as the colloid. Their concentration will gradually increase with distance, as the repulsive forces of the colloid are screened out by the positive ions, until equilibrium is again reached.

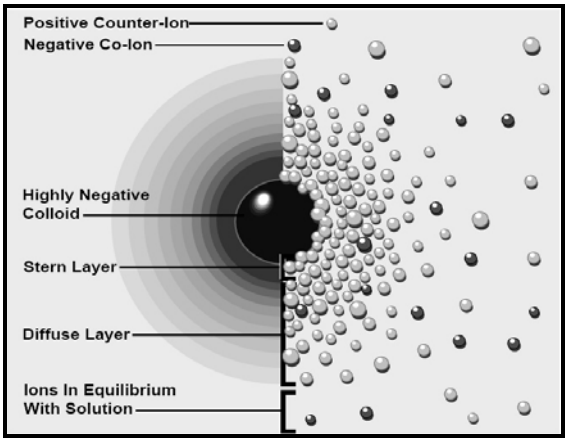

Figure 2.2- Schematic diagram representing the change in charge density around the colloid (left) and the distribution of positive and negative ions around the charged colloid (right) [17]

The diffuse layer is a charged atmosphere surrounding the colloid. The charge density at any distance from the surface is equal to the difference in concentration of positive and negative ions at that point. As shown in Figure 2.3, the charge density is greatest near the colloid and approaches zero as the concentration of positive and negative ions merge together away from the colloid.

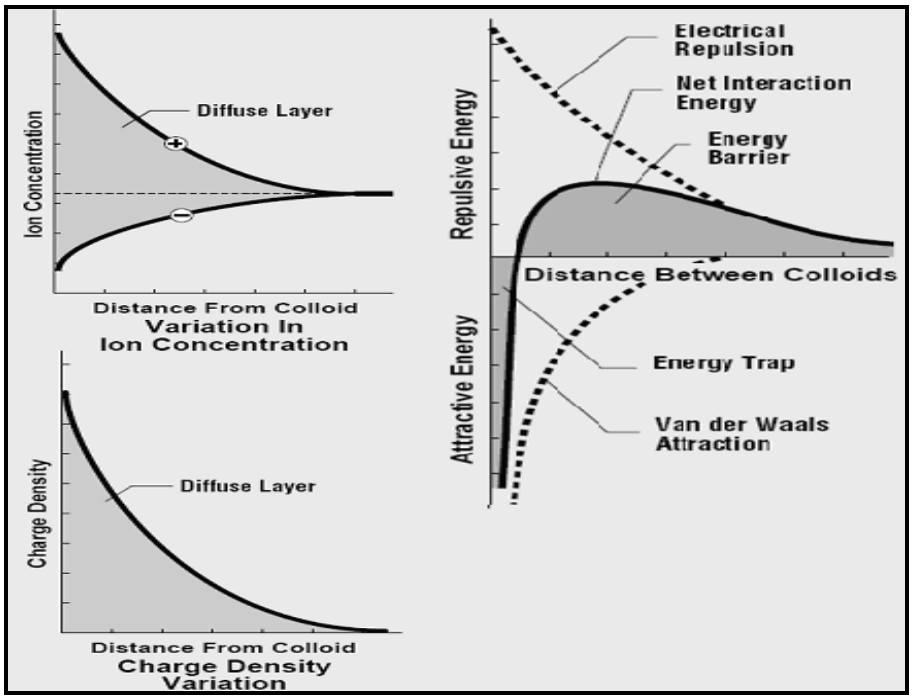

Figure 2.3- The variation of ion density in the Diffuse Layer (left) and the interaction of ions around the colloid (right) [17]

2.1.3.2 DVLO Theory

In 1940's four scientists, Derjaguin, Verwey, Landau and Overbeek developed the quantitative theory for the stability of colloidal systems known as the DVLO theory in which the stability of a particle in solution is dependent on the total interaction free energy, ΔG_T, defined as [18, 19, 20],

$$\Delta G_T = \Delta G_A + \Delta G_R + \Delta G_S \qquad \textbf{(2-1)}$$

where ΔG_A is the free energy of the van der Waals attractive forces, ΔG_R is the free energy of the electrical double layer repulsive forces and ΔG_S is the free energy of the solvent.

The attractive and repulsive terms are a result of Brownian motion as the particles approach each other. The latter term is often neglected, as it only makes a small contribution to the total free energy, thus the stability of a colloidal system is determined greatly by the balance of the attractive and repulsive forces. As can be seen in Figure 2.3, there is an energy barrier which prevents two particles adhering together as a result of the repulsive forces. If particles come together beyond this barrier the attractive forces will overcome the repulsive forces resulting in the formation of larger particles (agglomerates) thus it is favourable to have a dispersed system with high repulsive forces to be most stable and avoid flocculation.

It is also important to note that reactions occur in the direction that will reduce the surface energy of the system and so particles try to spontaneously reduce their total surface area by aggregating [18].

2.1.4 Zeta Potential

Zeta potential is the electric potential that exists at the shear plane of a particle. It estimates the stability and thus control of colloids in a suspension. By understanding the effect of colloidal behaviour on different parameters (e.g. viscosity, settling and effective size diameter) and the interaction between individual colloids, the performance and characteristics of a colloidal suspension can be improved and tailored. This leads to the ability to prevent undesirable properties of suspensions such as aggregation which leads to

other unstable states such as creaming (particles rise to the top if less dense than the dispersion medium) and sedimentation (particles fall to the bottom if more dense than the dispersion medium)[18].

The zeta potential is measured at the plane of shear, which is the hypothetical boundary that divides the double layer into those ions which move with the particles when an electric field is applied to the suspension and those that remain stationary.

The existence of electrical charges in the double layer of attached counter-ions in the Stern layer and the charged atmosphere in the diffuse layer interact with an applied electric field resulting in four distinct effects known as the electrokinetic phenomena [21]. These are:

1- *Electrophoresis*: the movement of a charged particle relative to the liquid it is suspended in under the influence of an applied electric field.
2- *Electroosmosis*: the movement of a liquid relative to a stationary charged surface under the influence of an electric field
3- *Streaming Potential*: the electric field generated when a liquid is forced to flow past a stationary charged surface
4- *Sedimentation potential*: the electric field generated when charged particles sediment

Figure 2.3 also shows the net interaction of ions when near the colloid surface, the interaction is dominated by Van der Waals attraction between the negative colloid with the direct positive ions surrounding it. This is then gradually 'interrupted' by the repulsion of similar positive ions both from the Stern layer and other positive ions trying to approach the colloid until the interaction is dominated by repulsion further away from the colloid.

2.1.5 Stability Mechanisms

There are 3 keys ways to stabilise a particle against aggregation, two of which can be seen in Figure 2.4 and all are defined as;

1-*Electrostatic Stabilisation*: this method introduces a charge on the particle surface causing repulsion between particles to occur.

2-*Steric Stabilisation*: in this method a polymer is adsorbed onto the particle surface to prevent particles from coming into close proximity preventing Van der Waals attractive forces from dominating.

3-*Electrosteric Stabilisation*: this is a combination of the first two methods in which a polymer with a charge is introduced to the particle surface. These are called polyelectrolytes.

For this research electrostatic stabilisation is of interest. There are three mechanisms in which the particles can become charged. The first is the ionisation of surface groups as acidic groups dissociate to give negative surfaces whilst basic surfaces take on a positive charge. The second is isomorphic substitution which is the exchange of a structural ion with one of a lower valency to produce a negative charge. Calcium carbonate has 2 crystal lattice ion species, Ca^{2+} ions and CO_3^{2-} ions. The third mechanism is specific ion adsorption in which ions from a surfactant or any other contaminate are adsorbed onto the surface. The impact of the addition of various surfactants/dispersants to the suspension can be investigated and analysed using this technique.

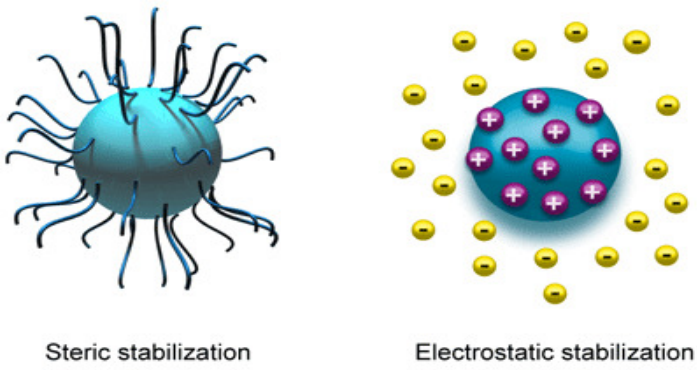

Figure 2.4- Steric stabilization (left) and electrostatic stabilization (right) of a particle [22]

The magnitude of repulsive forces depends on the pH of the suspension as well as the surface groups present. In an aqueous suspension, the pH is the most important factor affecting the zeta potential. The general case of a zeta potential-pH plot is that the more acidic the suspension the more positive the zeta potential charge as shown in Figure 2.5. When the zeta potential is zero at a given pH there is zero electrophoretic mobility and this is known as the iso-electric point.

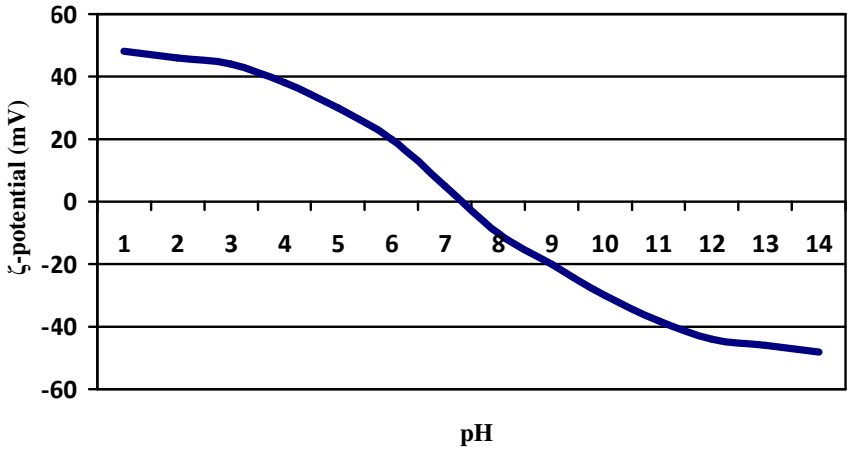

Figure 2.5- Zeta potential-pH plot example

2.1.6 Previous Studies

Defects in the calcite crystal structure can lead to a change in the surface charge as different crystal lattice ions are exposed. These exposed ions become the potential determining ions (PDIs). The PDIs can also vary at the calcite/water interface due to surface hydrolysis where the PDIs are Ca^{2+}, CO_3^{2-}, HCO_3^-, $CaHCO_3^+$, H^+ and OH^-. The latter two are the PDIs of the second order. Foreign ions in the surrounding solution can also become the PDIs through adsorption [23, 24].

Various studies have been conducted in determining the primary PDIs and the pH of the iso-electric point in which there is a variety in the experimental pH_{IEP} values obtained. The difference in these values can be observed from Smani *et al*, pH_{IEP} = 5.4, to Somasundaran and Agar, pH_{IEP} = 8.2 [25, 26].

In 2001 Vdović investigated the properties of 6 calcite samples of different origins. Two of these samples are synthetic calcites and have been labelled as Socal and Aldrich. The other four samples are of natural origin and are labelled as Kozjak (lake sediment), Jadran (sea sediment) and Mirna and Paravija (both limestone samples). As shown in Figure 2.6, the synthetic calcites have positive zeta potentials whereas the natural calcites are negative across the pH range investigated. Vdović also found pH_{IEP} = 9.5 in the synthetic calcites.

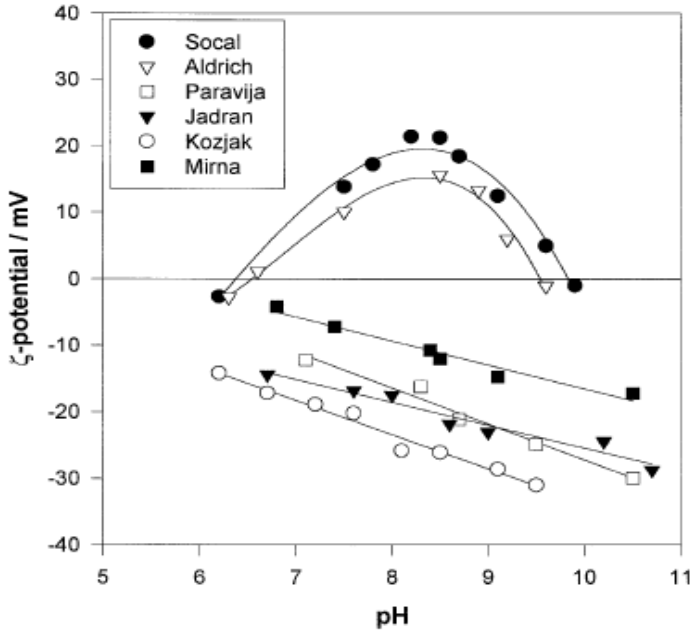

Figure 2.6- Zeta-potential dependence of calcite samples on the pH. Supporting electrolyte is 10^{-3} mol/dm^3 NaCl [24]

2.2-Rheology

2.2.1 Introduction

Rheology is defined as the scientific study of the deformation and flow of matter under various types of stress and strain. This area of study observes the relationship between stress, strain and time where stress is defined as force per unit area and strain is defined as change in dimension per unit dimension [27, 28].

Rheology measurements provide an indication of the colloidal state and interactions that are occurring such as hydrodynamic forces, Brownian motion and electrostatic forces. Studies have shown that small scale interactions between particles in suspensions can have a large effect on the rheology of the macro-scale. Rheology allows the prediction of which suspension formulations are likely to exhibit some form of aggregation [29]. This area of study is also of great importance for characterising materials during and at the end of production, to monitor process conditions and to also predict the performance of the materials under various constraints. Thus the rheological properties have a direct impact on

the design of processing equipment and rheological behaviour can be directly linked to product specifications and consumer acceptability [30].

2.2.2 Various Rheological Responses

When a stress is applied to a material there are three possible responses: viscous flow, elastic deformation or rupture. However, some materials can behave with a combination of these responses [28].

In the case of viscous flow and elastic deformation, the extreme cases are known as a Newtonian liquid and a Hookean solid respectively. When a material exhibits Newtonian behaviour it continues to deform as long as a stress is applied and has a constant viscosity as represented by the gradient in Figure 2.7(a). The relationship for a Newtonian liquid is

$$\tau = \mu \dot{\gamma} \qquad \textbf{(2-2)}$$

where τ is the shear stress, μ is the viscosity and $\dot{\gamma}$ is the shear rate.

A Hookean solid is defined as a material which deforms instantly when a stress is applied where the deformation is proportional to the applied stress and is reversible. The gradient of the linear stress-strain relationship in this case is the modulus.

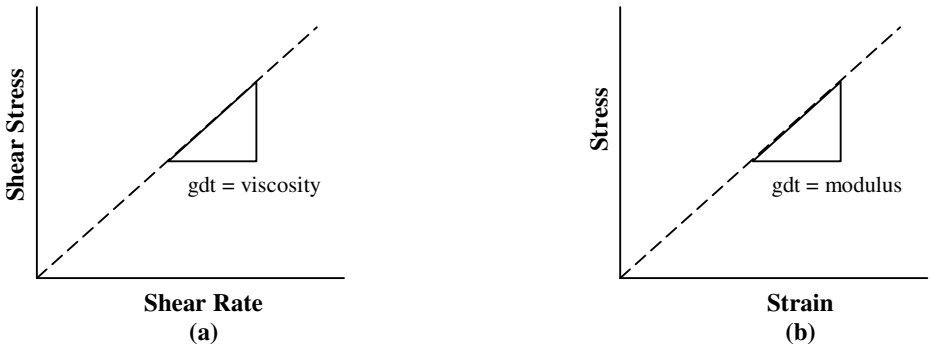

Figure 2.7- (a) Newtonian behaviour, (b) Hookean behaviour

The relationship represented in Figure 2.7(b) for normal stress, σ, and uniaxial strain (by stretching and squashing), ε_c, is given by;

$$\sigma = E\varepsilon_c \quad \textbf{(2-3)}$$

where E is the Young's modulus. If the Hookean material is twisted this relationship changes to;

$$\tau = G\gamma \quad \textbf{(2-4)}$$

where γ is the shear strain and G is the shear modulus.

2.2.3 Flow Behaviour

In the case of non-Newtonian fluids, the behaviour of the fluid can be time independent or time dependent. The time independent fluid behaviours are described as:

a. *Psuedoplastic Behaviour (shear thinning)*: this is when there is a gradual decrease in the viscosity with increasing shear rates due to a structural breakdown of the particles.
b. *Dilatant Behaviour (shear thickening)*: this is due to the disordered rearrangement of the structure which causes a viscosity change thus the viscosity increases as the rate of deformation increase.
c. *Viscoplastic Behaviour*: this behaviour is similar to shear thinning however the system does not flow until the shearing stress exceeds a value known as the yield stress

The time dependent fluid behaviours are linked to the psuedoplastic and dilatant behaviour and are defined as:

a. *Thixotropic*: this is reversible thinning which occurs when there is no equilibrium established between structural breakdown and reformation processes such that the number of structural interactions decreased with time and materials surfer reduction in the apparent viscosity.
b. *Rheopectic*: this is reversible thickening but is rare. This behaviour is obtained with shear thickening fluids in which the apparent viscosity increases the duration of deformation as there is a gradual development of structure by shear with time.

2.2.4 Flow Models

There are a number of flow models which can be applied to the time independent flow behaviours described for non-Newtonian fluids. Figure 2.8 shows how these behaviours differentiate on a shear stress/shear rate plot.

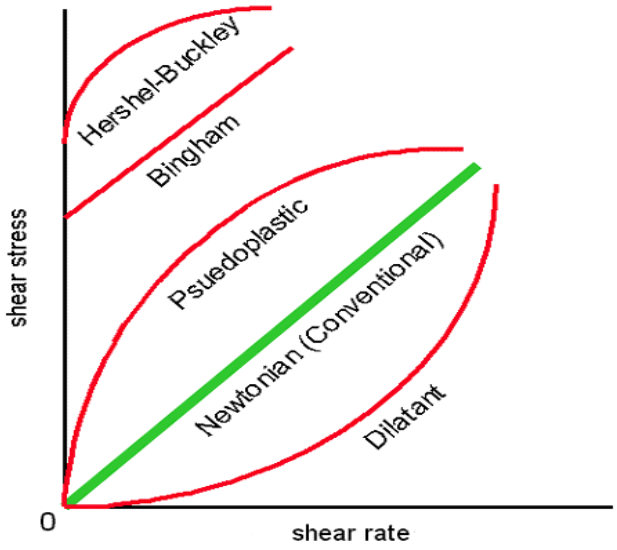

Figure 2.8- Different flow behaviours on a shear stress versus shear rate plot [31]

The most common model which can be applied to non-Newtonian fluids without a yield stress is the Power-Law model which is given as;

$$\tau = K\dot{\gamma}^{n} \Rightarrow \eta = K\dot{\gamma}^{(n-1)} \qquad \textbf{(2-5)}$$

where K is the consistency index, n is the power law index and η is the viscosity at a given shear rate. For psuedoplastic fluids n<1 and for dilatant fluids n>1 [32].

The Carreau model and the Ellis model can also be used to describe psuedoplastic behaviour. The Carreau model takes into account the limiting values of viscosity and is given by;

$$\frac{\eta - \eta_{\infty}}{\eta_0 - \eta_{\infty}} = \left[1 + \left(\lambda\dot{\gamma}\right)^2\right]^{(n-1)/2} \qquad \textbf{(2-6)}$$

where η_0 is the zero shear viscosity and η_∞ is the infinite shear viscosity. The Ellis model also predicts the zero-shear viscosity and if given by;

$$\frac{\eta_0}{\eta} = 1 + \left(\frac{\tau}{\tau_{1/2}} \right)^{\alpha - 1} \qquad \textbf{(2-7)}$$

where $\tau_{1/2}$ is the value of the shear stress at which the $\eta = \eta_0/2$. This model is generally difficult to use as it is not explicit in shear rate [32].

The most common model applied to psuedoplastic materials is the Cross model, as it can be applied to a wider range of shear rates. The model is given as;

$$\eta = \eta_\infty + \frac{\eta_0 - \eta_\infty}{1 + \left(C \dot{\gamma} \right)^m} \qquad \textbf{(2-8)}$$

where m is a parameter known as the Cross rate constant and C is the Cross time constant.

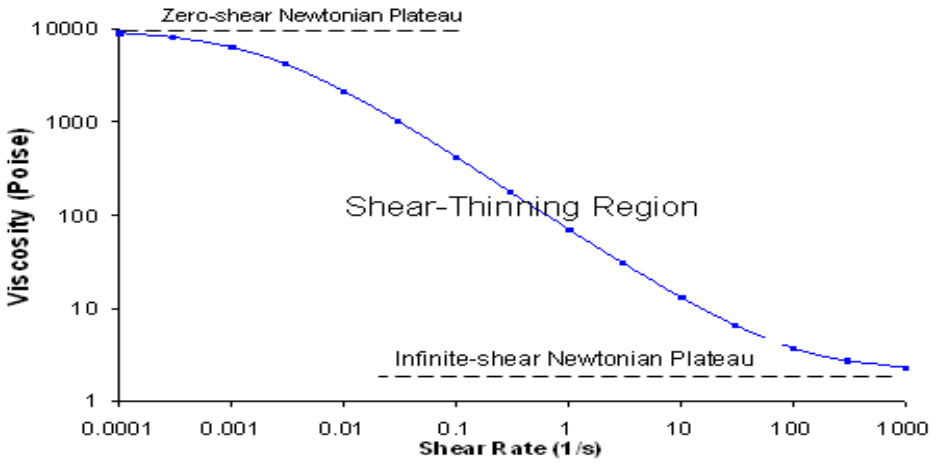

Figure 2.9- Typical viscosity profile for a dispersion, polymer solution or melt [33]

Figure 2.9 can be used to help explain the use of these models and in particular the Cross model. The zero shear viscosity is observed at the lower Newtonian plateau and the infinite shear viscosity can be taken from the infinite Newtonian plateau. These viscosities

help to predict the behaviour of the material at low and high shear rates and prove to be valuable in assessing the behaviour of suspensions.

The Cross rate constant in the Cross model measures the dependency of viscosity on the shear rate in the shear thinning region and thus the flow behaviour as when it is equal to zero Newtonian behaviour is observed.

A psuedoplastic material with a yield stress can be modelled using the Herschel-Buckley model given as;

$$\tau = \tau_y + K \dot{\gamma}^n \qquad \textbf{(2-9)}$$

where τ_y is the yield stress.

The Bingham model describes the yield behaviour typically observed in suspensions and is given by;

$$\tau = \tau_y + \eta_B \dot{\gamma} \qquad \textbf{(2-10)}$$

2.2.5 Viscosity of suspensions

In general, the viscosity of a suspension is greater than the viscosity of the liquid medium. The relative viscosity is the ratio between these viscosities [34]. Einstein developed a relationship between the relative viscosity and the volume fraction, f_p^v. In the case of dilute, Newtonian suspensions Einstein found the following relationship true for non interacting spherical particles;

$$\eta_{rel} = 1 + 2.5 f_p^v \qquad \textbf{(2-11)}$$

This relationship led to further work to develop similar relationships for more concentrated suspensions. The most widely accepted relationship for this case is the Krieger-Dougherty equation,

$$\eta_{rel} = \left[1 - \frac{f_p^v}{f_{cr}^v}\right]^{-K_H f_{cr}^v} \qquad \textbf{(2-12)}$$

where f_{cr}^v is the maximum volume fraction and K_H is the hydrodynamic shape factor [35].

Figure 2.10 shows how the relative viscosity and volume fraction of dispersed particles varied with changing value of the shape factor thus the solids loading of a suspension is a significant parameter to its rheological properties.

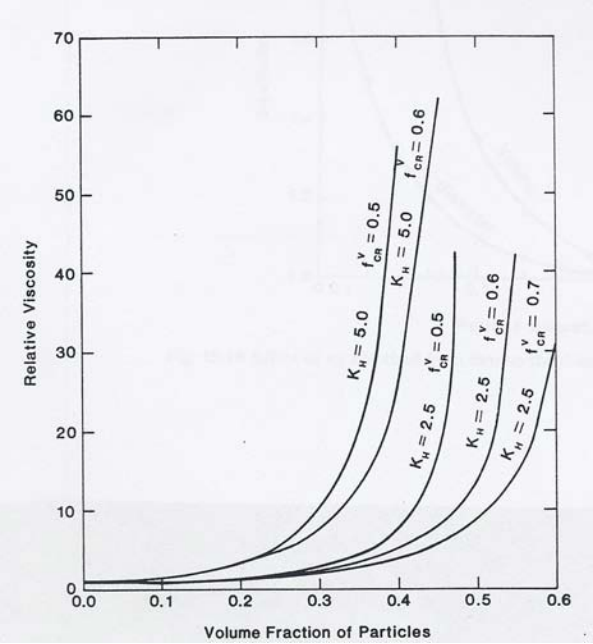

Figure 2.10- Dependence of relative viscosity on solids concentration of the Krieger-Dougherty equation [34]

2.3 Agglomerate Strength

2.3.1 Introduction

The most fundamental characteristic of any agglomerate is its strength. When unintentional agglomeration occurs, measuring the cohesive strength is most useful in

understanding the caking potential (the formation of a solid from the suspensions) [36, 37]. Although caking is undesirable for this research, obtaining the agglomerate strength of various samples will be beneficial to overcome industrial problems such as clogging of process equipment and optimising a suspension which produces weak agglomerate for redispersion after drying.

2.3.2 Diametrical Compaction and Die Pressing

It was proposed by Rumpf that, in order to obtain the agglomerate strength, the tensile strength should be determined by dividing the tensile force at failure by the cross-section of the agglomerate [37]. Diametrical compaction is a common technique used to obtain the strength of a single agglomerate by placing it between two parallel flat surface and applying an increasing load until the agglomerate fails (Figure 2.11(a)). An agglomerate can fail in one of the following three ways [38],

a. Tension fracture over the middle area of a test piece
b. Crushing due to compressive stresses near the points of loading
c. Compression fracture between the two points of loading

When testing agglomerates on the micron scale, this method can be very slow and difficult, leading to inaccuracies in the strength obtained.

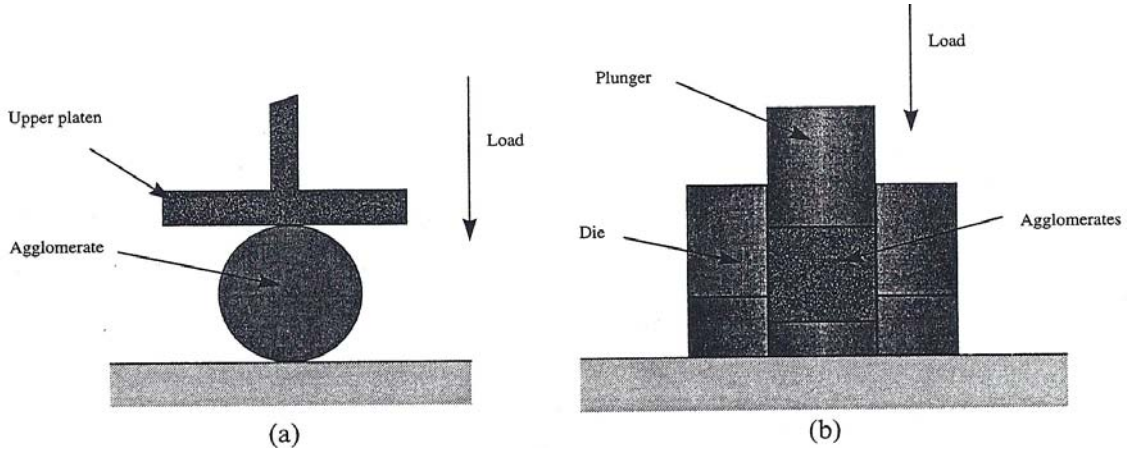

Figure 2.11- Schematic diagrams showing loading geometries of (a) diametrical compaction of an agglomerate, and (b) die pressing arrangement for a bed of agglomerate [38]

Die pressing, as shown in Figure 2.11(b), is a common method to use to obtain the agglomerate strength for small agglomerates as many can be tested at once. A load is applied at a controlled rate to the plunger which compresses the agglomerates within the die. The data obtained from this can be fitted to various models such as the Kawakita and Adams model as discussed later.

The packing characteristics are also of importance in these methods as this has a direct impact on the displacement of the bed of agglomerates. Table 2.1 shows how the number of contacts each particle has with another differs type of packing of the particles and the porosity [39].

Table 2.1- Packing Characteristics stated by Kawakita [39]

Type of packing	*Number of contacts*	*Porosity (%)*
Cubic	6	47.64
Orthorhombic	8	39.54
Rhombohedral	12	25.95
Tetragonalspheroidal	10	30.19

Although calcite is a rhombohedral crystal, the packing properties may differ due to the formation of agglomerates.

2.3.3 Kawakita Model

The Kawakita relationship [39] was derived by the observation of the relationship between pressure and volume and is supported by multiple compression theories. It is commonly used to represent the agglomerate strength, thus compression data, for powders in the fields of pharmaceuticals and powder metallurgy [40] and is as follows:

$$\frac{\sigma}{\varepsilon} = \frac{1}{ab} + \frac{\sigma}{a} \qquad \textbf{(2-13)}$$

where σ is the applied pressure, a and b are characteristic constants and ε is the degree of volume reduction which is equivalent to the uniaxial strain where h_i is the initial height of powder bed and h_p is the height at the current applied stress:

$$\varepsilon = \frac{h_i - h_p}{h_i} \qquad \textbf{(2-14)}$$

The characteristic constant of relevance is *b*, which has the dimension of the reciprocal of stress, and is directly related to the failure stress of an individual agglomerate.

2.3.4 Adams Model

Adams *et al.* carried out studies on the unaxial compaction of weak, porous granules which were made up of sand and held together by a polyvinylpyrrrolidone binder to form particles of 1.5-2.6 mm in diameter. The equation derived from this study used the Mohr-Coulomb macroscopic failure criterion and is given by [40];

$$\ln \sigma = \ln\left(\frac{\tau_0^{'}}{\alpha^{'}}\right) + \alpha^{'}\varepsilon_n + \ln\left(1 - e^{\left(-\alpha^{'}\varepsilon_n\right)}\right) \qquad \textbf{(2-15)}$$

where $\tau_0^{'}$ is the apparent strength of the single particles, $\alpha^{'}$ is the apparent coefficient of friction and the natural strain in the bed is given by $\varepsilon_n = ln\ (h_i/h_p)$.

At high strains the last term can be ignored. This provides a linear plot from which the apparent strength and coefficient of friction can be obtained.

2.3.5 Conventional Compaction Knee Approach

The data obtained from die pressing can also be interpreted by plotting the relative density against natural log of the applied pressure. As shown in Figure 2.12, the plot is linear until the point at which the agglomerate breaks down resulting in a change of the gradient. The knee approach extrapolates between the two linear relationship observed to find the agglomerate strength

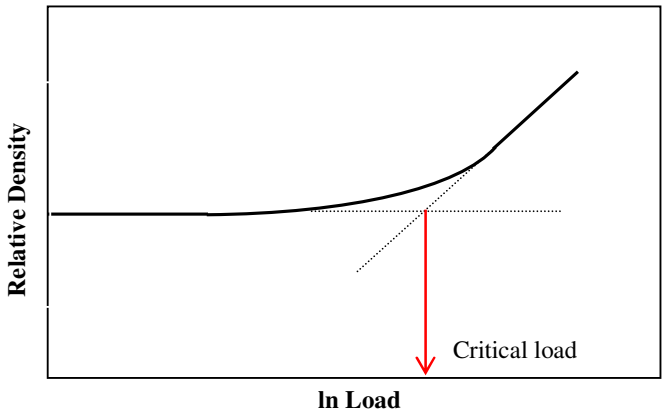

Figure 2.12- Agglomerate strength obtained from a relative density-ln load plot

2.3.6 Brazilian Test

As previously stated, on such a small scale the strength of a single agglomerate can be difficult to obtain. To further validate the agglomerate strengths obtained from die pressing, a load can be applied to each pellet, as shown in Figure 2.13, at a controlled rate until the pellet fails. This test is known as the Brazil test and examines the strength of a pressed pellet where the pressed pellet will be the strongest when formed from weaker agglomerates if all other material characteristic remain the same.

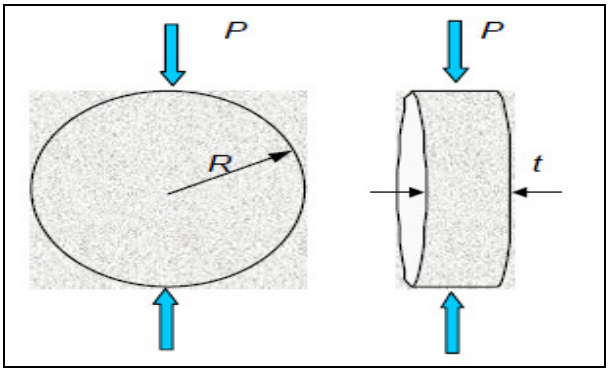

Figure 2.13- Brazilian test for indirect tensile strength [41]

The following equation is used;

$$\sigma_t = \frac{P}{\pi R t} \qquad \textbf{(2-16)}$$

where σ_t is the tensile stress, R is the radius, t is the thickness and P is the failure pressure.

2.3.7 Previous Studies

Experiments conducted by Yap *et al.* compared various models to obtain the agglomerate strength of a range of materials. The models investigated were the Heckel model, Kawakita model and the Adams model. The results obtained are shown in Table 2.2.

Yap *et al.* found that the Heckel model provided a poor fit for the date obtained due to the dependency of the yield stress of particles in the bed to the bed pressure. It was found that both the Kawakita and Adams models were able to fit to a wide range of bulk compression data and thus produced similar agglomerate strengths [40].

Table 2.2- The extrapolated compression parameter derived from Heckel, Kawakita and Adams models [40]

	Heckel parameter (MPa)	Kawakita parameter (MPa)	Adams parameter (MPa)
Eudragit® L100-55	57.1±8.6	27.0±10.7	34.8±12.0
Eudragit® L100	10.2±2.7	2.9±0.7	2.2±1.3
Eudragit® S100	9.7±2.9	3.2±0.9	2.8±1.8
Advantose™ 100	36.8±9.3	8.5±3.3	5.4±5.2
Calcium carbonate	15.7±2.6	3.6±0.6	3.0±1.3
Starlac™	11.7±1.9	2.9±0.8	2.1±1.5

2.4 Drying

2.4.1 Drying Mechanism

A key contributor to the formation of agglomerates is the moisture content as thin viscous films can form between particles causing them to bond. The total moisture content of a bulk material is made up of the free moisture also known as surface moisture, the bound moisture and inherent moisture. Free moisture can easily be removed by conventional drying, whereas bound moisture is physically or chemically absorbed onto a particle making it difficult to remove and inherent moisture cannot be removed by drying, as water molecules are trapped in the structure of the particle [36].

The drying process can be explained in the following five stages [42],

a. *Increasing Rate Period*- in the initial period the liquid is removed by evaporation and the rate increases on heating when the relative humidity is less than 100%. The free moisture is mostly removed in this stage.
b. *Constant Rate Period*- during this stage the drying rate is constant as the evaporation rate per unit area of the drying surface is independent of time. The product temperature is equal to the wet bulb temperature of the surroundings. Shrinkage may be seen as a result of the both the loss of interparticle liquid and external capillary stress and colloidal particles or molecules may migrate to the surface. This shrinkage and migration often leads to the falling rate period as the pores become unsaturated.
c. *Critical Point*- This is the point at which shrinkage stops before the drying rate begins to decrease as the liquid is evenly distributed. It is at this point the breaking or cracking of particles is likely to happen.
d. *First Falling Rate Period*- the evaporation of liquid in the unsaturated pores occurs when the evaporation rate is higher than the rate of internal liquid transport. The temperature of the evaporation surface can approach the dry bulb temperature.
e. *Second Falling Rate Period*- the slope changes for the second falling rate period as the remaining free liquid can only be removed by thermal diffusion of the liquids vapour to the particle surface.

The drying rate of slurries is highly dependent on the solids concentration, as more particles will trap more moisture slowing down the overall drying rate of the process.

2.4.2 Drying Parameters

The internal parameters which affect the drying process and rate are the moisture content, the drying ratio and the latent heat. The external parameters are of the drying air and are the dry and wet bulb temperature (thus the relative humidity), the humidity ratio, the temperature and enthalpy. The drying air temperature and also the drying air flow rate are the main controllable parameters which determine the quality of the dried product. The drying temperature must not exceed the known temperature which is likely to cause undesirable changes in the sample and both parameters must be controlled to avoid rapid

drying rates. This is because higher drying rates may result in the formation of hard drying surfaces which promote moisture migration to the surface [43].

The understanding of the critical control parameters during drying processes are of great importance when considering the redispersibility of dry powders as various drying techniques can create additional thermal stresses, such as heat for spray drying and freezing for freeze drying, which leads to the destabilisation of the particles. On the nano and micron scale this can lead to aggregation of particles providing an undesirable size distribution. The controls of these parameters are also important to avoid morphology of the dried particles [44].

2.4.3 Drying Processes

2.4.3.1 Spray Drying

The spray drying process evaporates the moisture from an atomised feed by mixing the spray with a drying medium, typically air. When the desired moisture content of the sprayed particles is reached the product is separated from the air. The sample which is sprayed can be a solvent, dispersion, emulsion or suspension [45]. Spray drying can be an expensive process and more so with a low solids content in the sprayed sample [46].

Figure 2.14 shows a schematic diagram of the spray drying process in which the mixing of the spray and the drying medium occurs in the same direction (co-current). This gives a lower residence time in comparison to a counter-current spray drying system. The spray cylinder, marked as 3, can operate as an open system, where the drying medium is electrically heated at point 1 and is exhausted to the atmosphere after the drying process, or as a closed system, where the drying medium is typically an inert gas which is recycled back into the process.

When the sprayed droplets come into contact with the drying medium, a saturated vapour film quickly form at the droplet surface and evaporation takes place. This then cools the droplet, creating a temperature and moisture gradient in the cylinder. These gradients and the high surface area favour heat and mass transfer, resulting in rapid drying of the particles.

The product is removed from this stage reducing the possibility of any heat damage from the drying medium entering at the top of the cylinder. The inertial forces of the cyclone, shown at 4, separate the desired product.

The particle size obtained from this process is dependent on the spray flow rate, as particles become smaller as the rate is increased, and the spray concentration where more concentrated samples result in the formation of larger particles. The formation of larger particles is also dependent on the aspirator speed. When a high speed is used a shorter residence time is obtained resulting in an increase of residual moisture. This moisture can cause the particles to bond. This is also the case if there is a larger temperature difference between the inlet and outlet temperature where a higher pump speed lowers the outlet temperature. Thus there are many parameters which affect the overall average particle size obtained although this method produces a more uniform size distribution than other drying techniques [45].

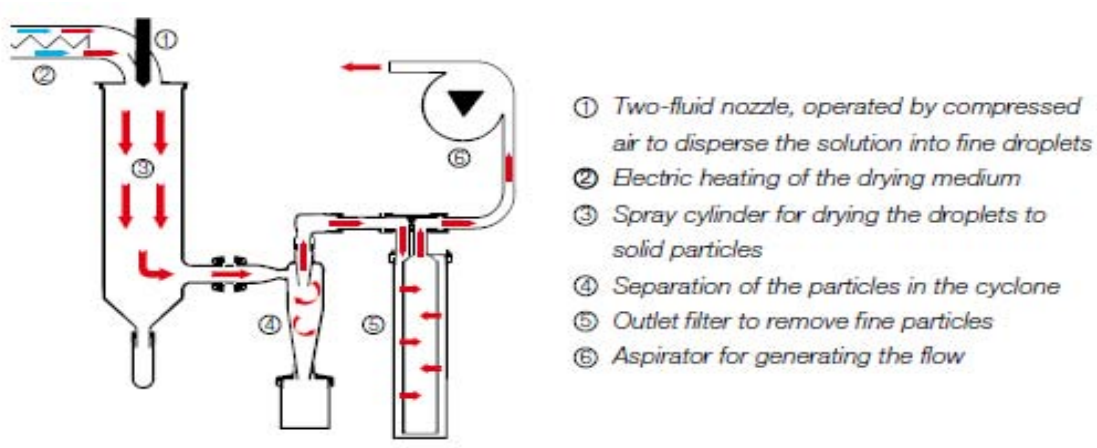

Figure 2.14- Schematic diagram of a lab scale spray drier [47]

2.4.3.2 Freeze Drying

Freeze drying is a drying process which avoids the liquid-vapour interface by freezing the liquid in the structure of a particle and then undergoing sublimation under vacuum [42]. It is quite a slow and expensive process and consists of the following three stages [48, 49],

a. *Freezing Stage (solidification)* - in this stage the suspension is frozen below its triple point to ensure it does not melt in the following stages. As the water

molecules form ice crystals, the concentration of the remainder suspension increases and the viscosity increases as a result until further crystallisation cannot occur. Finally the concentrated liquid solidifies but the bound moisture does not freeze.

b. *Primary Drying Stage (ice sublimation)* – in this stage the pressure is controlled by the use of a vacuum to transfer heat to the frozen solution from the tray or shelf it is sitting on. When the ice sublimes water vapour is produced and transfers from the dried area of the product to the sample surface and then through the chamber to a condenser. The condenser allows the water vapour to re-solidify. After this step the sample contains pores which are where the ice crystals were formed.

c. *Secondary Drying Stage (desorption of unfrozen water)* – this stage is primarily for the removal of the bound moisture which did not freeze in the first stage and is dependent on the samples adsorption isotherms. Generally the temperature is increased from the primary drying stage and the pressure is lowered to promote desorption of the water molecules [49, 50].

Freeze drying is most likely to cause less damage to the sample on a larger scale, especially during rapid freezing, as this helps to keep the shape and structure of the product. On the smaller scale, the rapid formation of ice crystals can cause some defects and breakdowns of structures leading to the formation of agglomerates aided by the presence of the bound moisture.

3 Methodology

3.1 Materials

The materials used in this research were Carbilux (99.9% calcite, Imerys Minerals), Hydrochloric Acid (37%, Sigma Aldrich), Sodium Hydroxide (98%, Sigma Aldrich), Acetone (99.9%, Sigma Aldrich), Dispex A40 (CIBA), Glycerol (99%, BDH), Igepal (Sigma Aldrich), and Rinse Aid (5-15% non-ionic surfactants, Finish Consumer Service).

3.2 Experimental Methods

3.2.1 Altering the pH of Carbilux

The pH of Carbilux was altered to allow the plotting of a conventional figure of zeta potential as a function of pH. A dilute suspension of Carbilux was prepared by adding 0.27 g of the sample to 500 cm^3 of distilled water (overall concentration 4mM). Various pH levels were obtained using a titration technique of 0.1 mol dm^{-3} acid and base solutions of Hydrochloric Acid and Sodium Hydroxide respectively. All suspensions were left for 2 hours before measurements were taken.

3.2.2 Addition of Various Dispersants

Various dispersing agents were added to Carbilux at 0.5 wt% by solids and then passed through a centrifuge mixer at 3500 rpm (DAC 150 FV) for 120 seconds to aid the mixing process. Cyro-SEM and rheology analysis was conducted on Carbilux samples with the addition of Dispex A40 and Glycerol. The zeta potential was also obtained of these samples in addition to Carbilux with Igepal (a non-ionic detergent), Rinse Aid and Acetone which was used to reduce the surface tension.

3.2.3 Sample Preparation for Rheological Comparison of Washed and Acetone Treated Carbilux

The Carbilux sample specification from Imerys Minerals states a small amount of a dispersant assumed to be similar to Dispex A40 is used. The project aimed to study the re-dispersion of Carbilux after drying, and so it was decided to investigate what effect removing this dispersant and other impurities would have on the sample using a washing technique as described here.

Three samples were prepared; Carbilux-unwashed, Carbilux-Washed, and Carbilux washed and rinsed with acetone (Carbilux-Acetone). As Carbilux is highly concentrated it was first diluted with distilled water using a 1:2 ratio Carbilux to water. It was then passed through a Hermle z200a centrifuge system at 5000 rpm for 15 minutes, causing the particles to separate from the suspension and collect at the bottom of the tube. The excess liquid was poured off and distilled water was added. The particles were redispersed by putting the tube into a Whatman ultrasonic bath before removing the water through the same centrifugation method, thus washing the particles.

For the Carbilux-Washed sample, the particles were redispersed in distilled water and put into a conventional oven along with the unwashed sample to dry at 130^{o}C. For the Carbilux-Acetone sample, the particles were redispersed in acetone and left to dry in a fume cupboard.

The dried samples were then ground down and passed through a 710 μm sieve. The rheological properties of all three samples were compared by redispersing the particles in distilled water at various solids loadings using a DAC 150 FV centrifuge mixer at 3000 rpm for 60 seconds.

3.2.4 Sample Preparation to Compare Various Drying Techniques

3.2.4.1 Various Samples Prepared

Four samples were prepared to investigate the difference in the powder properties after oven drying, freeze drying and spray drying procedures. Two of the samples were unwashed material comprising Carbilux-unwashed and Carbilux-pH where the pH was

altered to the most stable zeta potential previously found. The Carbilux-Washed and Carbilux-Acetone sample were washed as mentioned in section 3.1.3. In this case, the Carbilux-Acetone sample was redispersed in distilled water after most of the acetone had evaporated in the fume cupboard for safety in the drying techniques. All samples were diluted using distilled water to approximately 37 wt% by solids.

3.2.4.2 Oven Drying

All four samples were dried in a conventional oven at 130^{o}C in 500ml glass beakers. To prepare the powders for later study, the samples were ground and passed through a 300 µm sieve after drying.

3.2.4.3 Freeze Drying

To obtain powders from a freeze drying technique a lab scale BOC Edwards freeze drier was used. Each sample, of 500 ml, was poured into a tray of liquid nitrogen and a vacuum was applied with the temperature kept at -170^{o}C. The sample was left for 2 days to ensure all of the liquid crystals had sublimed and evaporated leaving a powder.

3.2.4.4 Spray Drying

Spray dried powders of the four samples were obtained using a Büchi Mini Spray Dryer B-290 in the co-current flow mode. The inlet temperature was set at 220^{o}C, the aspirator at 100% and a pump flow rate of 40% (approximately 250 ml/hr). The outlet temperature was measured at 130-135^{o}C and each sample of 500ml took 2-3 hours to dry.

3.3 Analytical Methods

3.3.1 Microscopy

3.3.1.1 Optical Microscopy

A thin section of approximately 30 µm of marble from an extraction site, similar to where the calcite for Carbilux is removed, was prepared courtesy of Imerys Minerals. The surface of the thin section was polished, allowing examination under an Olympus petrological optical microscope, and observed both under cross polarised and plane

polarised light at a low magnification of 50x. An Olympus Metallurgical Microscope was used to observe opaque minerals using reflected light.

3.3.1.2 Environmental Scanning Electron Microscopy (ESEM)

A scanning electron microscope (SEM) is a type of microscope that uses a high-energy beam of electrons to scan the surface of a sample, as opposed to a light source in ordinary optical microscopes which has limited resolution due to diffraction. The beam interacts with the atoms of the sample providing signals and thus information on the samples surface topography to form an image of greater resolution [51, 52, 53]. A schematic representation of a SEM is shown in Figure 3.1.

ESEM holds the same basic principles as SEM but the sample can be examined in its natural state without any modification or preparation at any gas compositions, at temperatures ranging from ambient temperature to 1500^{o}C and at pressures of up to 30 torr [54].

A Phillips XL30 ESEM-FEG was used to obtain images in various techniques. To observe the drying process of Carbilux a droplet was put onto a stub and loaded into the sample chamber. By controlling the pressure of the sample chamber the humidity is controlled allowing the droplet to be viewed at different stages as it dries on the stub. The pressure was reduced in stages from 5.3 torr (100% humidity) to 3 torr (50-55% humidity) and images were taken at an acceleration voltage of 10 kV and a spot size of 3-4.

The ESEM also has facility to analyse samples by Cyro-SEM. Various Carbilux samples with different dispersants were rapidly frozen in liquid nitrogen in an attempt to capture its dispersed phase using an acceleration voltage of 3kV and a spot size of 4.

Images were taken of the powders produced by various drying techniques. The powders required to be sputter coated using gold particles in order to increase their conductivity in the ESEM. The accelerated voltage was set at 20kV and a spot size of 4 was used to take images at various magnifications.

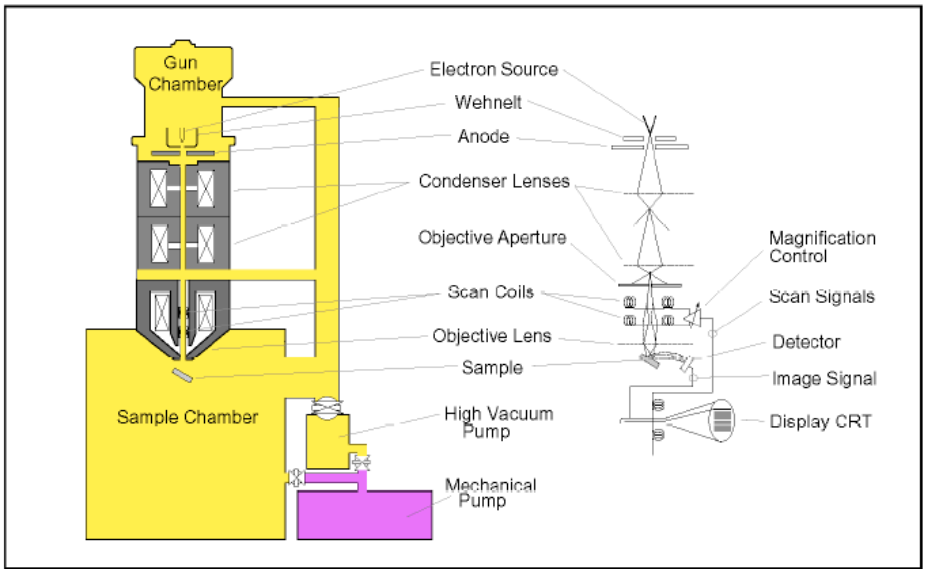

Figure 3.1- A schematic representation of a Scanning Electron Microscope [55]

An Oxford INCA 300 X-ray Energy Dispersive Spectrometer (EDS) is incorporated within the ESEM used. A thin layer of carbon coating was applied to the sample slide to aid conductivity thus enabling the detection of the element content. Using backscattering electrons with an acceleration voltage of 20 kV and spot size of 4, the composition of various sites were obtained and analysed by the INCA system.

3.3.2 XRD Analysis

For the X-ray diffraction (XRD) analysis a PANalytical X'Pert Pro Multi Purpose Diffractometer was used. An x-ray beam is emitted towards the sample at different angles and Braggs Law is applied to determine the composition of the sample. Raw material analysis was conducted on a dried Carbilux cake which was placed into a bulk holder and probed between 10-140^{o}. The wavelength was set at 1.542 Angstroms as the small wavelength enables the detection of small variations of the material. A copper X-ray source is used to control the photon energy level as it is found to eliminate the changes of varying photon energy levels caused by decay. To excite the electrons, a voltage of 40mV is supplied to the copper and a current of 40mA is used to obtain the large number of photons required for emission [56].

3.3.3 Zeta Potential Measurements and Particle Size Analysis

The zeta potential is measured using a Zetamaster (Malvern Instruments Ltd, UK) by electrophoresis phenomena. The velocity of a particle in a unit electric field and the zeta potential is related by the Henry equation,

$$U_E = \frac{2\varepsilon\zeta f(\kappa a)}{3\eta} \qquad \textbf{(3-1)}$$

where U_E is the electrophoretic mobility, ζ is the zeta potential, ε is the dielectric constant, η is the viscosity and $f(\kappa a)$ is Henrys function which is a measure of the ratio of the particle radius and of the electrical double layer thickness [21].

The sample to be measured must be conductive and dilute. In cases where the sample is not conductive small amounts (1-2 ml) of an inert electrolyte, such as Potassium Chloride, can be added. The sample is then injected in 5 ml quantities to ensure the area that is probed for electrophoretic mobility is completely full.

The particle size distribution of Carbilux in its raw slurry form and of the powders obtained from various drying techniques were measured using the Mastersizer 2000 particle size analyser (Malvern Instruments Ltd, UK) which is combined with a Hydro SM small volume sample dispersion unit. This unit enable the size analysis of both wet and dry samples in which only a small quantity is needed which is determined by the programme during use.

3.3.4 Surface Area Analysis

The surface areas of the powders produced from various drying techniques were obtained using physical gas adsorption using a Micromeritics ASAP 2010.

The instrument calculates the Langmuir surface area and the BET surface area from plots of both equations. Langmuir's theory assumes only monolayer molecular adsorption occurs whereas the BET equation is an extension of the Langmuir theory and assumes gas molecules adsorb onto each layer infinitely and the adsorbed layers do not interact [57].

3.3.5 Rheology Methods

A TA Instrument AR500 shear rheometer was used to conduct all rheological tests. The AR500 can function as a controlled-stress or a controlled-rate instrument. The controlled-stress technique is most commonly used as most real-life situations can be simulated using these measurements. In this technique the stress can be applied and released whilst providing information on the interactions of the sample material.

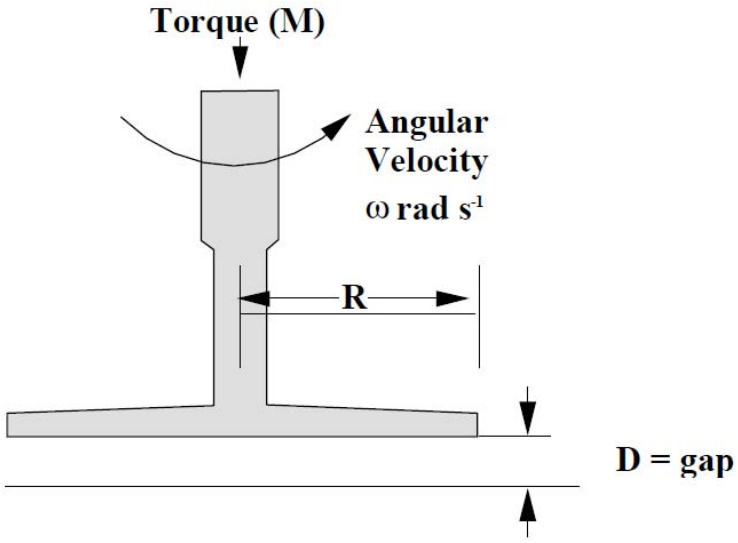

Figure 3.2- Parallel Plate Geometry [58]

There are 3 main geometry types: cone and plate, parallel plate and concentric cylinders. Parallel plates, as shown in Figure 3.2, allow systems containing particles to be measured more effectively and so this geometry was uses for all Carbilux dispersions. It is commonly stated that the geometry gap must be at least 10 times the size of the largest particle in the sample.

Various diameters of flat plate geometries were used to probe the Carbilux slurry and both controlled stress and controlled rate techniques were used for different samples.

3.3.6 Compressive Load Tests

Compressive load test were conducted using the Instron Model 4467 model and Bluehill 2 software. The various powders prepared by the different drying techniques were weighed

at 1 g and loaded into a 9 mm diameter die. A 30 kN load cell was used to compress the powders at a ram speed of 1 mm min^{-1} to a maximum load of 1.2 kN (18.9 MPa) and the displacement was recorded by the software.

4 Results and Discussion

4.1 Characterisation of Raw Materials

4.1.1 Optical Microscopy of Raw Mineral Slide

The calcium carbonate sample provided by Imerys Minerals is known to be predominately calcite, the most stable polymorph of calcium carbonate. It has also been stated there is some dolomite present which has the chemical formula $CaMg(CO_3)_2$.

Using the transmitted light optical microscope, the following images of the sample under cross polarised and plane polarised were obtained at a low magnification of 50x.

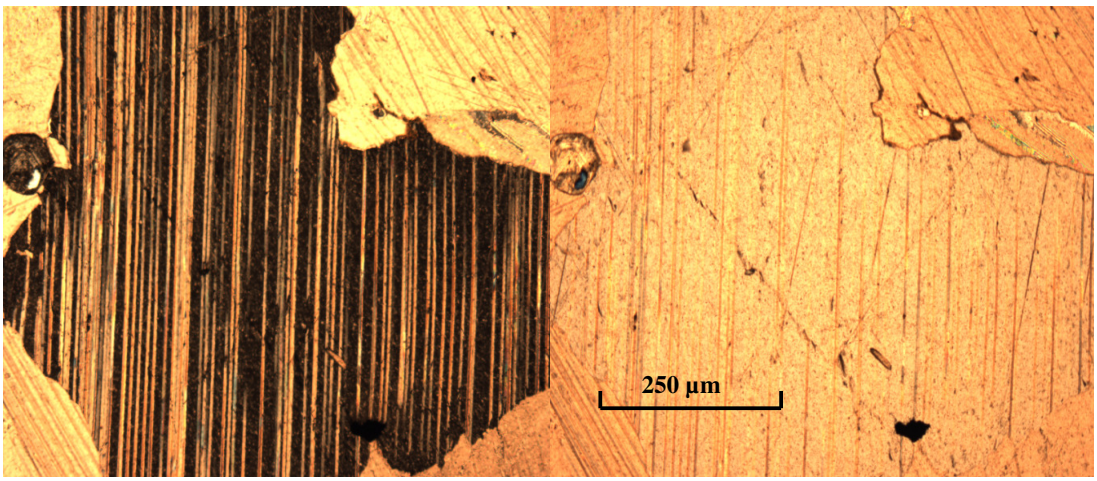

(a) **(b)**

Figure 4.1- Optical images of a large crystal in extinction with twin lamella in a) cross polarised light, b) plane polarised light

Calcite is an optically negative uniaxial mineral in which twinning is very common. From Figure 4.1 the twinning characteristic of calcite is quite clearly observed [59].

Figure 4.2 shows images taken of another spot on the sample slide. It is clear that there are some opaque minerals in cross and plane polarised light surrounded by hydrothermal alteration products in a vein system running across the sample.

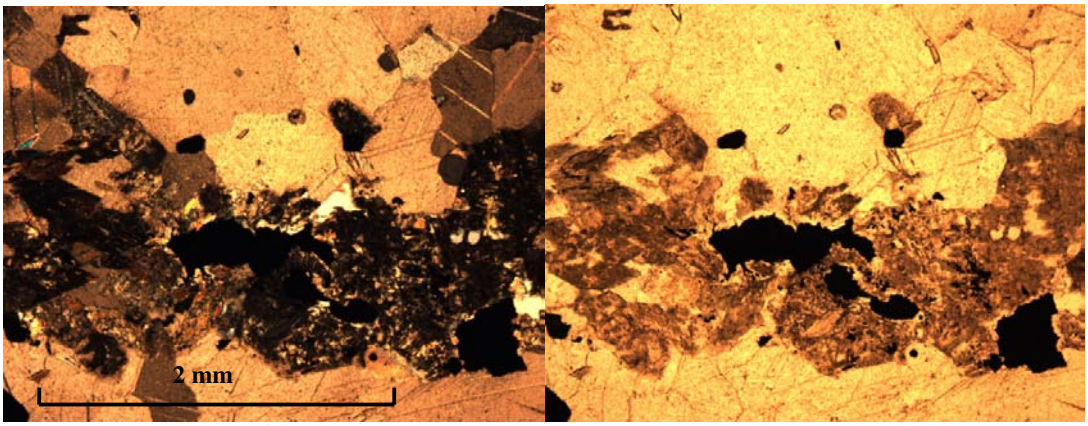

(a) (b)

Figure 4.2- Optical images of Contamination Mineral in (a) cross polarised light and (b) plane polarised light

The reflected light optical microscope showed highly reflective opaque minerals on the sample slide as shown in Figure 4.3. Although here the reflected particle appears white, it was observed to be pale yellow which is an indication that pyrite is most probably present [59].

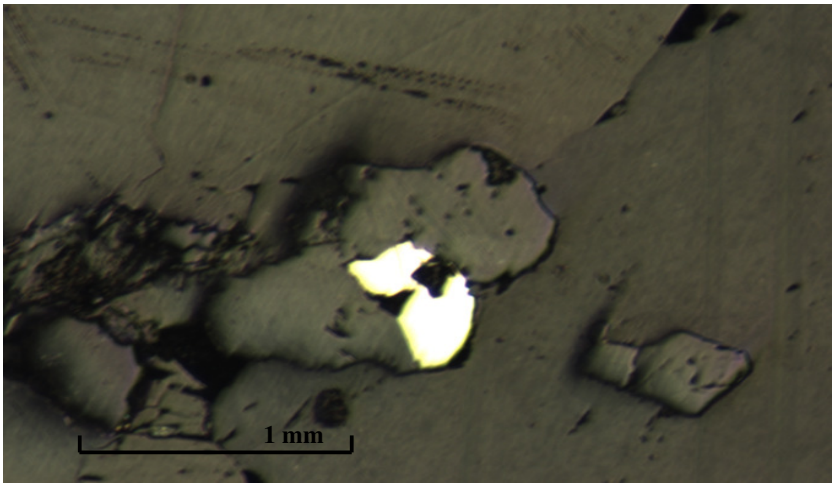

Figure 4.3-Reflected light Image of a site on the sample slide

4.1.2 EDS Analysis of Slide

Using the ESEM Inca energy dispersive system, images were taken at various locations across the sample slide and the composition determined by the Inca software. The SEM image taken in Figure 4.4 shows the presence of a fibre on the sample slide. These were

found at many sites but did not produce a varied spectrum and thus it can be deduced that they are irrelevant in this analysis.

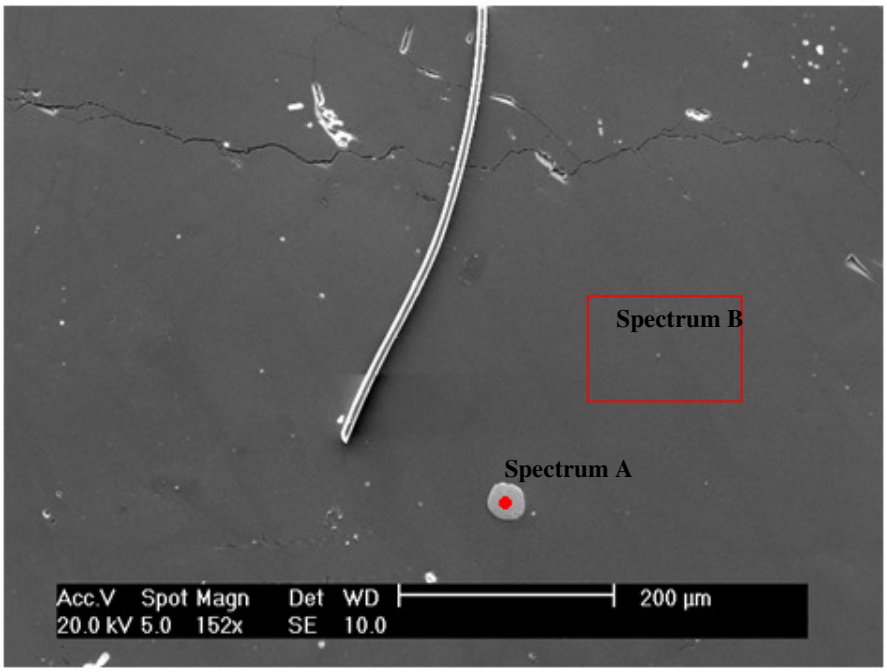

Figure 4.4- SEM image of Area 1 of which EDS spot analysis conducted

Table 4.1- Composition Table of spectrum A

Element	Weight%	Atomic%
S K	38.74	52.97
Ca K	0.36	0.39
Fe K	58.81	46.17
W M	0.61	0.15
Pb M	1.49	0.31
Totals	100.00	

Table 4.2- Composition of spectrum B

Element	Weight%	Atomic%
O K	57.23	77.28
K K	0.27	0.15
Ca K	41.31	22.27
Fe K	0.44	0.17
Sn L	0.76	0.14
Totals	100.00	

Table 4.1 shows spectrum A consists of mainly iron (Fe) and sulphur (S). The chemical formula of pyrite is FeS_2 and thus this spectrum further supports the presence of pyrite in the sample slide as observed in Figure 4.3. Table 4.2 shows spectrum B consists of mainly calcium and oxygen suggesting the main surface of the sample slide consists of calcium carbonate as carbon cannot be detected.

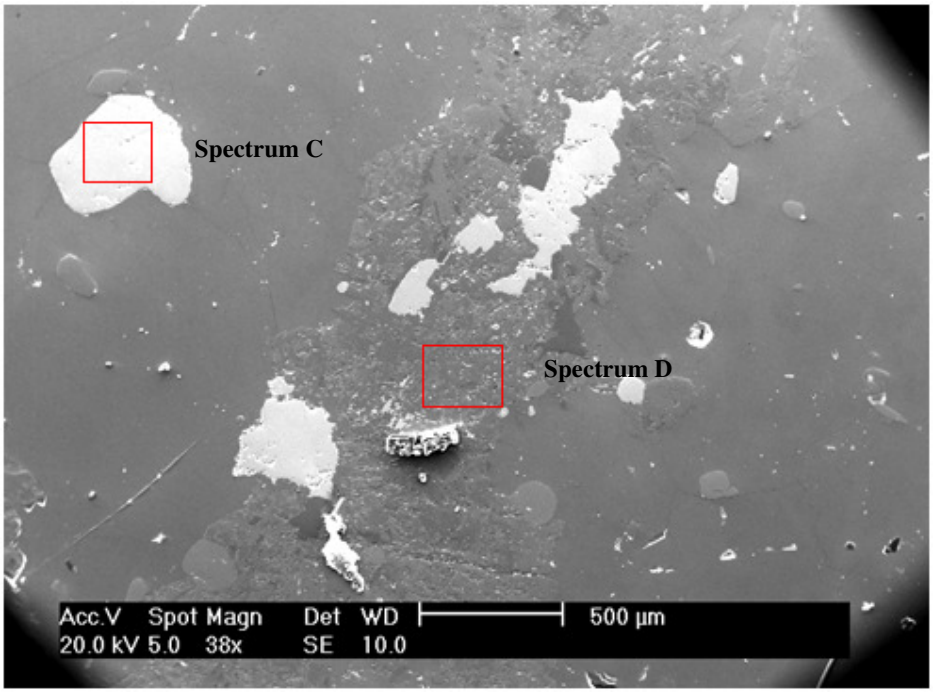

Figure 4.5: SEM image of Area 2 of which EDS spot analysis is conducted

Table 4.3- Composition Table of Spectrum D

Element	Weight%	Atomic%
O K	47.69	64.96
Mg K	2.98	2.67
Al K	10.45	8.44
Si K	17.53	13.60
S K	0.34	0.23
K K	0.48	0.26
Ca K	11.55	6.28
Ti K	0.66	0.30
V K	0.21	0.09
Fe K	8.12	3.17
Totals	100.00	

Figure 4.5 shows a different area on which EDS spot analysis was conducted. The spectrum composition of C was similar to spectrum A. All the whiter areas in this image have the same composition, suggesting there is a significant presence of pyrite. The smoother areas of this image shared similar spectrum compositions to Table 4.2, thus the presence of calcium carbonate. Table 4.3 suggests a strong presence of the alteration

product wollastonite, which has the chemical formula $CaSiO_3$. There is also the possibility of the presence of augite, a calcium magnesium iron silicate with the chemical formula $(Ca,Na)(Mg,Fe,Al)(Al,Si)_2O_6$. However, as previously stated, Imerys Minerals have observed the presence of dolomite which has the chemical formula $CaMg(CO_3)_2$ and thus spectrum 3 may possibly be a combination of wollastonite and dolomite only. Other areas of similar appearance in the SEM images consisted of a similar spectra.

4.2 Carbilux Characterisation

4.2.1 XRD Results

The XRD results obtained from Carbilux oven dried at 130°C are shown over the 2θ range 10-140°. Figure 4.6b shows the number of peaks occuring in the range of 2θ = 20-90°. The single peak at 29.5° is of calcite and shows that the material is mono crystalline. The peaks visible at 36.5°, 43.5° and 48.5° show aragonite may be present in the sample.

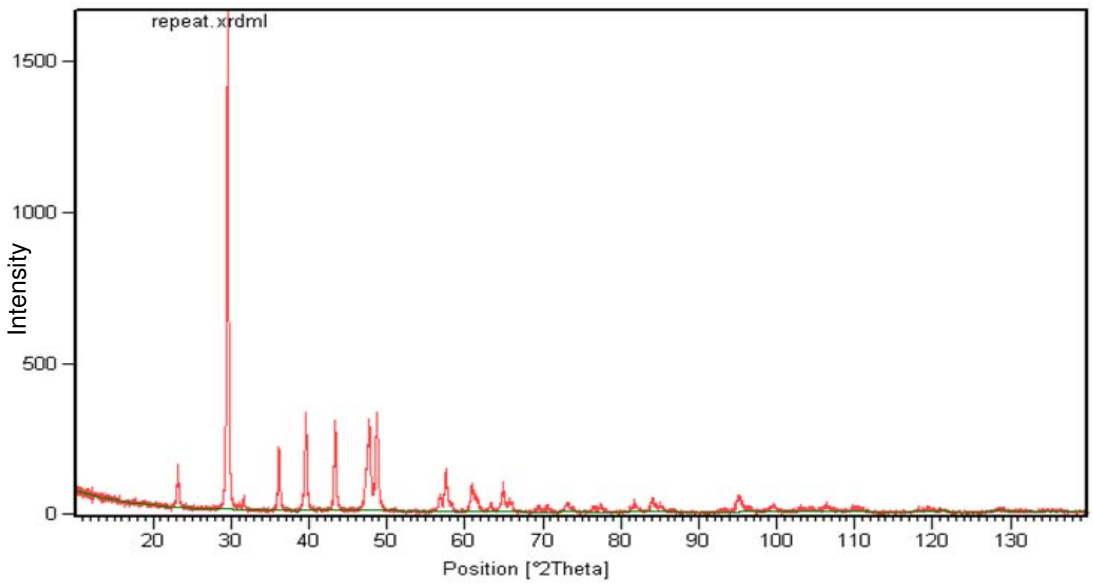

Figure 4.6a- XRD Analysis of Carbilux oven dried at 130°C for 10 minutes where 2θ = 10-140°

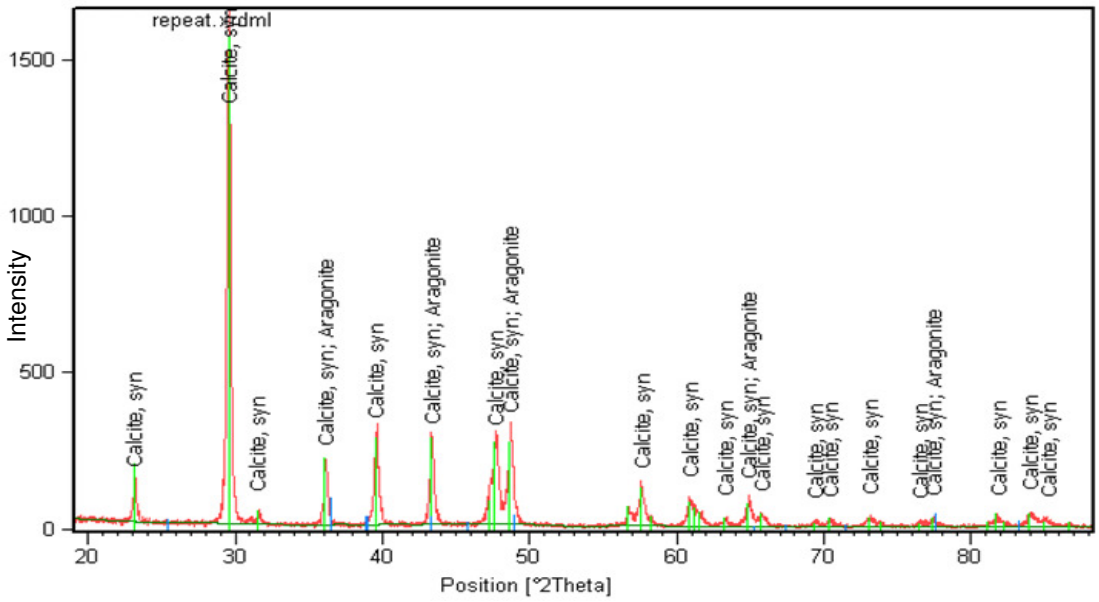

Figure 4.6b- XRD Analysis of Carbilux oven dried at 130°C for 10 minutes where 2θ = 20-90°

In previous literature, aragonite is said to change to calcite between 400-500°C due to its instability [60]. Hacker *et al.* suggests the transformation of aragonite to calcite does not occur in the absense of volatiles at temperatures below 200°C, such as the case in recent studies by Zhaodong *et al.*, where with the addition of sodium dodecyl benzene sulfonate causes aragonite to become vaterite at 90°C and calcite at 120-150°C [61,62]. The Carbilux sample analysed here was only dried to 130°C suggesting this is not a sufficient temperature to transform the aragonite present.

4.2.2 Particle Size

The particle size distribution data given by Imerys Minerals states the calcite particles are 0.3-4 µm in diameter. The size distribution obtained in Figure 4.7 shows a curve with two peaks with a relatively uniform volume percentage where the smallest and largest particles detected as 0.12 µm and 3.311 µm respectively. At the 90th percentile the particles are below 1.625 µm and the average particle size is 0.585 µm. In comparison to the dada provided the sample size distribution was found to be smaller.

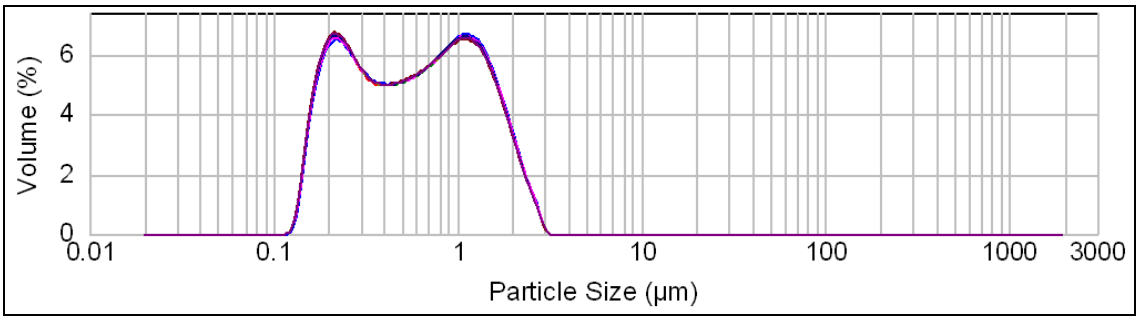

Figure 4.7- Particle Size Distribution of Carbilux

Imerys Minerals also state that Carbilux has a weight percentage of 75% by solids. By removing the moisture the weight percentage was found to be 74.3% by solids when drying at 130^{o}C.

4.2.3 Effect of pH on Zeta Potential

The zeta potential measurement of Carbilux at different pH values is shown in Figure 4.8 in which an order 4 polynomial trend line has been used to fit the data. The experiments were repeated 20 times and the results show zeta potential is negative across the pH range evaluated. When a dilute suspension of Carbilux was left to reach equilibrium the pH_{eq} was 9.5 and at this pH value the zeta potential obtained was -24.8 mV. For a stable system a zeta potential of +/-30 mV is generally observed and is achieved here when the pH is greater than 10, after which a steep increase in the negative potential can be seen [18]. An iso-electric point could not be found.

The pH is 8.29 of the bulk, undiluted Carbilux sample. The zeta potential can be estimated to approximately -25 mV, indicating that Carbilux may be a slightly unstable system in the current form.

Comparing these results with the values obtained in experiments by Vdović (2001) shown in Figure 2.6, it can be seen that the relationship is similar to other natural calcite samples where the zeta potential is always negative and decreases with the addition of acid and increases with the addition of the base. This negative zeta potential trend amongst natural calcites is usually the result of organic matter adsorption which acts as a coating, thus changing the surface potential, and can also be incorporated in the structure [24]. The

Carbilux sample has an organic polymer dispersant and possibly accounts for this behaviour.

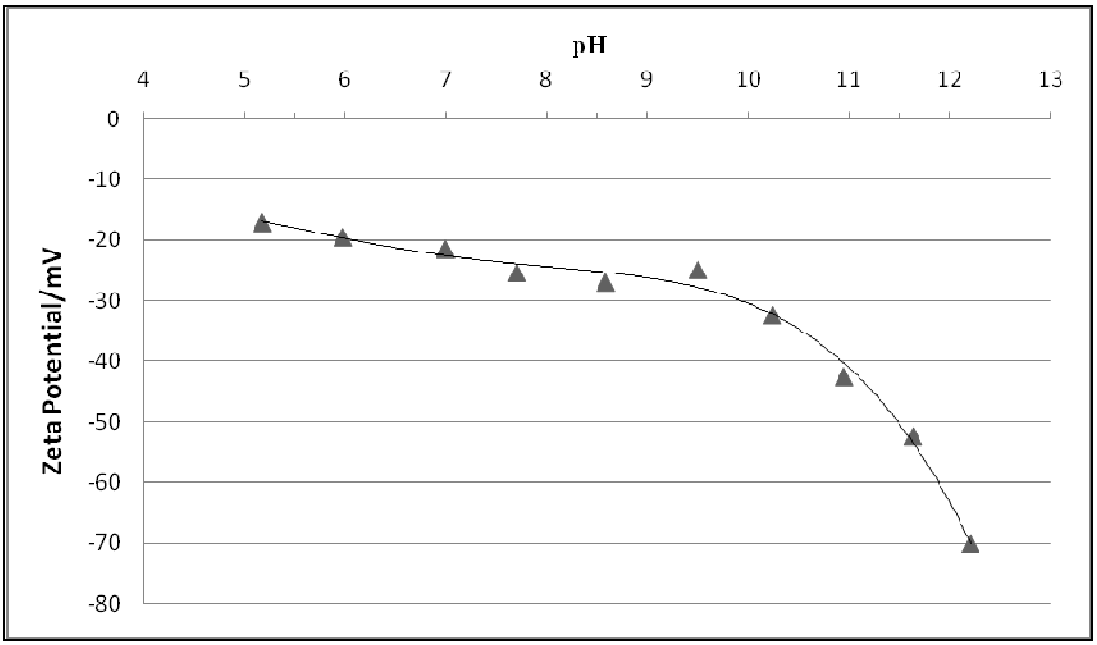

Figure 4.8- Zeta Potential at different pH solutions of Carbilux

4.3 Use of Various Dispersants

4.3.1 Zeta Potential

The Carbilux sample specification states it contains a dispersant similar to Dispex A40 at an optimised weight percentage by solids set by Imerys Minerals to meet their customer requirements. The zeta potentials obtained on the addition of various dispersants are shown in Table 4.4. Adding Dispex A40 continues to stabilise the system suggesting Imerys Minerals have not necessarily used the optimum amount for colloidal stability. Igepal has also improved the colloidal stability slightly whereas the dispersant glycerol has decreased the zeta potential. Acetone and Rinse Aid are known to reduce the surface tension but have not affected the system's stability greatly.

From these initial tests, it was concluded that changing the pH allowed greater control of the system stability, as can be seen in Figure 4.8.

Table 4.4- Zeta Potential of the addition of various dispersants to Carbilux at 0.5 wt% by solids

Dispersant Added	Zeta Potential (mV)
None	-23.94
Dispex A40	-27.31
Igepal	-24.89
Glycerol	-23.81
Rinse Aid	-24.54
Acetone	-23.97

4.3.2 Rheological Differences

A maximum shear stress of 200 Pa was applied to the Carbilux sample, Carbilux with the addition of Dispex A40 and Carbilux with the addition of Glycerol in a continuous ramp step up and step down to produce flow curves. A 40 mm flat plate geometry was used for these tests.

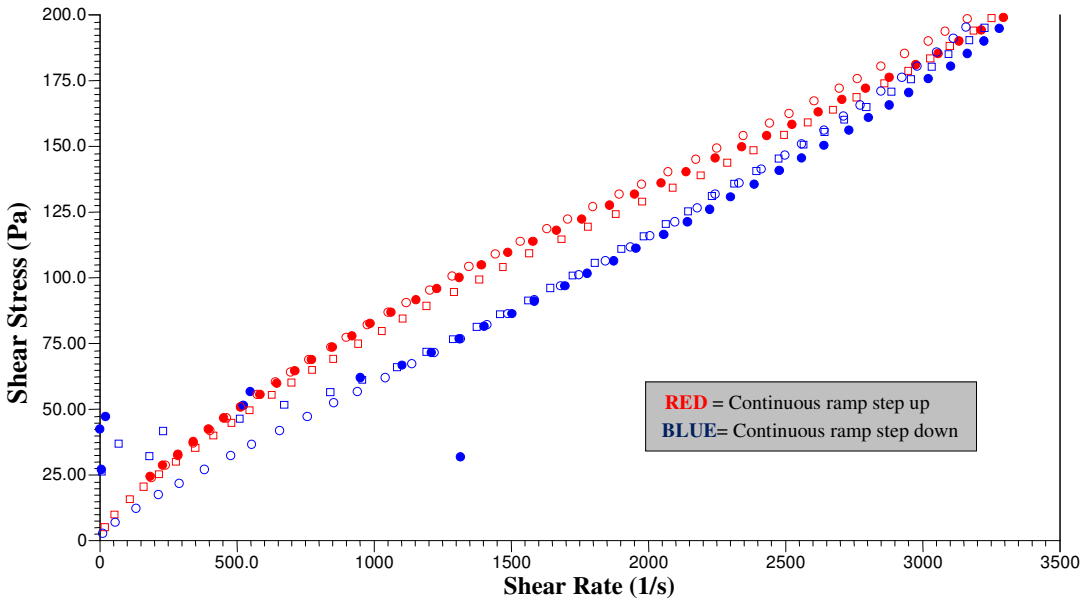

Figure 4.9- Shear stress versus shear rate of Carbilux

Figure 4.9 shows at 200 Pa the sample Carbilux attains a shear rate of approximately 3250 s^{-1} giving an apparent viscosity of 0.061 Pa.s. The flow curve shows that as the applied stress is increased the sample is showing shear thinning behaviour before it becomes

Newtonian. As the stress applied is decreased the sample remains Newtonian, suggesting the breakdown occurring is irreversible.

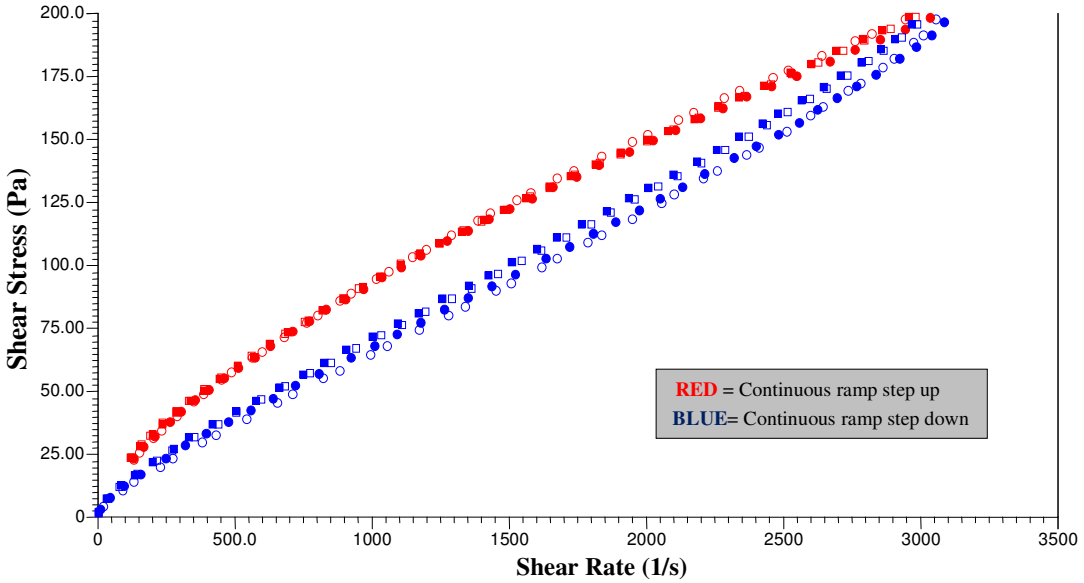

Figure 4.10- Shear stress versus shear rate of Carbilux with the addition of Dispex A40

The addition of Dispex A40 results in the shear rate decreasing to 3050 s^{-1} at 200 Pa giving an apparent viscosity of 0.065 Pa.s. The flow curve in Figure 4.10 shows a similar trend to the Carbilux sample where the sample shear thins when a stress is applied and becomes closer to Newtonian as the particles do not re-aggregate when the stress is reduced. As mentioned previously, Carbilux already contains a similar dispersant to Dispex A40. Although the addition of this dispersant has increased the stability of the system, as determined by the zeta potential analysis, the apparent viscosity has increased slightly. This suggests that in addition to changing the colloidal chemistry by coating the particles, in excess the organic polymer remains in suspension thickening the system.

Figure 4.11 shows the rheology results of Carbilux with the addition of Glycerol. At an applied shear stress of 200 Pa, the average shear rate obtained is 11,500 s^{-1}, giving an apparent viscosity of 0.016 Pa.s. This clearly shows that the addition of Glycerol lubricates the system and reduces the apparent viscosity significantly. The flow curve shows initially some shear thinning occurs before the sample is Newtonian and when the stress is reduced it continues to shear thin further, reducing the apparent viscosity. This

dispersant does not improve the zeta potential of the system, but clearly has an impact on the viscosity of the medium.

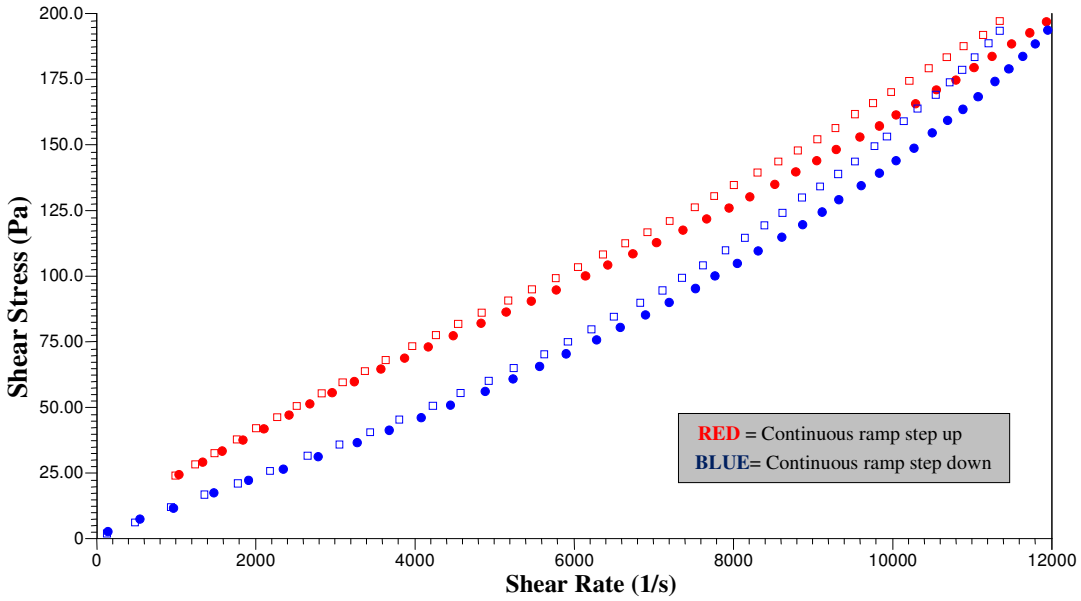

Figure 4.11- Shear stress versus shear rate of Carbilux with the addition of Glycerol

In all 3 cases, further investigation is required to determine if the shear thinning behaviour is reversible.

4.3.3 Cyro-SEM Images

This technique was used to see if there are significant differences visible in the samples with the addition of various dispersants. Figure 4.12 shows examples of images taken of Carbilux on it is own and with the addition of Dispex A40 and Glycerol. It is difficult to see from these images if the addition of the dispersant has any effect. However, as seen in the rheology results, Carbliux with Dispex A40 had similar properties to just Carbilux and both share similar SEM images. The addition of Glycerol lubricated the system and as can be seen from Figure 4.12(c) the particles appear to be more free than in Figure (a) and (b). It may the case that the particles visible in all 3 images are ice crystals on the surface of the sample and therefore this needs further investigation.

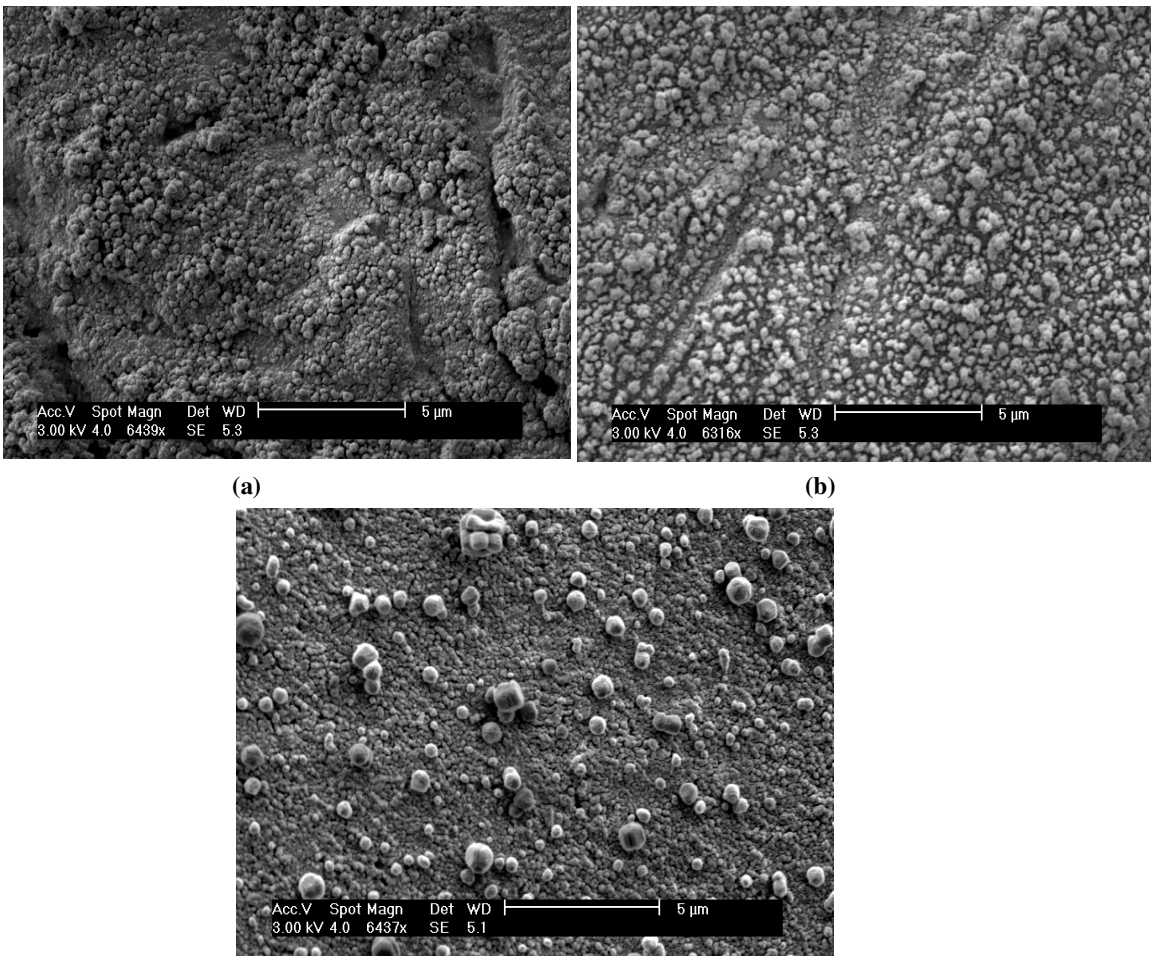

(a) **(b)**

(c)

Figure 4.12- Cyro-SEM images of a) Carbilux, b) Carbilux with Dispex A40, and c) Carbilux with Glycerol

4.4 Rheological Comparison of Washing Carbilux and Affect of Acetone Rinsing

The rheological effects of washing Carbilux and washing and rinsing the sample with acetone were investigated using shear rate controlled experiments, where a continuous ramp was applied to all samples from 0-10,000 1/s.

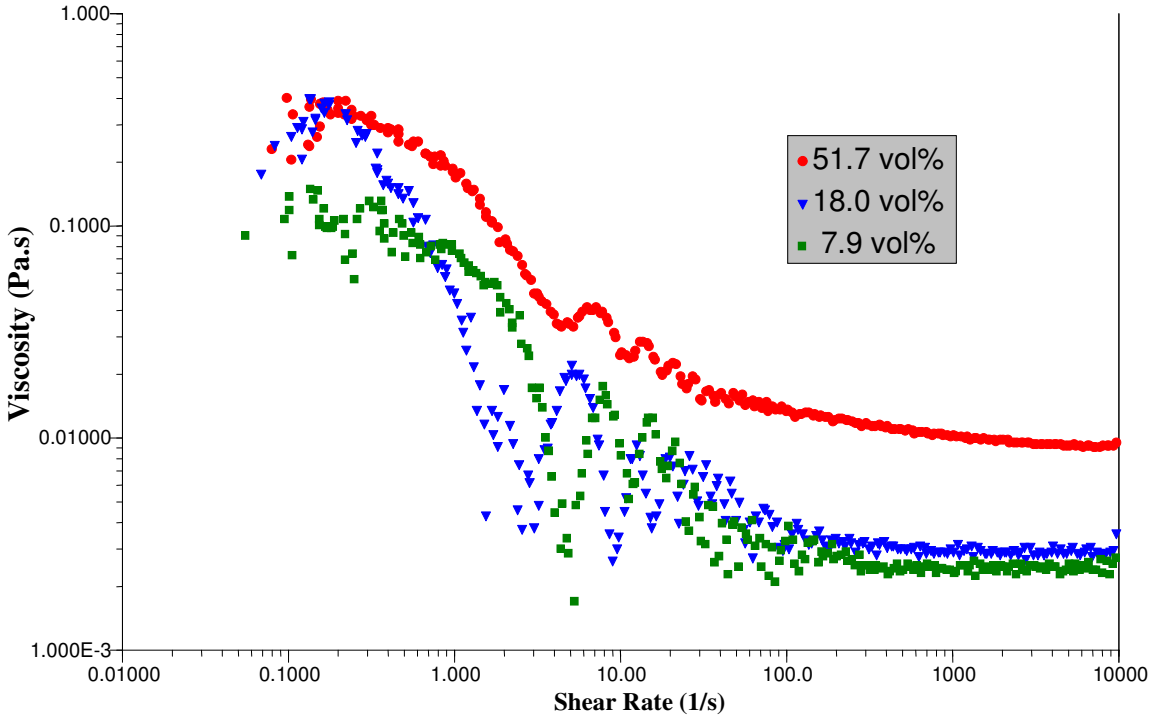

Figure 4.13- Viscosity versus shear rate of Carbilux unwashed at various solids loading

Figure 4.13 shows the rheological behaviour of the Carbilux sample under these conditions at various solid loadings. At first a Newtonian plateau is obtained at low shear rates, followed by a power law shear thinning region which flattens out to the upper (second) Newtonian plateau. Trends containing low shear and high shear viscosity plateaus, η_0 and η_∞ respectively, with a shear thinning region in between are typical features of a stable, concentrated colloidal suspension and can be modelled by the Cross relationship [63]. The curve form is present in all solid loadings, indicating stability of the colloidal system. As the solid loading is decreased, the viscosities also decrease as is expected with the addition of more fluid. This probably follows a relationship similar to that of Krieger-Doherty. The signal is noisy between shear rates of 1-100 1/s, particularly at lower solid loadings, and needs further investigation.

When Carbilux is passed through a washing system, and in addition rinsed with acetone, the suspensions of redispersed powders at lower concentrations in Figures 4.14 and 4.15 show similar stable behaviour to Figure 4.13.

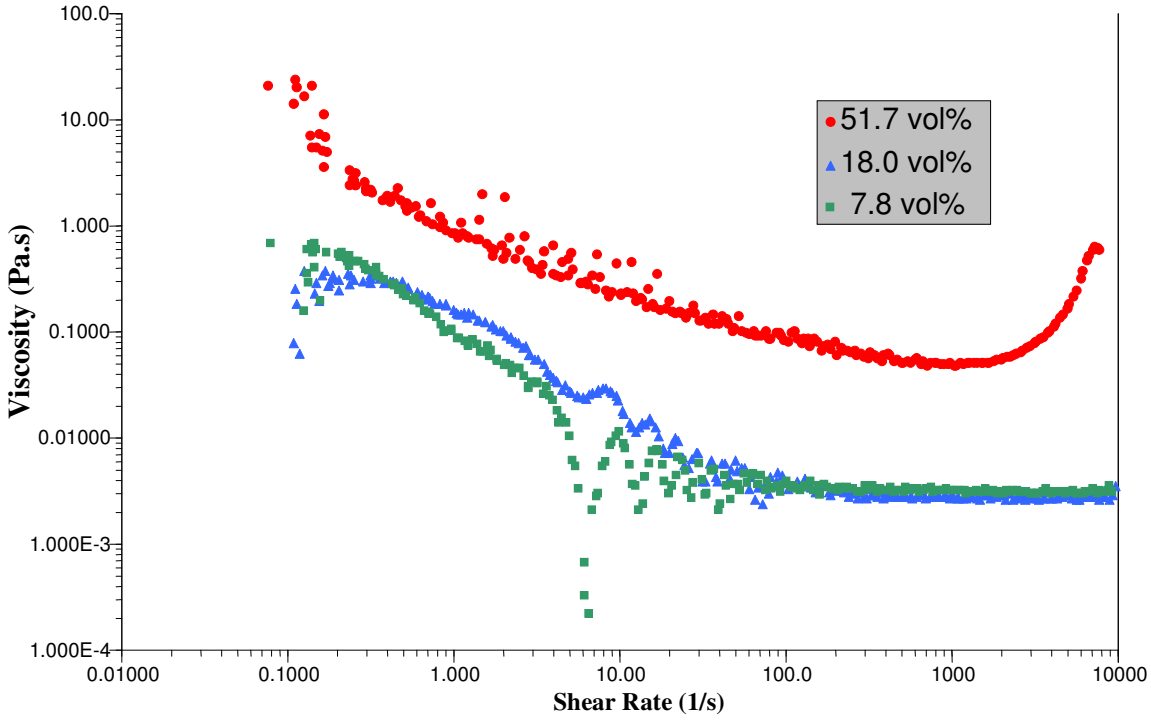

Figure 4.14- Viscosity versus Shear rate of Carbilux washed at various solids loading

At the higher concentrations (51.7 vol% by solids) these two samples show that at some critical shear rate in the upper Newtonian plateau, around 1000 1/s, the viscosity increases. This shear thickening behaviour, which is sometimes observed in suspensions, is governed by the viscosity of the medium, the particle size and the magnitude of interparticle repulsions [64]. This could be an indication of some form of flocculation or even aggregation as when particles break down from an ordered structure in the shear thinning region they may reform as less ordered flocculated structures in the shear thickening region creating a resistance. The less ordered structure also dissipates more energy during flow due to particle 'jamming' which increases the viscosity of the system [63]. Thus at higher solid loadings these two sample have become unstable.

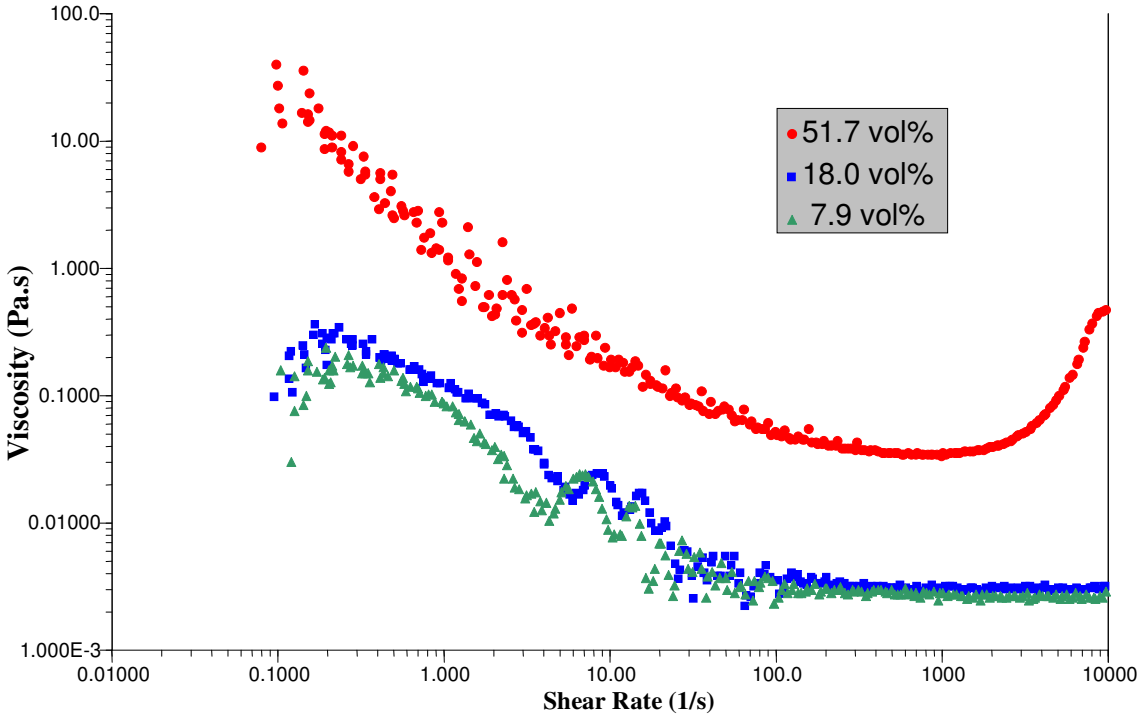

Figure 4.15- Viscosity versus shear rate of Carbilux rinsed with Acetone at various solids loading

4.5 Further Rheology Tests

The results obtained in section 4.4 showed some form of oscillation occurring and a region of shear thickening in the higher solids concentration samples suggesting some form of particle build up. This may also have been due to the sample drying out under the rheometer and so similar tests were conducted on the Carbilux sample under various geometries to investigate this further. As an alternative to investigating the various solids loadings, these tests were conducted by using a fresh bulk sample for each geometry used, in which the bulk sample was re-mixed for some tests or left to settle for others. This was done to investigate the effect of particles sedimenting from the suspension on the system. All tests had a geometry gap set at 50 µm.

The tests conducted on Carbilux under a 40 mm flat plate geometry are presented in Figure 4.16. Tests 1 and 2 were of the well mixed bulk sample. As observed in Figure 4.13, these tests follow the same trend for stable, concentrated suspensions. Tests 3 and 4 were conducted on the bulk sample after a settling period of 4 minutes and tests 5 and 6 were

conducted after a further settling period of 4 minutes. As the sample settles the shear thinning region is less prominent and the viscosity decreases suggesting the larger particles in the sample have sedimented from the suspension and thus a sample of finer particles was probed in the final tests. The oscillation observed in previous experiments reduces as the viscosity and shear thinning behaviour decreases.

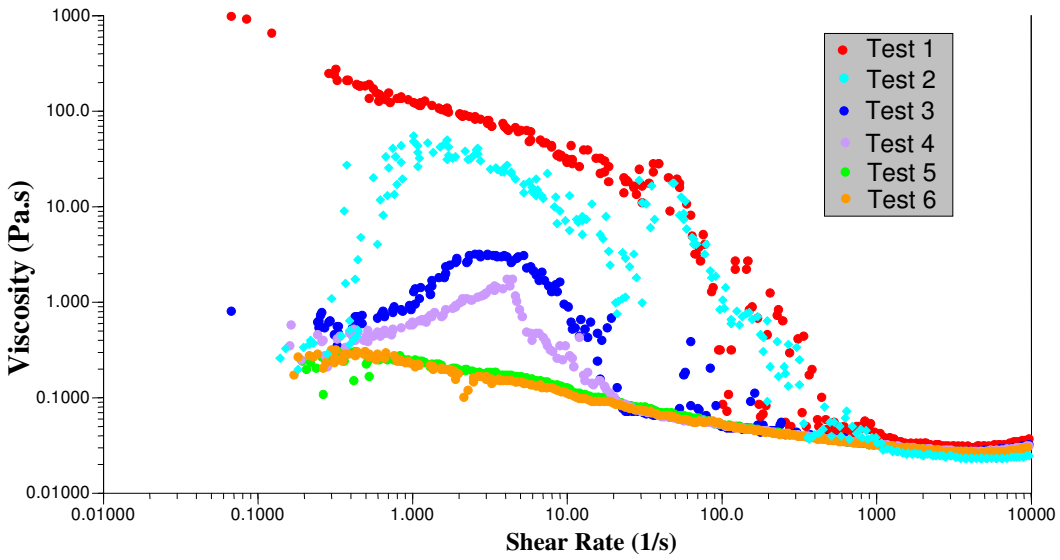

Figure 4.16- Viscosity versus shear rate of Carbilux using 40 mm flat plate geometry

Using 20 mm flat plate geometry shows similar trends in tests 1-3 of the well mixed bulk sample and test 4-6 of the sample after 4 minutes of settling. The settled samples again show reduced viscosities and shear thinning behaviour compared to the well mixed samples. However, a small shear thickening region can be seen after the Newtonian plateau suggesting Carbilux may be unstable.

Tests 1-2 in Figure 4.17 are also of a fresh sample and tests 3-6 have been allowed to settle before being probed using 10 mm flat plate geometry. The results are similar, but in this case the settled samples have an increased oscillation between shear rates of 1-10 1/s.

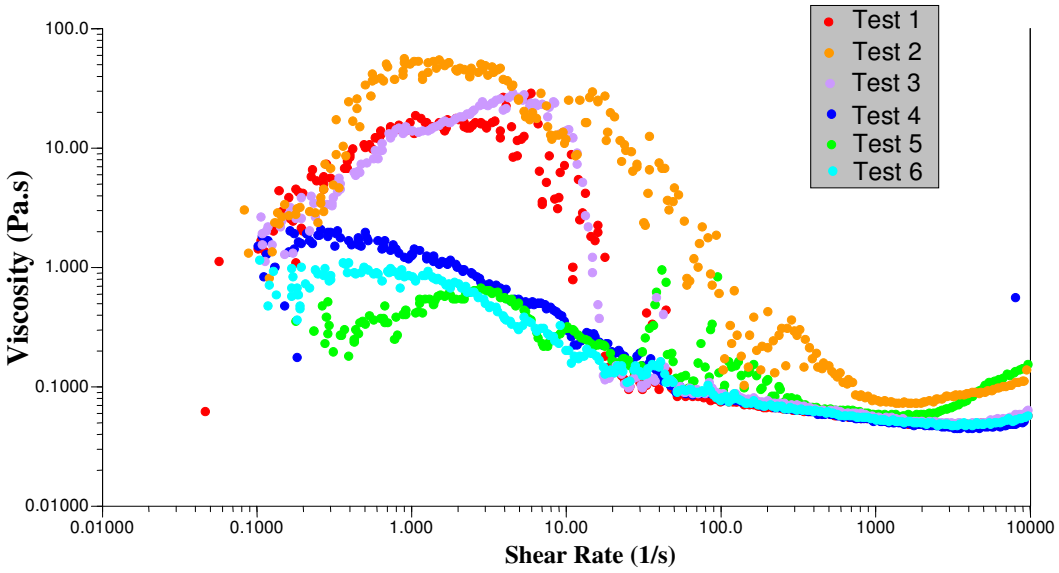

Figure 4.17- Viscosity versus shear rate of Carbilux using 20 mm flat plate geometry

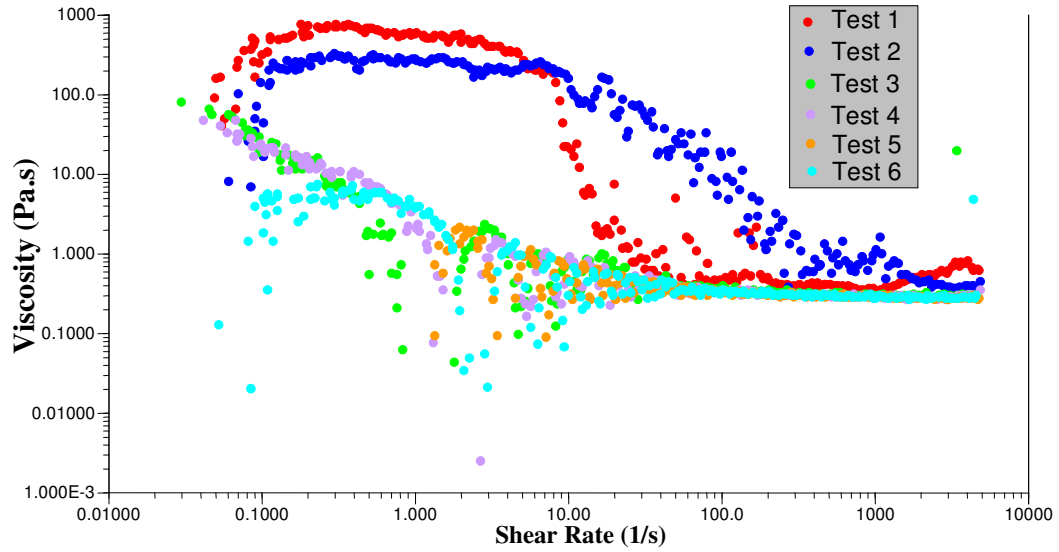

Figure 4.18- Viscosity versus shear rate of Carbilux using 10 mm flat plate geometry

It is difficult to tell from these tests if the oscillation phenomenon occurring is a result of the sample. Further investigation is required by using different rheometers to be certain that this is not the result of the rheometer used.

4.6 Drying Phenomena using ESEM

Figures 4.19 and 4.20 are SEM images of the Carbilux slurry taken under varying pressures thus varying the humidity of the same area at different magnifications. The initial wet sample in Figures 4.19(a) and 4.20(a) show poor contrast and particles are barely visible. This is due to there being no conductive coating of the submerged particles. The images in Figures 4.19(b) and 4.20(b) have become darker as the pressure has decreased and the sample is drying. At the low magnification it is difficult to see any changes in the sample during this drying process.

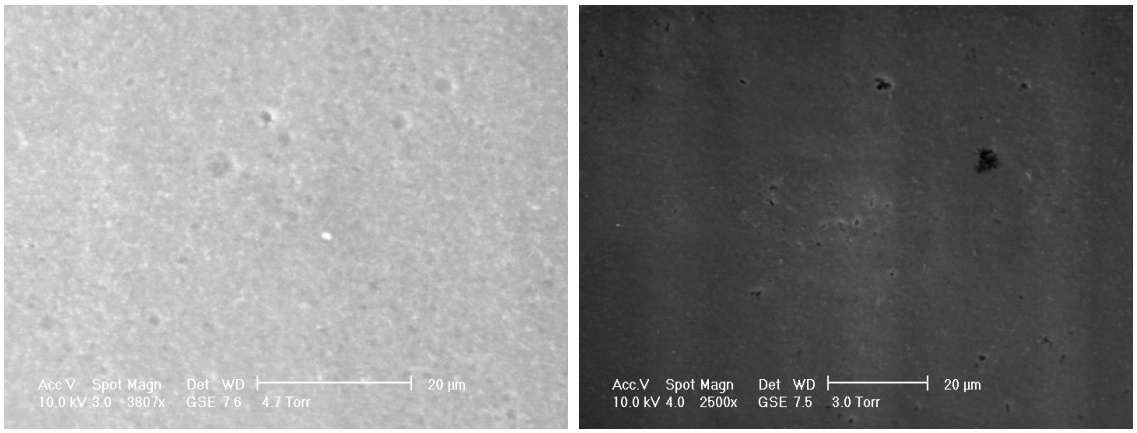

(a) **(b)**

Figure 4.19- ESEM Images of Carbilux at (a) 4.7 Torr and (b) 3 Torr at low magnifications

However, in Figure 4.20 the moving of the particles circled can be seen as drying occurs but there is no indication of particles coming together during this process and thus is difficult to observe the drying process using this technique.

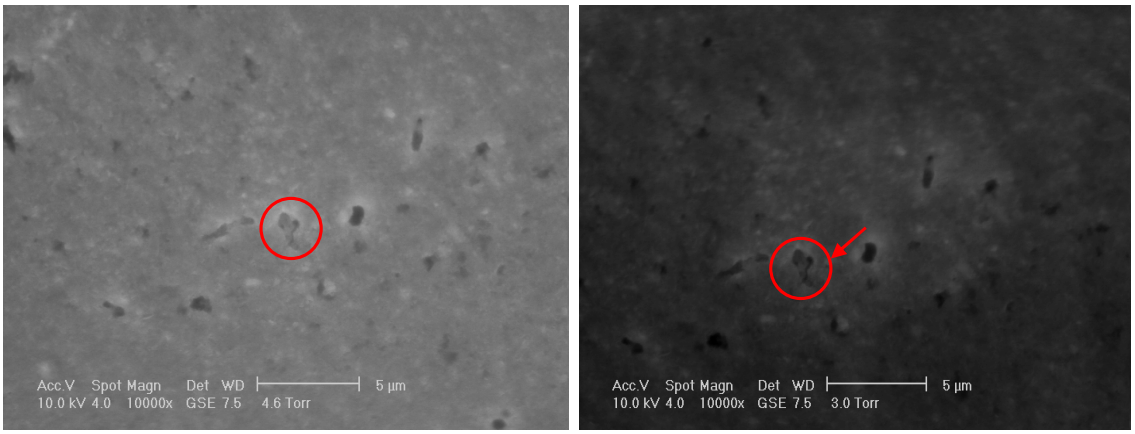

(a) **(b)**

Figure 4.20- ESEM Images of Carbilux at (a) 4.6 Torr and (b) 3 Torr at high magnifications

4.7 Powder Comparison from various Drying Techniques

Powders were obtained using various drying techniques on four different Carbilux samples. Two of the samples were unwashed, Carbilux-Unwashed and Carbilux-pH, where the pH was altered to 12, as the most stable zeta potential was previously found under this condition. The other two samples, Carbilux-Acetone and Carbilux-Washed, were prepared as stated in section 3.2.4.1. All four samples were oven dried, freeze dried and spray dried and are compared using various analytical techniques.

4.7.1 Particle Size Analysis

The particle size distributions of the powders obtained from the 4 samples using oven drying, freeze drying and spray drying were found using laser diffraction and the surface area by calculation from this data. These are presented in Table 4.5 and the particle size distributions are displayed accordingly in Figures 4.21-4.32 where the lines represent repeat tests.

Table 4.5- Particle size data of powders obtained from various drying techniques

		Specific surface area (m2/g)	d(0.1) (µm)	d(0.5) (µm)	d(0.9) (µm)
	CaCO3	14.200	0.195	0.585	1.625
OVEN DRY	Carbilux	0.304	20.750	123.496	302.590
	Carbilux-pH	0.535	12.724	111.722	291.398
	Carbilux-Acetone	2.105	0.750	52.743	202.687
	Carbilux-Washed	2.725	0.693	36.099	187.813
FREEZE DRY	Carbilux	1.130	2.338	10.327	47.987
	Carbilux-pH	0.831	3.203	16.224	84.452
	Carbilux-Acetone	0.297	20.648	97.877	268.738
	Carbilux-Washed	0.366	15.944	74.082	301.384
SPRAY DRY	Carbilux	2.545	0.953	4.065	9.441
	Carbilux-pH	2.510	1.024	3.878	8.592
	Carbilux-Acetone	3.735	0.640	2.984	7.070
	Carbilux-Washed	3.145	0.770	3.301	8.186

The surface area calculation conducted by the Mastersizer assumes the particles are solid with no pores and is based on the particle size distribution. These are later compared to the surfaces areas obtained by gas adsorption in section 4.7.3.

4.7.1.1 Oven Dried Samples

The particle size analyses of the oven dried samples are reflective of the sample preparation technique, as the dried sample cakes were passed through a 300 µm sieve. The average particle sizes are 123.5 µm, 111.7 µm, 52.7 µm and 36.1 µm from Figures 4.21-4.24 respectively. These sizes reflect the peaks shown in the Figures where the size distributions of Carbilux and Carbilux-pH show a large peak at around 150 µm with a small proportion of powder in the 1 µm region. In comparison, the size distributions of Carbilux-Acetone and Carbilux-Washed show an increased proportion of powder in the 1 µm region decreasing the average particle size. This increased proportion of fines suggests that under the relatively mild dispersion process of the particle size analyser, the particles are more weakly agglomerated once the organic dispersant in Carbilux has been removed through the wash cycles in Carbilux-Acetone and Carbilux-Washed.

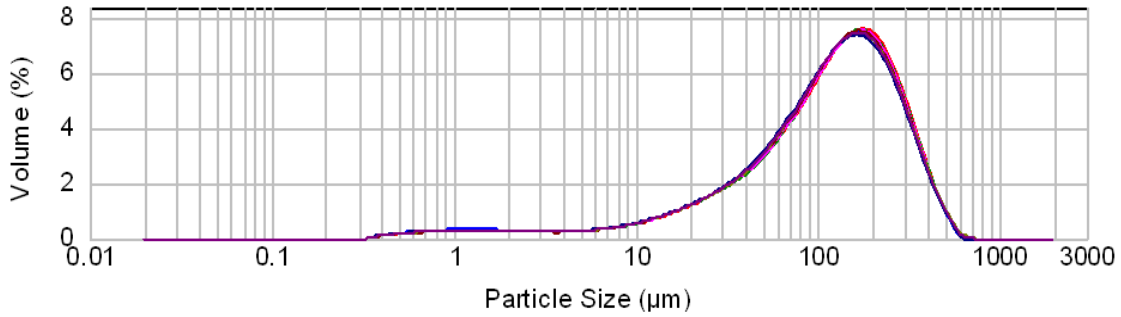

Figure 4.21- Particle size distribution of Carbilux oven dried at 130°C

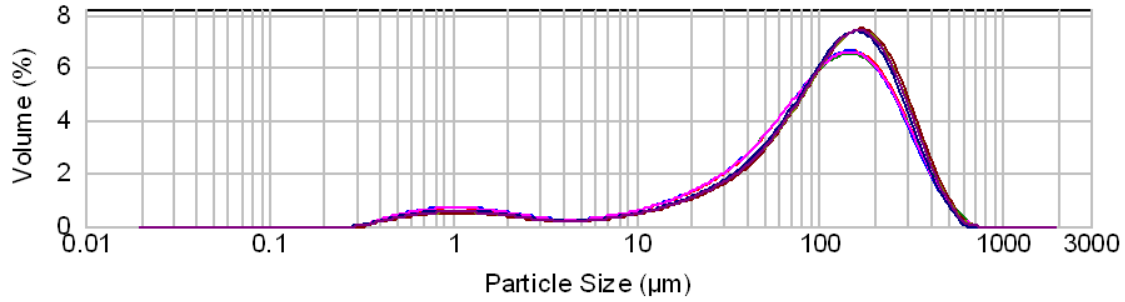

Figure 4.22- Particle size distribution of Carbilux-pH oven dried at 130°C

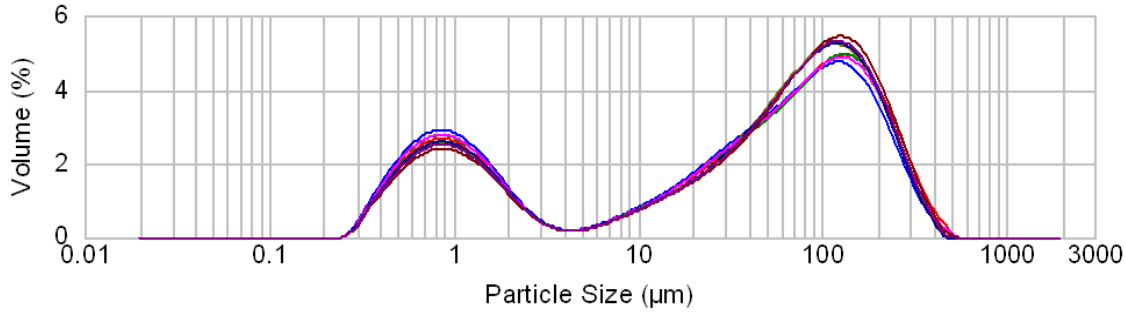

Figure 4.23- Particle size distribution of Carbilux-Acetone oven dried at 130°C

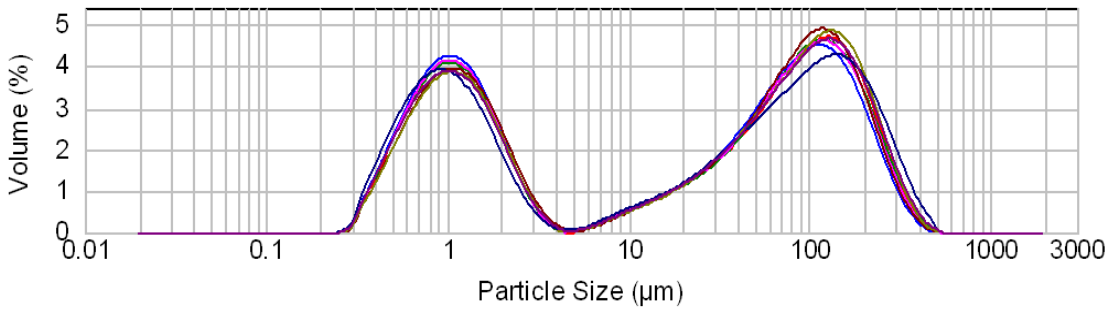

Figure 4.24- Particle size distribution of Carbilux-Washed oven dried at 130°C

4.7.1.2Freeze Dried Samples

The freeze dried samples all show a more uniform, broader size distribution. The Carbilux and Carbilux-pH samples also show similar size distributions in this drying technique with average particles sizes of 10.3 µm and 16.2 µm respectively. These are much lower than the Carbilux-Acetone and Carbilux-Washed samples where the particle size increases and the peaks are shifted to the right on the removal of the organic dispersant in Carbilux. The average particle sizes of these two samples are 97.9 µm and 74.1 µm respectively. A small volume percentage of fine particles can also be seen in Figures 4.25 and 4.26. These distributions suggest the removal of the organic dispersant in the wash cycles influences the freezing process by altering the water crystal form, thus changing the structure and producing larger particles after the sublimation process. This is further investigated using SEM.

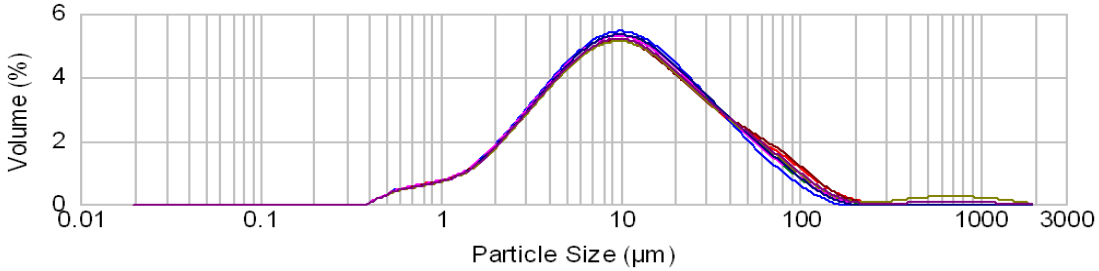

Figure 4.25- Particle size distribution of Carbilux freeze dried

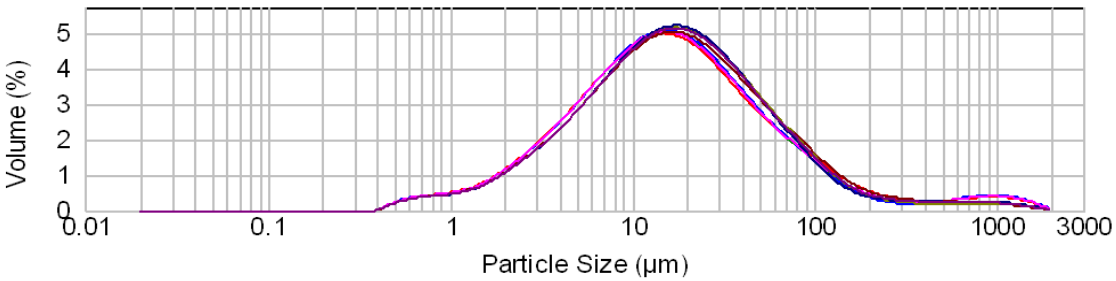

Figure 4.26- Particle size distribution of Carbilux-pH freeze dried

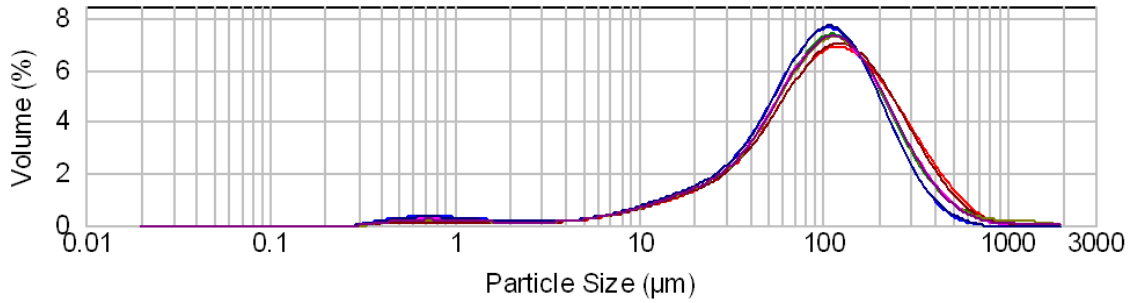

Figure 4.27- Particle size distribution of Carbilux-Acetone freeze dried

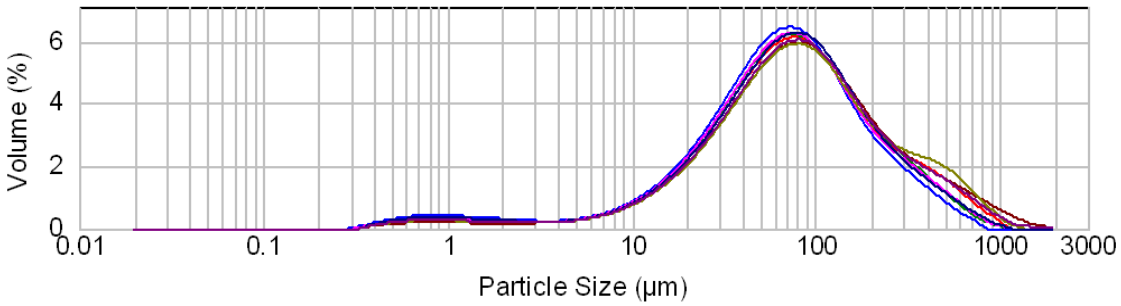

Figure 4.28- Particle size distribution of Carbilux-Washed freeze

4.7.1.3 Spray Dried Samples

The particle size distribution graphs of all the spray dried samples show similar distributions and the average particle sizes are 4.07 µm, 3.89 µm, 2.98 µm and 3.30 µm from Figures 4.29-4.32 respectively. This drying technique has produced particles of a smaller size than the freeze drying and oven drying which is reflective of the droplet drying process as spray drying is highly dependent on the size of the equipment. The volume percentage of fines increases from Figure 4.29-4.32, indicating weaker bonding between particles in the Carbilux-Acetone and Carbilux-Washed samples.

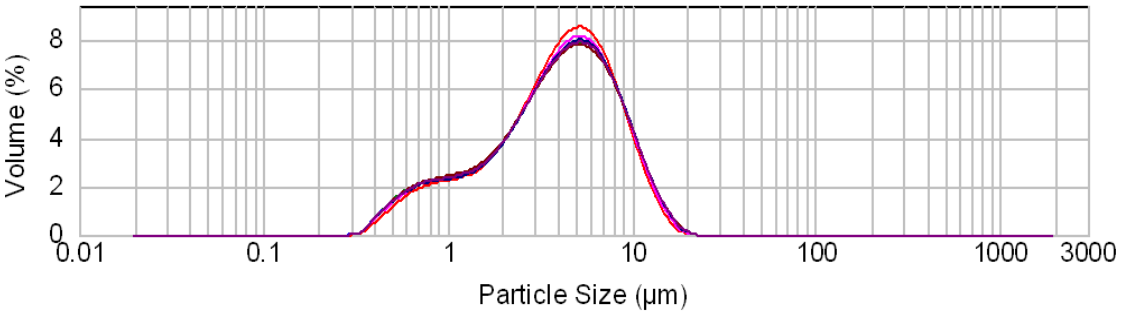

Figure 4.29- Particle size distribution of Carbilux spray dried

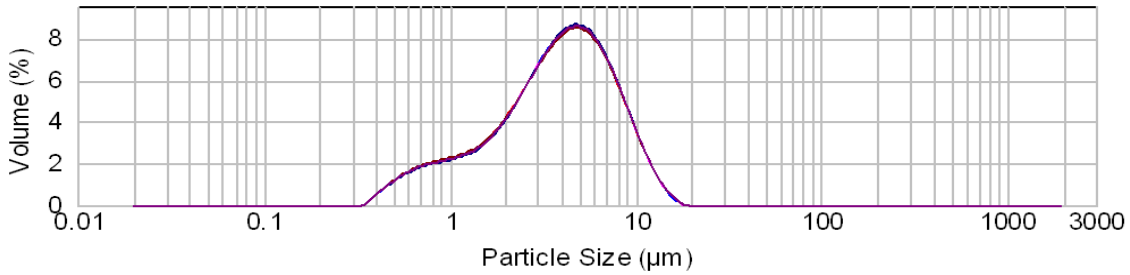

Figure 4.30- Particle size distribution of Carbilux-pH spray dried

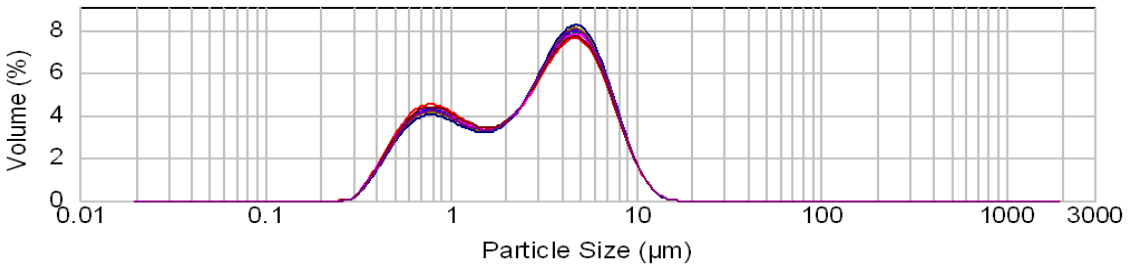

Figure 4.31- Particle size distribution of Carbilux-Acetone spray dried

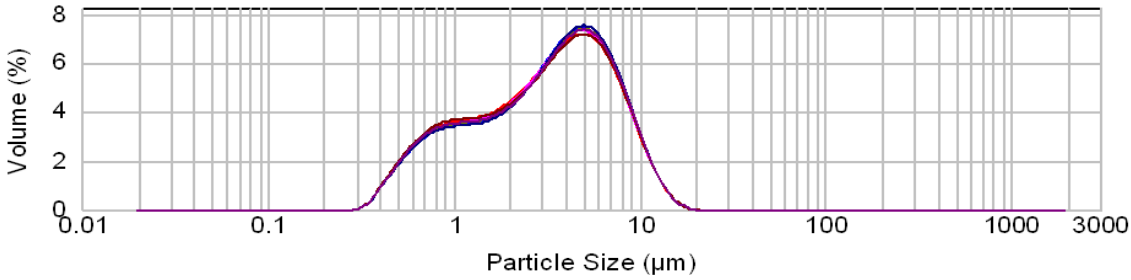

Figure 4.32- Particle size distribution of Carbilux-Washed spray dried

4.7.2 SEM Images

SEM images were taken of all the powders prepared to confirm the particle size distributions obtained and to see if the various drying techniques have affected the shape and structure of the particles formed. Images of each powder are taken at low and high magnifications.

4.7.2.1 Oven Dried Samples

The particles observed in Figure 4.33 for all 4 samples show a varied size distribution, particularly in images (c) and (d) where large clumps can be seen. This reflects the size distribution date presented in Figures 4.21-4.24.

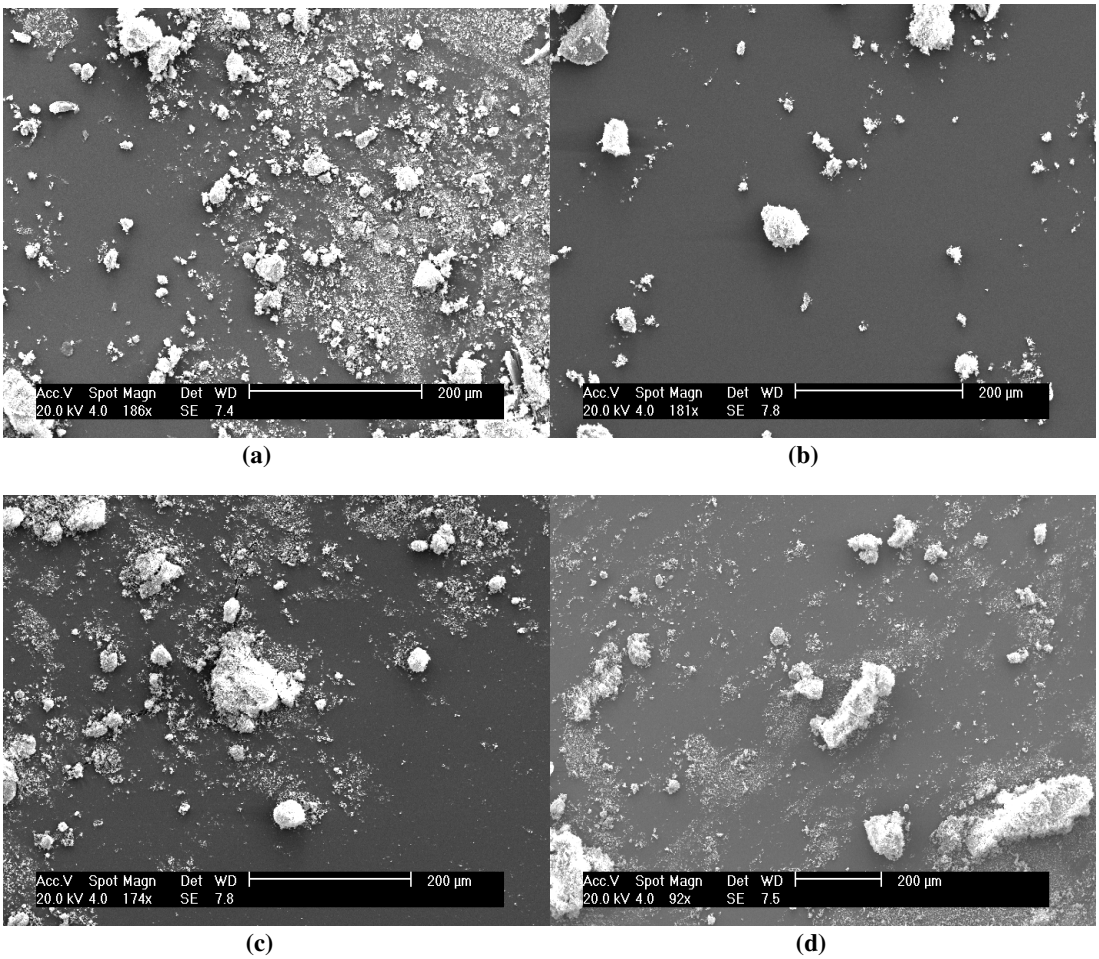

Figure 4.33- Low magnification SEM images of powder formed by oven drying of (a) Carbilux, (b) Carbilux-pH, (c) Carbilux-Acetone and (d) Carbilux-Washed

The fines observed in the size distributions of Carbilux-Acetone and Carbilux-Washed can be seen more clearly in Figures 4.34(c) and (d) where they are near the surfaces of the larger particles. In Figure 4.34 (a) and (b) the number of free fines are much less and seem to have formed stronger agglomerates. This supports the size distribution graphs of all four samples.

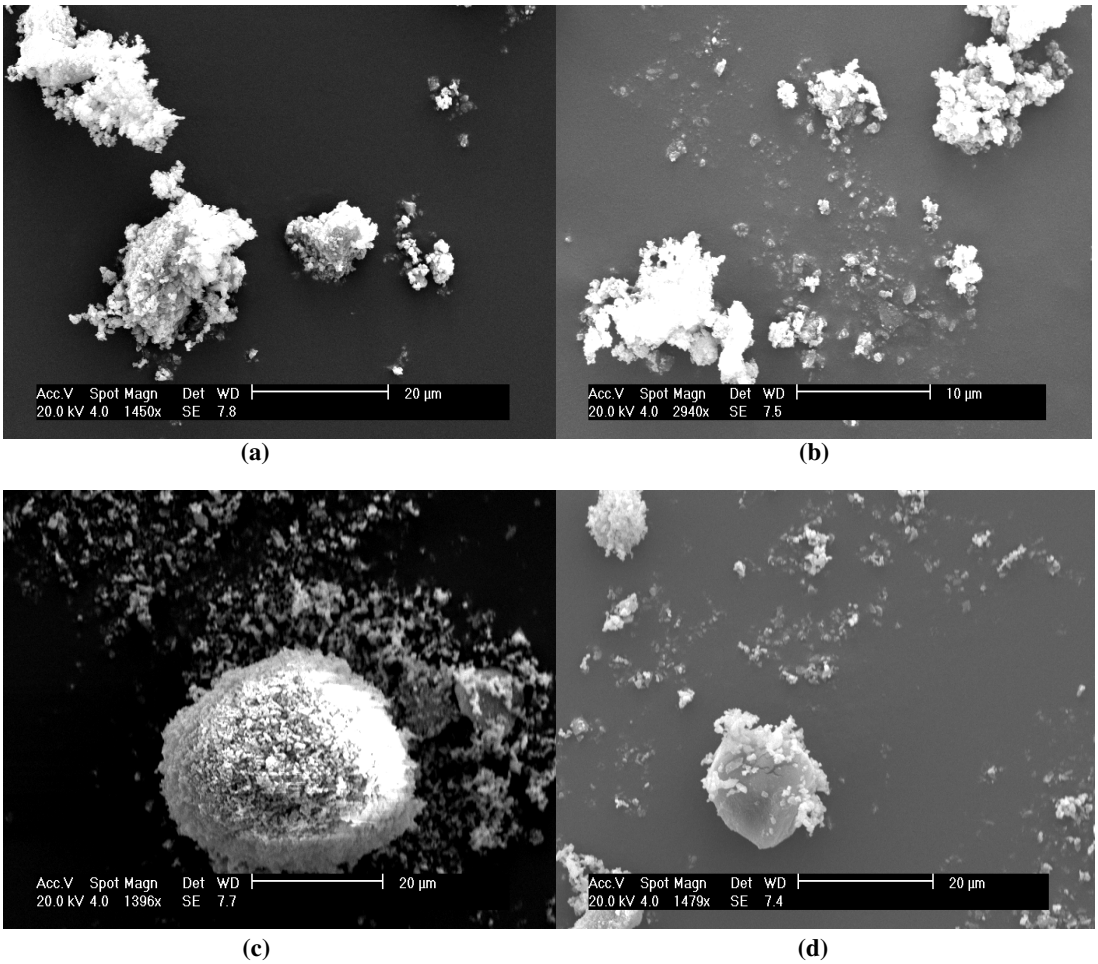

(a) **(b)**

(c) **(d)**

Figure 4.34- High magnification SEM images of powder formed by oven drying of (a) Carbilux, (b) Carbilux-pH, (c) Carbilux-Acetone and (d) Carbilux-Washed

The particle shape of oven dried Carbilux and Carbilux-pH are irregular compared to Carbilux-Acetone and Carbilux-Unwashed where they appear much rounder. This may be due to the weaker interactions with the fine particles in the later systems and suggests these are softer agglomerates.

4.7.2.2 Freeze Dried Samples

The particle size distributions of the freeze dried samples are also supported by the SEM images. Figures 4.35(a) and (b) show a finer particle size distribution in comparison to the other two samples. The Carbilux-Acetone and Carbilux-Washed samples, in (c) and (d) respectively, are much more angular, whereas the Carbilux and Carbilux-pH particles appear to be more needle like.

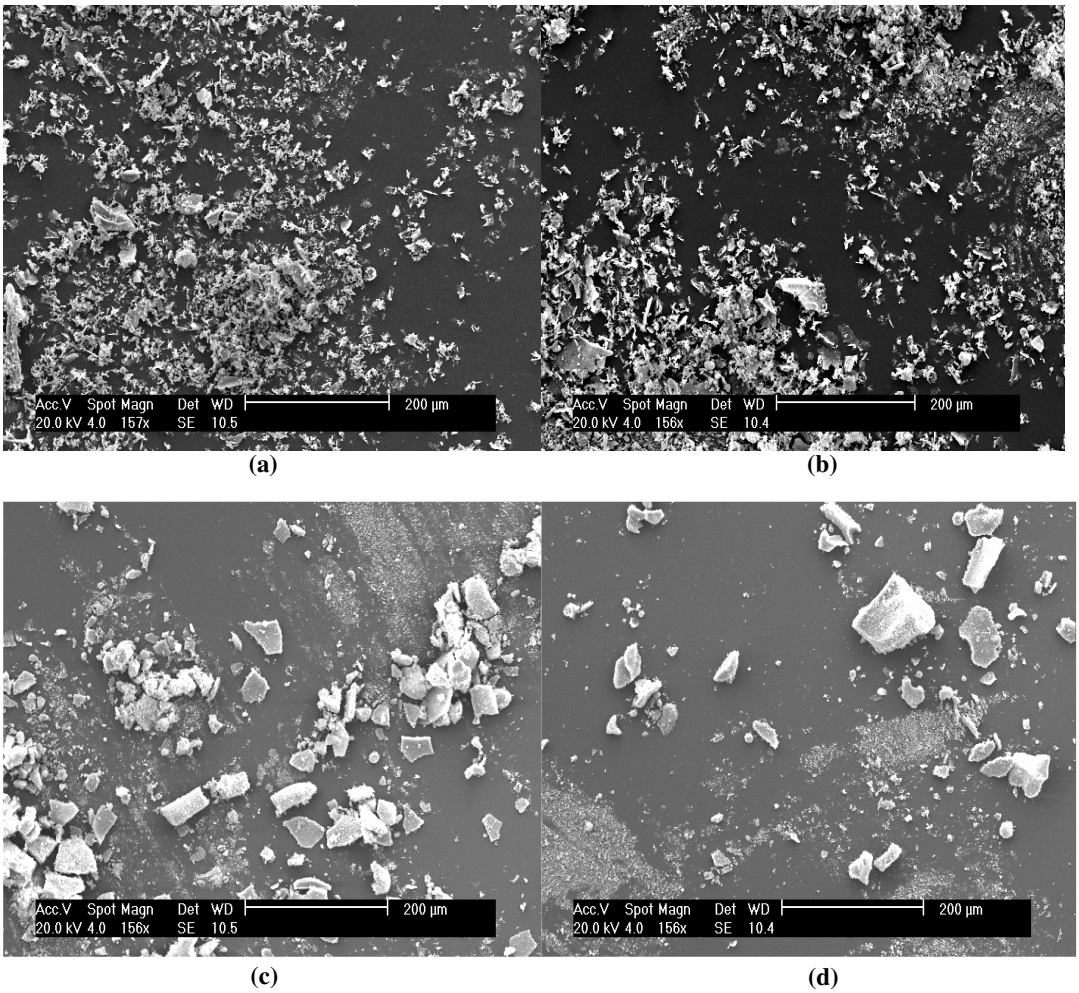

Figure 4.35- Low magnification SEM images of powder formed by freeze drying of (a) Carbilux, (b) Carbilux-pH, (c) Carbilux-Acetone and (d) Carbilux-Washed

The higher magnification SEM images in Figure 4.36 show how the fines have strongly bonded to the Carbilux-Acetone and Carbilux-Washed sample as indicated in the size distribution graphs. These images also suggest that the organic dispersant present in Carbilux and Carbilux-pH has formed larger crystals, forming porous structures after sublimation as can be seen in Figure 4.36(b). Figure 4.36(a) appears to show the

breakdown of such a porous structure suggesting these are weaker agglomerates thus the reducing the average particle size. The removal of this dispersant appears to have formed a more solid agglomerate in the freeze drying process.

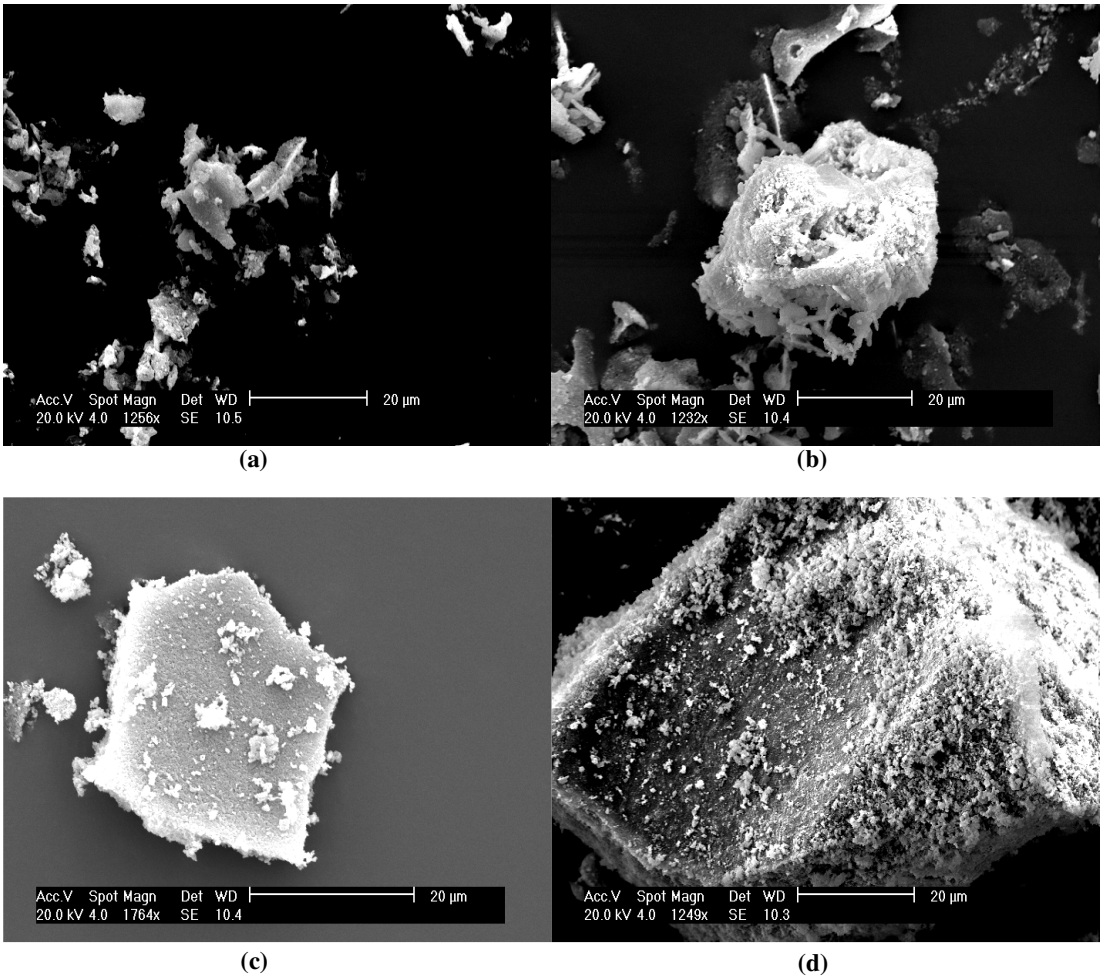

Figure 4.36- High magnification SEM images of powder formed by freeze drying of (a) Carbilux, (b) Carbilux-pH, (c) Carbilux-Acetone and (d) Carbilux-Washed

4.7.2.3 Spray Dried Samples

The low magnification SEM images in Figure 4.37 reflect the uniform size distributions obtained in Figures 4.29-4.32. It is clear that these samples are much finer than the powders obtained from oven drying and freeze drying.

The shape of the particles in all 4 samples is spherical, as shown in the higher magnification images in Figure 4.38, which is reflective of the spray drying technique.

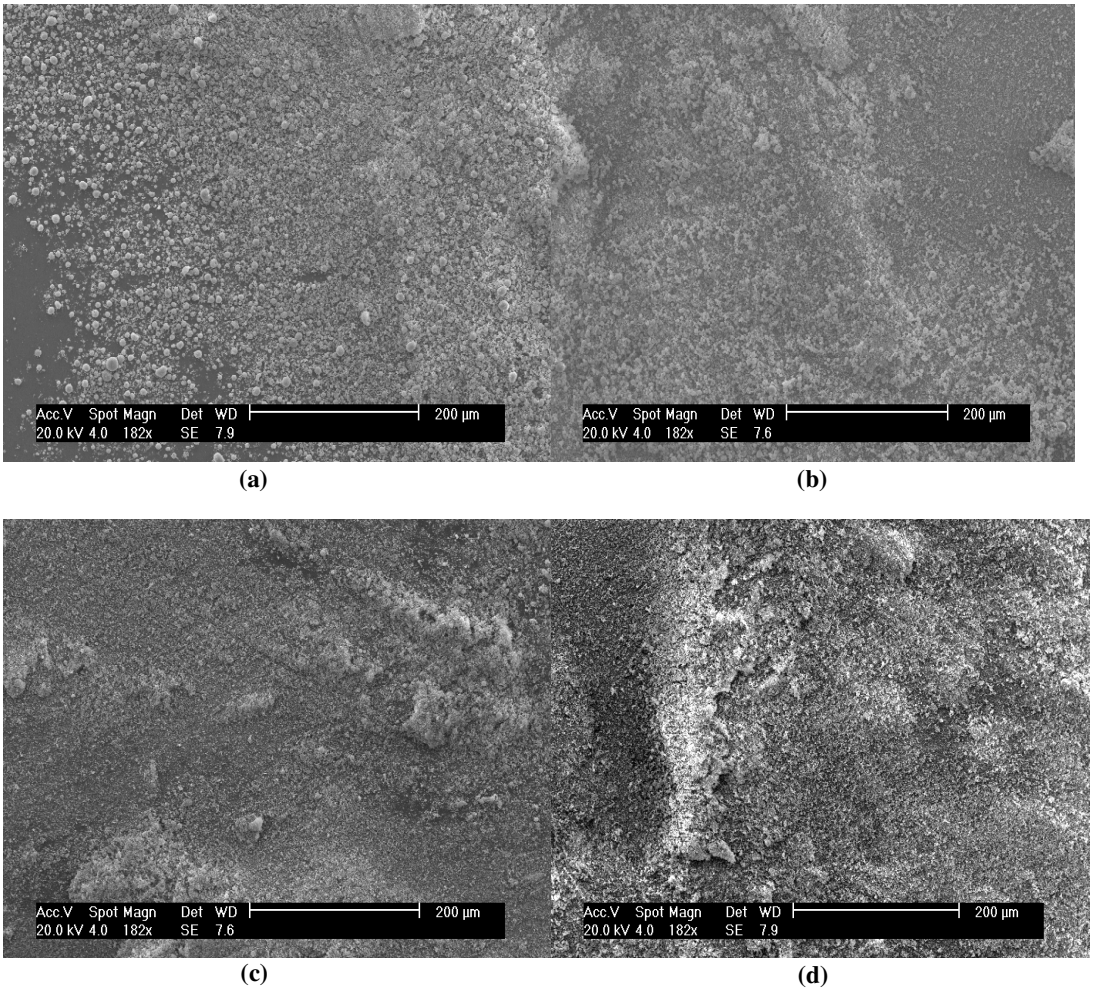

(a) **(b)**

(c) **(d)**

Figure 4.37- Low magnification SEM images of powder formed by spray drying of (a) Carbilux, (b) Carbilux-pH, (c) Carbilux-Acetone and (d) Carbilux-Washed

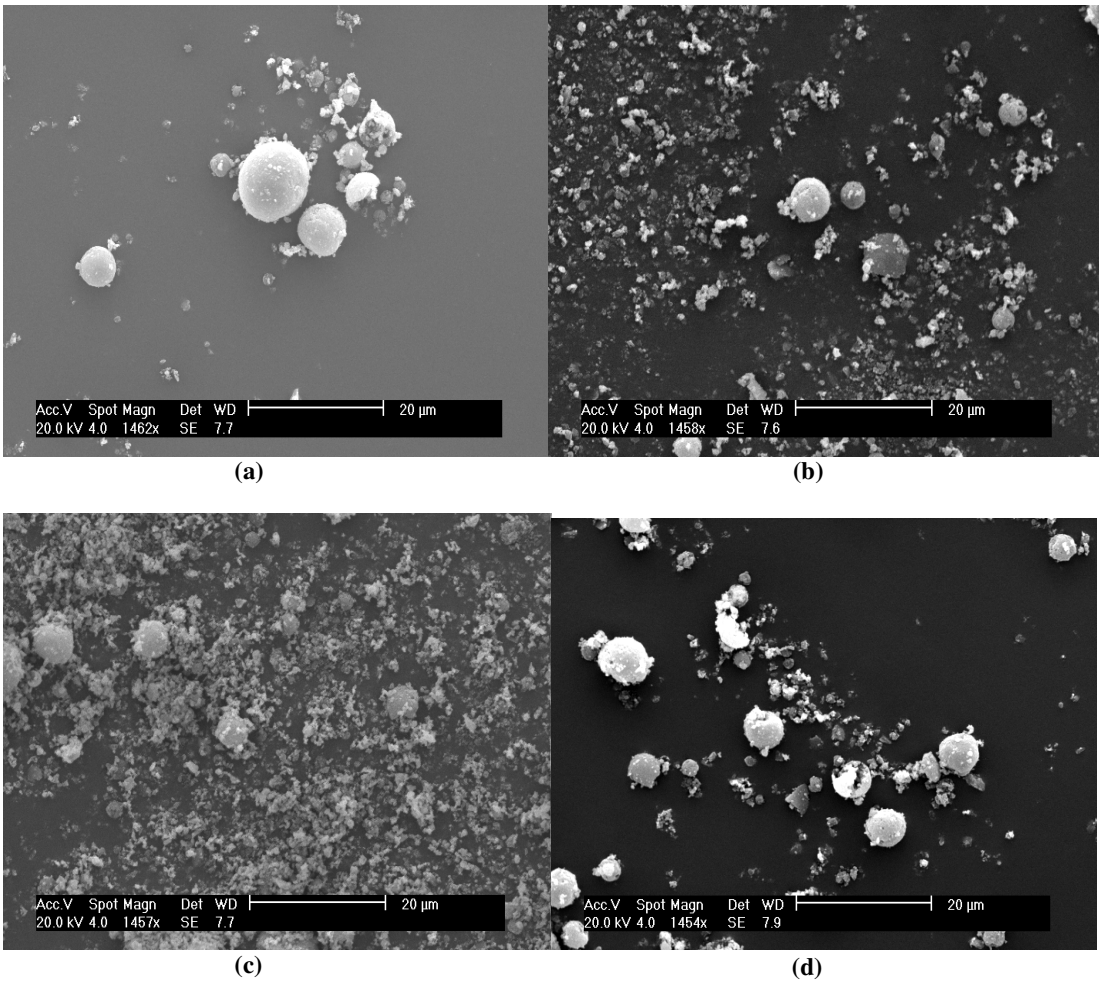

Figure 4.38- High magnification SEM images of powder formed by spray drying of (a) Carbilux, (b) Carbilux-pH, (c) Carbilux-Acetone and (d) Carbilux-Washed

4.7.3 Surface Area

The surface areas of the powders given in Table 4.5 were derived mathematically using the particle size distribution. In gas adsorption the surface areas of all primary particles, unless otherwise aggregated, are measured and are presented in Table 4.6. These results are not reflective of the size distribution of the agglomerates obtained for each powder, as in this method the gas permeates the open pores of the sample. As a result, the surface areas presented in Table 4.6 are significantly higher than those present in Table 4.5. The exception to this is the surface area calculated for the oven dried Carbilux.

Taking into consideration the BET surface area, the oven dried Carbilux has the highest surface area value of 15.5 m^2/g which is similar to the surface area calculated in the laser diffraction technique, given as 14.2 m^2/g, for the original, wet Carbilux sample. However, the average particle size has increased from 0.585 µm for the raw sample, to 123.5 µm, for the oven dried Carbilux, suggesting the particles have formed large, porous agglomerates. When agglomerates form, the area is reduced because the particles are touching or bridging, as is the case for the oven dried Carbilux-pH, Carbilux-Acetone and Carbilux-Washed samples. These samples all have similar surface areas, but the average particle size is much larger for Carbilux-pH, suggesting this sample is also more porous, whereas the other two have formed smaller, high density agglomerates.

Table 4.6- BET and Langmuir surface area of powders obtained from various drying techniques

Surface Area:		BET (m^2/g)		Langmuir (m^2/g)	
OVEN DRY	Carbilux	15.5457	±0.0582	21.5395	±0.5663
	Carbilux-pH	10.3776	±0.0921	14.3488	±0.2759
	Carbilux-Acetone	10.0373	±0.0766	13.8735	±0.2950
	Carbilux-Washed	10.5534	±0.0489	14.7473	±0.3947
FREEZE DRY	Carbilux	10.6163	±0.1999	14.6574	±0.1351
	Carbilux-pH	10.6634	±0.1262	14.5492	±0.2400
	Carbilux-Acetone	11.7864	±0.0929	16.3564	±0.3405
	Carbilux-Washed	10.6882	±0.0710	14.8819	±0.3472
SPRAY DRY	Carbilux	12.9947	±0.1143	18.0015	±0.3571
	Carbilux-pH	11.6669	±0.0945	16.1849	±0.3431
	Carbilux-Acetone	10.9026	±0.1139	15.0964	±0.2483
	Carbilux-Washed	10.3466	±0.0796	14.355	±0.2838

The freeze dried Carbilux-Acetone and Carbilux-Washed samples have a higher surface area and average particle size than the freeze dried Carbilux and Carbilux-pH samples. This suggests the latter two samples have formed smaller high density agglomerates as the surface area has reduced. The SEM images of these samples contradict these results as it shows these samples to be more porous than the washed samples. However, the increased surface area in the Carbilux-Acetone and Carbilux-Washed sample may be due to the high number of fine particles agglomerated to the larger particles, as shown in Figure 4.36(c) and (d), forming a rough surface and thus greater surface area than if the agglomerates had a smooth surface.

The spray dried samples all have similar size distributions and average particle sizes but the surface areas of Carbilux-Acetone and Carbilux-Washed samples are significantly lower than the surface areas of Carbilux and Carbilux-pH samples, suggesting they are more agglomerated in a high density form.

4.7.4 Zeta Potential Measurements

The zeta potential of the Carbilux sample before any drying was found to be -23.94 mV. Table 4.7 shows the zeta potential values obtained for the four samples after the three various drying techniques. From the oven dried samples Carbilux-pH and Carbilux-Washed appear to have slightly improved the stability of the redispersed suspension to -24.24 mV and -24.10 mV respectively, compared to the original sample. Carbilux and Carbilux-Acetone oven dried samples have a reduced zeta potential. The presence of the organic dispersant in the unwashed samples does not correlate to these results suggesting it has been removed in the drying process.

Table 4.7- Zeta potentials obtained of redispersed powders from various drying techniques

		Zeta Potential (mV)
OVEN DRY	Carbilux	-22.740
	Carbilux-pH	-24.238
	Carbilux-Acetone	-21.767
	Carbilux-Washed	-24.100
FREEZE DRY	Carbilux	-19.211
	Carbilux-pH	-17.977
	Carbilux-Acetone	-19.400
	Carbilux-Washed	-19.070
SPRAY DRY	Carbilux	-17.953
	Carbilux-pH	-20.257
	Carbilux-Acetone	-19.800
	Carbilux-Washed	-20.629

The freeze dried samples all have reduced zeta potentials with Carbilux-pH having the lowest value of -17.997 mV. The spray dried samples also have reduced zeta potentials, but in this case the Carbilux sample has the lowest zeta value of -17.953 mV.

As previously stated, the general rule for a stable system is a suspension with a zeta potential of +/-30 mV. From Table 4.7, it is apparent that the drying technique which produces the most stable samples is conventional oven drying followed by spray drying and finally freeze drying. This may have an impact on the rheological results of each sample as the more stable samples should produce a dispersed system with a lower viscosity.

4.7.5 Rheology

The rheological properties of all the samples were investigated using 40 mm flat plate geometry and shear rates in a continuous ramp step from 0-1000 1/s were applied. All samples were redispersed in distilled water to obtain the original weight percentage of 74.3 wt% (51.7 vol%) by solids. An inefficient mixing process was used for this to help determine which preparation and drying method worked best under these rheological conditions to give redispersible properties. Samples were taken at random from within the mixing pot and, as a consequence of this, the samples were not necessarily uniform as they sediment with time. It has been shown in section 4.5 that sedimentation influences the results and this, in conjunction with other sampling errors, may have been active here.

4.7.5.1 Oven Dried Samples

Carbilux and Carbilux-pH oven dried samples have a much larger average particle size compared to the other two oven dried samples. This is reflective in Figures 4.39 and 4.40 in which these two samples have a lower viscosity range compared to Figures 4.41 and 4.42, Carbilux-Acetone and Carbilux-Washed respectively. This could be due to the increased number of free fines in the Carbilux-Acetone and Carbilux-Washed samples. Generally increasing the fines content increases the viscosity as the number of particle-particle interaction increases and it also fills the voids in between the larger particles thus increasing the viscosity. It may also be the case that there are fewer but larger agglomerates in the former systems leading to a viscosity decrease.

The redispersed oven dried Carbilux sample in Figure 4.39 shows the occurrence of shear thickening before the sample shear thins and finally reaches a Newtonian plateau at high shear rates. This could be due to the larger particles locking together at the lower shear rates, creating some resistance to the flow or possibly some particle build up. As the shear

rate is increased, the rheometer acts as a mixer which breaks down the particles until the sample behaves in a similar manner to the original Carbilux slurry. The noise in the tests may be the result of the mixing process. The different tests clearly show that sedimentation is occurring in tests 3 and 4. This reduces the shear thickening and thinning regions and also the viscosity, but they all follow similar trend.

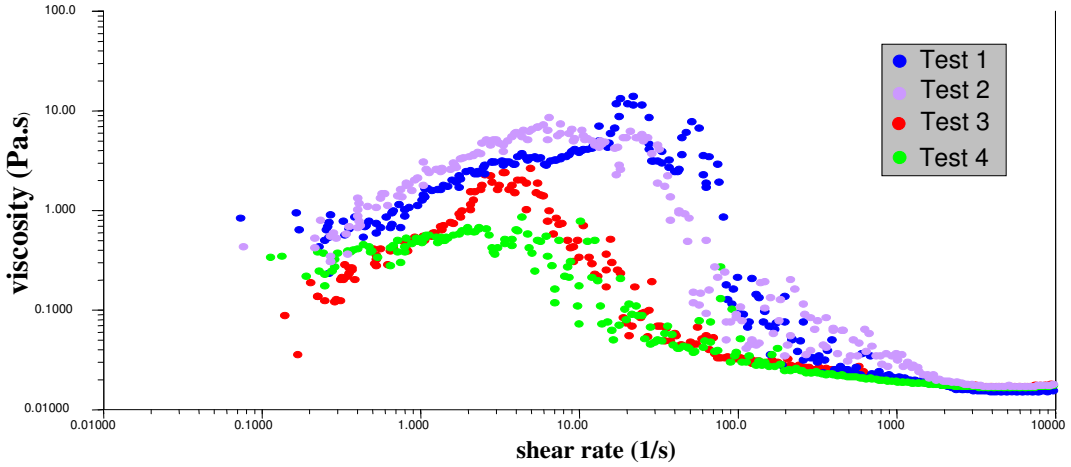

Figure 4.39- Viscosity versus shear rate of redispersed oven dried Carbilux

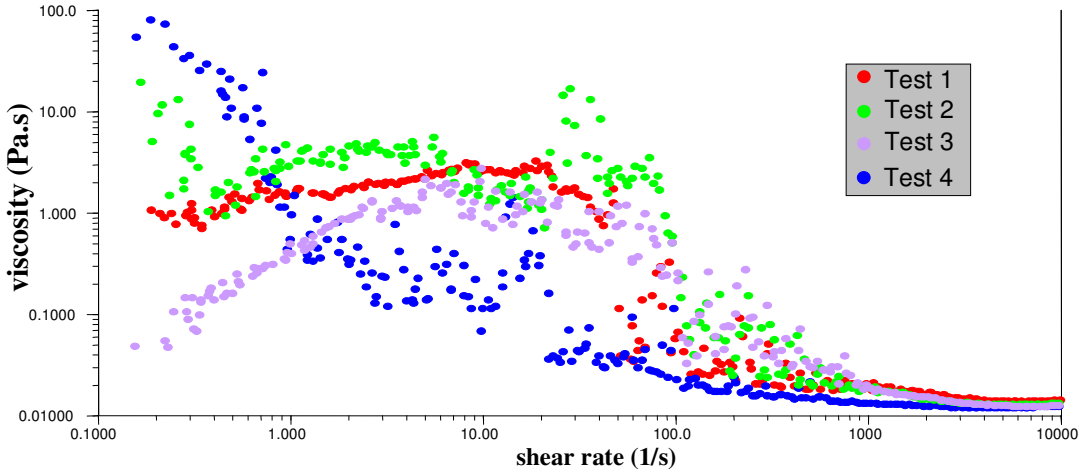

Figure 4.40- Viscosity versus shear rate of redispersed oven dried Carbilux-pH

Figure 4.40 shows the results of the Carbilux-pH sample. In this case there is evidence of shear thickening occurring at low shear rates and the same trend is observed as the Carbilux sample in the well mixed tests, 1-3. The sample probed in test 4, after sedimenting, shows shear thinning behaviour at low shear rates.

The Carbilux-Acetone and Carbilux-Washed samples in Figures 4.41 and 4.42 respectively can be directly compared to their size distribution graphs. The shear thickening behaviour in both cases has reduced in comparison to the Carbilux and Carbilux-pH samples. The severity of shear thickening if often alleviated by widening the particle size distribution and both of these samples have a broader size distribution in the dried form [64]. It is therefore been suggested that they are more dispersible.

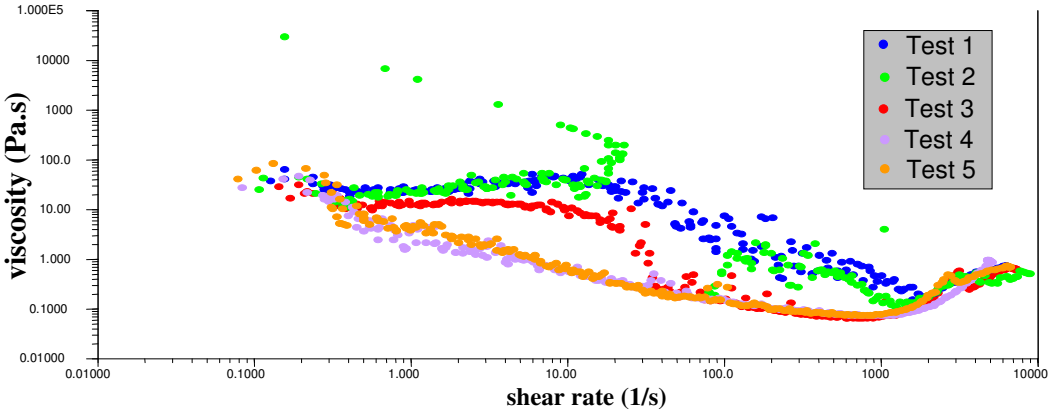

Figure 4.41- Viscosity versus shear rate of redispersed oven dried Carbilux-Acetone

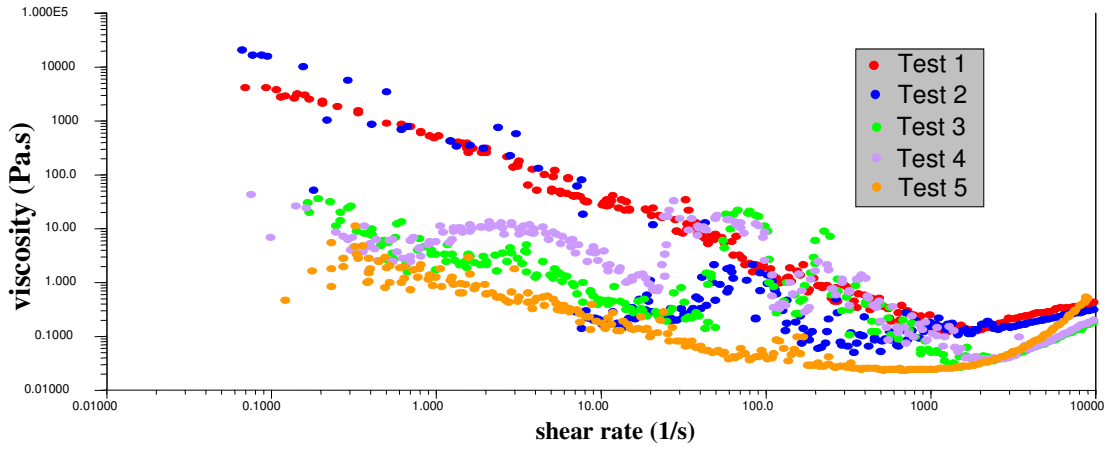

Figure 4.42- Viscosity versus shear rate of redispersed oven dried Carbilux-Washed

In both Figures 4.4.1 and 4.42, the viscosity decreases with each test as more agglomerated particles of the samples have sedimented in the mixing pot. The noise in both Figures has decreased, suggesting these samples are better dispersed as the rheometer mixes the

sample with increasing shear rates. However, in both cases shear thickening phenomena are observed at high shear rates, as also observed in earlier rheology tests, and may be due to the removal of the organic dispersant through the washing process and thus the destabilisation of the dispersion mechanisms of the original Carbilux sample.

4.7.5.2 Freeze Dried Samples

The freeze dried redispersed Carbilux sample in Figure 4.43 shows the same behaviour as the oven dried sample in Figure 4.39, but with increased viscosities. The average particle size of this sample is much smaller at 10.3 µm compared to 123.5 µm of the oven dried sample. The same volume fraction is used for these samples and so the decreased particle size of this sample means there are more particles present, and this may account for the increase in viscosity, as there are more particle-particle interactions occurring. This is also the case for the Carbilux-pH sample, although the trend has changed.

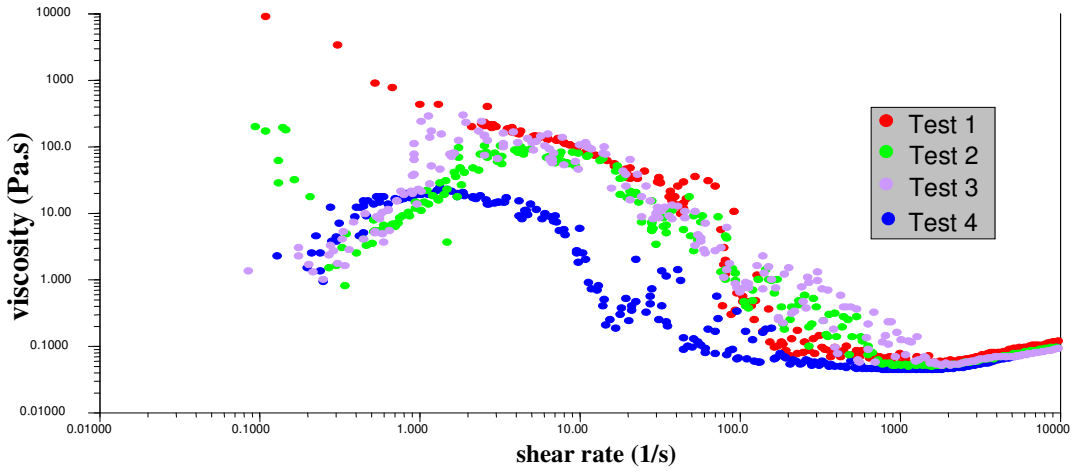

Figure 4.43- Viscosity versus shear rate of redispersed freeze dried Carbilux

Figure 4.44 shows there is a small Newtonian plateau followed by shear thinning and an upper Newtonian plateau at the higher shear rates. The graph also shows that between the shear rates of 1-5 1/s there are fewer results obtained. This was due to the sample drying out slightly before sufficient shear force was applied by the rheometer to obtain further readings. Although the viscosity has increased in this sample, the results obtained have very little noise suggesting a well dispersed relatively stable system.

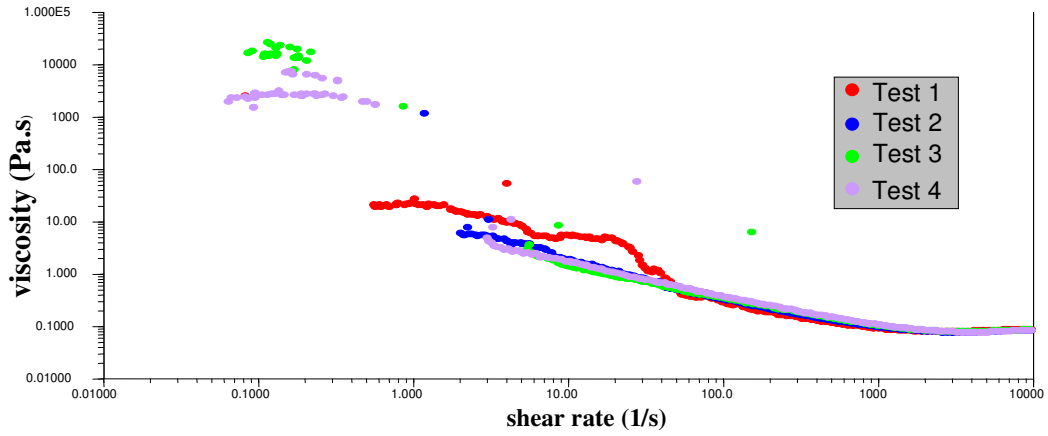

Figure 4.44- Viscosity versus shear rate of redispersed freeze dried Carbilux-pH

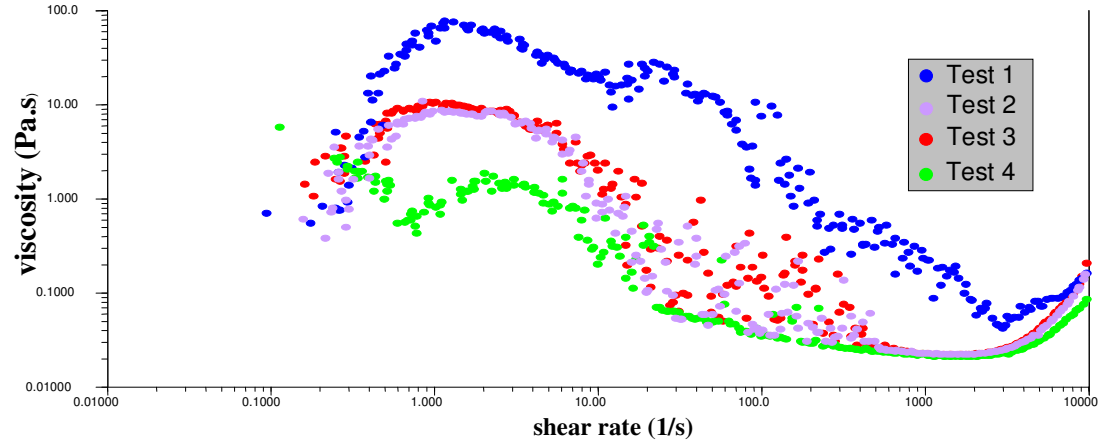

Figure 4.45- Viscosity versus shear rate of redispersed freeze dried Carbilux-Acetone

The same trend observed in Figure 4.43 occurs in the Carbilux-Acetone and Carbilux-Washed samples, but the viscosity has decreased. The oven dried Carbilux-Acetone and Carbilux-Washed samples had an increase in viscosity compared to these samples when freeze dried, indicating the removal of the organic dispersant has a different effect in this drying method. However, this decrease in viscosity may also be due to the particles in these samples having a much larger average particle size, due to agglomeration, thus the number of particle in the system has decreased reducing the effects of interparticulate interactions. There is less noise in Figure 4.45 than in Figure 4.46, suggesting the Carbilux-Acetone sample is better dispersed. Generally a better dispersion leads to a lower viscosity, but in the Carbilux-Washed sample there is indication the particles are relatively hard and coarse and thus not dispersing well, lowering the sample viscosity.

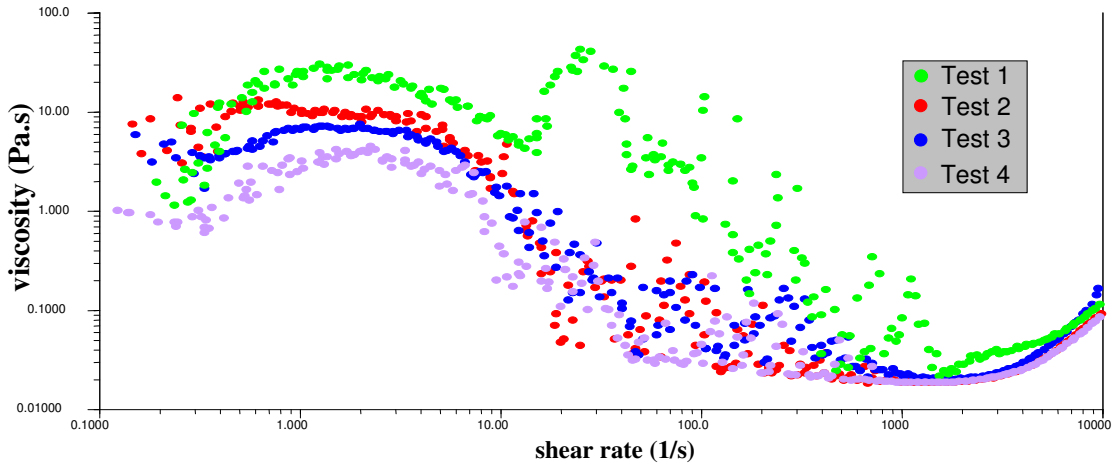

Figure 4.46- Viscosity versus shear rate of redispersed freeze dried Carbilux-Washed

4.7.5.3 Spray Dried Samples

The average particle sizes of the spray dried samples are 4.07 µm, 3.88 µm, 2.98 µm and 3.30 µm for Figures 4.47-4.50 respectively. The viscosities obtained in these samples are similar across all tests as a similar number of particles are present in each sample thus the magnitude of particle-particle interactions affecting the viscosity is approximately the same. The Carbilux and Carbilux-pH samples show a similar trend to the same samples obtained from the other drying techniques, but in these spray dried samples the noise has reduced suggesting they are better dispersed systems.

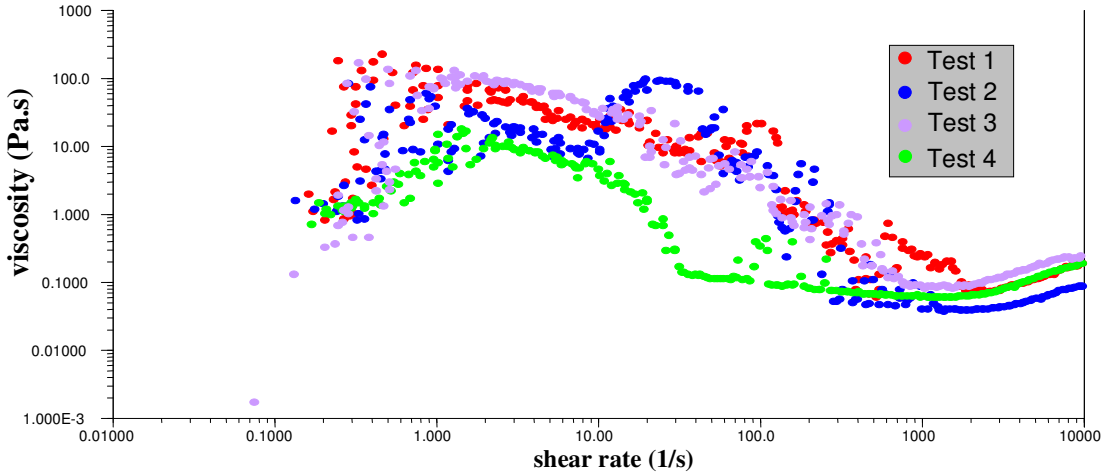

Figure 4.47- Viscosity versus shear rate of redispersed spray dried Carbilux

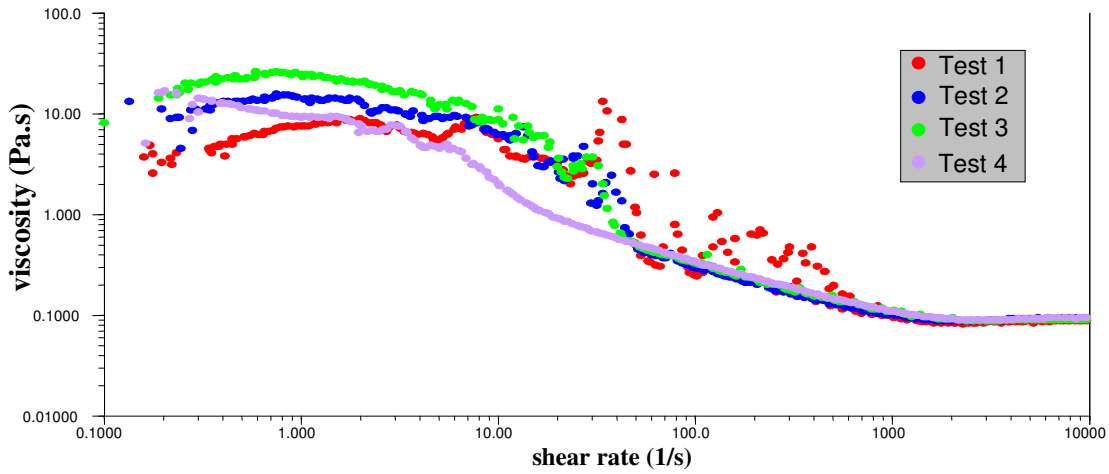

Figure 4.48- Viscosity versus shear rate of redispersed spray dried Carbilux-pH

The Carbilux-Acetone sample in Figure 4.49 also shows a similar trend for tests 1-3 which were well mixed. However, the upper Newtonian plateau region is small and the sample shows shear thickening behaviour almost immediately after the shear thinning region. This is also observed in the Carbilux-Washed sample and in the same samples which were freeze dried. The organic dispersant has been removed from all of these samples which further supports that the dispersant used by Imerys improves the stability of the system at higher shear rates. Test 4, after sedimentation, has a strong power law shear thinning region before shear thickening at the high shear rates, indicating the shear thickening behaviour is true for all solid loadings of this sample.

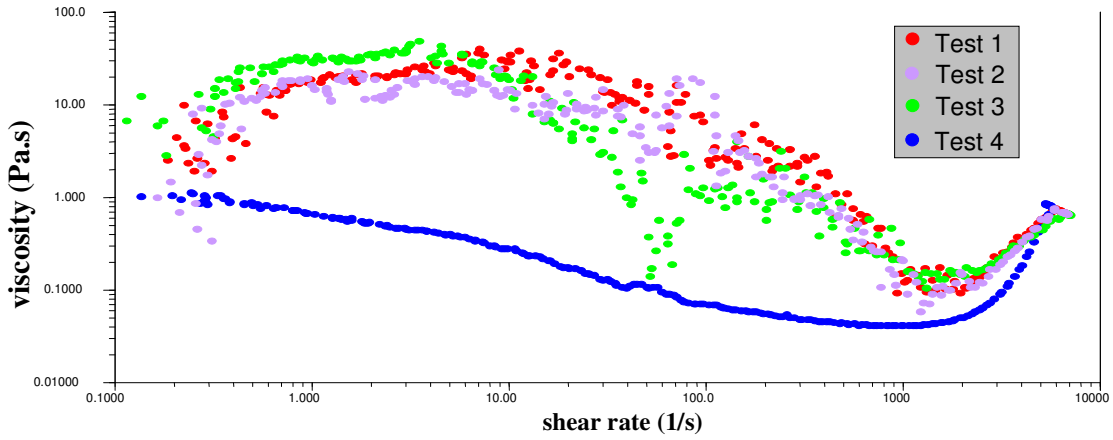

Figure 4.49- Viscosity versus shear rate of redispersed spray dried Carbilux-Acetone

Tests 1-3 of the Carbilux-Washed sample in Figure 4.50 were as mixed and show an increased level of noise compared to tests 4-6 in which finer particulates are present after

larger particles have sedimented in the mixing pot. This increased noise is also present in the freeze dried sample and further suggests the sample does not disperse well following the removal of the organic dispersant.

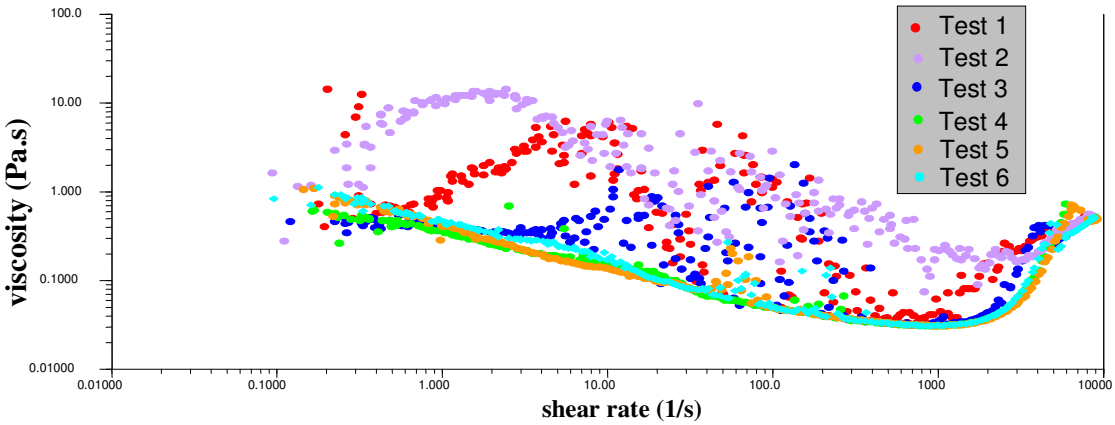

Figure 4.50- Viscosity versus shear rate of redispersed spray dried Carbilux-Washed

4.7.6 Agglomerate Strengths

The agglomerate strengths calculated from the Kawakita and Adams models and by the Knee compaction curve are present in Table 4.8. Only the freeze dried Carbilux sample results could be obtained from the freeze dried samples as these powders caused the die to stick providing unreliable results. This may be due to the needle like structure discussed in section 4.7.2.

The calcium carbonate agglomerate strength values obtained by Yap *et al.*, presented in Table 2.2, are shown as an indication of the magnitude of agglomerate strength. The Kawakita and Adams agglomerate strength found in the study of Yap *et al.* are 3.6 MPa and 3.0 MPa respectively. The magnitudes of the agglomerate strengths obtained in Table 4.8 are extremely large using the Kawakita model and small when using the Adams model. When obtaining these values, it was difficult to obtain the linear relationship stated by Kawakita, as the data from these compressive tests produced a curve on the Kawakita plot. This shows this model is not suitable for this data, contradictory to the findings of Yap *et al*. When applying the Adams model to the data, the linear region from which the parameters can be found is obtained. However, these strengths appear to be very small which may be the result of not applying a high enough load on the powders to produce the

pellets. The Knee compaction curve approach has provided realistic agglomerate strengths and is comparable to the particle size and shapes obtained in the particle size distributions and SEM images of the powders.

Table 4.8- Agglomerate strengths obtained using Kawakita, Adams and Knee Compaction Curve Methods

		Kawakita- 1/b (MPa)	Adams- τ (MPa)	Knee Compaction (MPa)
OVEN DRY	Carbilux	1552.38	0.00185	5.56
	Carbilux-pH	602.69	0.00269	3.73
	Carbilux-Acetone	289.61	0.00154	2.72
	Carbilux-Washed	163.62	0.00135	2.38
FREEZE DRY	Carbilux	62.64	0.01637	5.50
	Carbilux-pH	-	-	-
	Carbilux-Acetone	-	-	-
	Carbilux-Washed	-	-	-
SPRAY DRY	Carbilux	273.38	0.00177	5.59
	Carbilux-pH	771.29	0.00174	3.90
	Carbilux-Acetone	917.63	0.00151	3.60
	Carbilux-Washed	304.20	0.00128	2.26

The particle size distributions of the oven dried samples showed the Carbilux-Acetone and Carbilux-Washed sample contained more fines, suggesting weaker bonds between particles. From Table 4.5, the agglomerate strengths obtained using the Knee compaction curve approach are much weaker for these two samples compared to Carbilux and Carbilux-pH. The free fines in the spray dried powders increased from Carbilux to Carbilux-pH to Carbilux-Acetone and finally Carbilux-Washed. The agglomerate strengths obtained are again reflective of the samples that contain the most free fines having weaker bonds, thus weaker agglomerate strengths.

When comparing the effect of different particle shapes of the samples across the three drying techniques, it is expected that the spray dried powders would have better packing than the oven dried powders as the particles are more spherical, followed by the freeze dried powders which are quite angular. Although only the Carbilux sample can be compared, it is clear that the agglomerate strength is the weakest for the freeze dried sample.

These results show that the agglomerates are generally weaker in samples of a wider particle size distribution and that the shape of the particles can also affect the agglomerate strength. The removal of the organic dispersant in the original Carbilux slurry also has an effect on the agglomerate strength as the dispersant tends to cause the particles to bond strongly through the drying process.

5 Conclusion

The primary aim of this research was to produce dried powder from a Carbilux suspension which was redispersible after drying. To investigate this, the colloidal chemistry of the original Carbilux slurry was adjusted through various additions of dispersants and washing processes to produce feeds for a variety of drying methods. The resultant powders were tested for redispersibility.

The effect of changing the pH on the zeta potential was investigated where the equilibrium pH was found to be 9.5. The iso-electric point could not be found as all zeta potentials were negative, which is characteristic of natural calcites. It was found that Carbilux has a greater colloidal stability at a pH greater than 10, which is impractical for storage and transport as it requires more safety measures to be taken.

Various dispersants were added to Carbilux where the addition of Dispex A40, a dispersant similar to the organic dispersant added by Imerys, improved the zeta potential from -23.94 mV to -27.31 mV, stabilising the colloidal system further. In a shear stress controlled rheology test, the apparent viscosity of this sample increased, which is a known phenomenon when too much dispersant is added. The addition of Glycerol did not improve the zeta potential but lubricated the system, thus reducing the apparent viscosity from 0.061 Pa.s to 0.016 Pa.s.

Shear stress controlled rheology tests on Carbilux showed shear thinning typical of a polymer stabilised colloidal suspension. Using various geometries the sample was shown to be a concentrated stable suspension with a lower Newtonian plateau at low shear rates, followed by a power law shear thinning region which levelled off to an upper Newtonian plateau at high shear rates. An oscillation phenomena was also observed, but it could not be determined if this was characteristic of Carbilux.

To investigate various drying techniques, four Carbilux samples were prepared. Two of the samples were washed to investigate the removal of the dispersant already present, one of which was rinsed with acetone to reduce the surface tension during drying. The pH was changed to 12 for one of the unwashed samples and the other remained in the form

provided by Imerys. Powders were obtained from these samples using conventional oven drying, freeze drying and spray drying.

The samples produced from these drying processes were all of different morphology. The oven dried samples were generally coarser, reflective of the sample preparation technique as the dry cake was passed through a 300 μm sieve. The particle size distributions of the oven dried samples, in which the dispersant was removed, were broader with an increased number of fines as the powders following drying are more easily broken down by the sieving process indication weaker agglomeration. The freeze dried samples were generally finer in agglomerate size, but the opposite trend was observed for the washed samples as the powders were coarser, reflecting the influence of organic dispersant in the freeze dry process. The spray drier produced powders of uniform size, reflecting the atomisation process. A slight increase in the number of fines was also observed on the removal of the dispersant. It would therefore appear that the method of drying, in combination with the conditioning of the feed slurry, influences the morphology and dispersibility of the calcite.

From the BET surface area analysis of these powders it can generally be concluded that although the agglomerate sizes are different, the primary particles are loosely connected together in each system, as the surface area is only slightly reduced by the agglomeration process.

The removal of the organic dispersant resulted in a less negative zeta potential and therefore a less stable system on redispersion. Rheological evidence of these samples showed a shear thickening behaviour of the system in the high shear rate region, indicating the organic dispersant improved the stability in this region and thus the redispersibility properties.

The rheological traces of the washed samples were less noisy in the oven dried samples as the powders dispersed better. However, the removal of the dispersing aid increased the viscosity in the oven dried and spray dried samples. The relationship is complex as it would be expected better dispersed systems lead to a reduced viscosity but the washing process removed much of the colloidal stability. The washed freeze dried samples followed this behaviour.

All rheology results obtained showed a strong correlation between the particle size distributions and rheological properties. The redispersed systems all had the same volume fraction of powder and so when the average particle size is smaller the number of particles in the system increased. This led to an increase in particle-particle interactions, thus increasing the viscosity of the sample.

The agglomerate strength test suggests the removal of the organic dispersant weakened the agglomerates as the organic dispersant acts as a binder. The particle size distribution analysis also supports this to some extent but the rheological evidence tends to be less conclusive as different aspects of particle agglomeration and colloidal stability are competing. Where the feed to be dried contains the organic dispersant, then remnants of this remain in the dried product causing the formed agglomerate to be harder. However, when placed in water, the remnant organic can act as a dispersing aid countering the adverse drying result. On the other hand, where the calcite has been washed to remove the organic dispersant and also had the surface tension lowered to improve drying, the agglomerates formed are weaker, but the redispersed suspension has no mechanism to create a stable suspension and so the viscosity may rise.

6 Future Work

To further investigate the complex properties and relationships in this research it would be beneficial to work closely with a fresh clean bulk sample of pure rhombohedral calcite. This could be ground to the desired particle size distribution, in this case 0.3-4 µm, to represent the Carbilux sample.

Various dispersants and surfactants can be added to this fresh sample to gain better control of the system by finding the optimum volume percentage by solids. Although the amount of dispersant added to Carbilux by Imerys has been optimised to meet customer requirements in its multiple uses, it may not necessarily be the recommended amount to improve its redispersible rheological properties.

The oscillation phenomena in the rheology results obtained in this research require further investigation to determine if this is caused by an error of the sampling or rheological equipment, or if it is a characteristic of natural calcite.

The rheological tests also showed clear evidence of interparticulate interactions. It would be beneficial to investigate the forces between the calcite particles on such a small scale by using more recently developed techniques such as atomic force microscopy (AFM).

Further agglomerate strength tests would be beneficial to validate the findings of the results in this research. The Kawakita and Adams model were not the best fit for the data obtained from these tests and so the investigation of other models is recommended. It would also be advised to correlate the agglomerate strength tests to a crushing test, such as the Brazilian test described in section 2.3.6, to further validate the agglomerate strengths found.

Environmental scanning electron microscopy (ESEM) could be useful in understanding the drying process, but in this research the samples were too saturated and so it is recommended to use samples with reduced solid loadings.

References

[1] Palchik, N.A. (2005). *Polymorph modifications of calcium carbonate in gallstones.* Journal of crystal growth. **283**. 450-456

[2] Eriksson, R., Meta, J., Rosenholm, J.B. (2008). *The calcite/water interface II. Effect of added lattice ions on the charge properties and adsorption of sodium polyacrylate*. Journal of colloid and Interface science. **326**. 396-402

[3] Imerys Minerals. *Calcium carbonate.* Available: http://www.imerys-perfmins.com/calcium-carbonate/eu/calcium-carbonate.htm. Last accessed 28 March 2009.

[4] Eriksson, R., Meta, J., Rosenholm, J.B. (2007). *The calcite/water interface I. Surface charge in indifferent electrolyte media and the influence of low-molecular-weight polyelectrolyte*. Journal of colloid and Interface science. **313**. 184-193

[5] Sayan, P. (2005). *Effect of sodium oleate on the agglomeration of calcium carbonate*. Cryst. Res, Technol. **40**, No. 3, p226-232

[6] Tegthoff, F.W., Rohleder, J., Kroker, E. (2001). *Calcium carbonate: from the cretaceous period into the 21st century*. Birkhäuser

[7] Imerys Minerals. *Carbilux.* Available: http://www.imerys-perfmins.com/eu/ProductDetail.asp?PID=12. Last accessed 28 March 2009.

[8] Encyclopaedia Britannica. (2009). *Calcite*. (2009). Available: http://www.britannica.com/EBchecked/topic/88899/calcite. Last accessed 12 April 2008

[9] Adams, M. (2008). *Colliods and Rheology lecture notes*. Chemical Engineering: The University of Birmingham

[10] Malvern. (2009). *Stabilised Colloidal System Image*. Available: http://www.malvern.de/LabGer/industry/colloids/Stabilized_colloid_system.gif. Last accessed 20 May 2009

[11] Danforth, S.C. *Powder Selection*. Ceramic Powder Processing. Department of Ceramics, Rutgers-The State University of New Jersey. **Vol. 3**

[12] Shaw, D. J. (1992). *Introduction to Colloid & Surface Chemistry*. Elsevier Science Ltd. 4th ed. 174-199

[13] Hermans, J.J. (1953). *Flow Properties of Disperse Systems*. Amsterdam: North-Holland Publishing Company. 133-143.

[14] Perrins, J. (1916). *Atoms*. Constable and Company Ltd. 4th ed. 120

[15] Chalmers, A. (2008). *Atomism from the 17th to the 20th Century*. The Stanford Encyclopedia of Philosophy. Available: http://plato.stanford.edu/archives/fall2008/entries/atomism-modern/. Last accessed 18 July 2008

[16] Sonntag, H., Strenge, K. (1969). *Coagulation and Stability of Disperse Systems*. John Wiley & Sons. 22

[17] Zeta Meter. (2008). *Zeta Potential*. Available: http://www.zeta-meter.com/5min.pdf. Last accessed 9 January 2009

[18] Takeo, M. (1999). *Disperse Systems*. Wiley. 203-213

[19] Derjaguin, B., Landau, L. (1941). *Theory of the stability of strongly charged lyophobic sols and of the adhesion of strongly charged particles in solutions of electrolytes*. Acta Physico chemica URSS. **14**, 633

[20] Verwey, E.J.W., Overbeek J.Th.G, (1948). *Theory of the stability of lyophobic colloids*. Amsterdam: Elsevier

[21] Malvern. (2008). *Zeta Potential: An Introduction in 30 minutes*. Available: http://www.malvern.co.uk. Last accessed 9 January 2009

[22] Malvern. (2008). Colloid Stabilisation. Available: http://www.malvern.com/LabEng/industry/colloids/Stabilization.gif. Last accessed 18 May 2009

[23] Moulin, P., Roques, H. (2003). *Zeta potential measurement of calcium carbonate*. Journal of Colloid and Interface Science. **261**. 115-126

[24] Vdović, N. (2001). *Electrokinetic behaviour of calcite-the relationship with other calcite properties*. Chemical Geology. **177**. 241-248

[25] Smani, M.S., Blazy, P., Cases, J.M. (1975). Trans. Soc. Mining ASCE. **258**. 168

[26] Somasundaran. P., Agar, G.E. (1967). *The zero point of charge of calcite*. Colloid Interface Science. **24**. 433-440

[27] Whorlow, R.W. (1992). *Rheological Techniques*. Ellis Horwood, 2nd ed. 1

[28] Cogswell, F.N. (1981). *Polymer Melt Rheology*. John Wiley & Sons. 6

[29] Wilson, H. J. (2004). *The effect of Different Particle Contacts on Suspension Rheology*. Department of Applied Mathematics, University of Leeds

[30] Dalwadi, D.H. (2006). *A Normal-Force Sensor for Quantitative Normal Stress Measurements*. American Laboratory

[31] Pacific Northwest National Laboratory. (2008). *Flow Behaviour image*. Available: http://www.technet.pnl.gov/sensors/macro/projects/images/macro81lg.gif. Last accessed 5 May 2009

[32] Dorf, R.C. (2005). *The engineering handbook*. CRC Press. 2nd ed. Chapter 37

[33] Cunningham, N. (2009). *Making use of Models: The Cross Model*. Available: www.rheologyschool.com. Last accessed 22 August 2009

[34] Reed, J.S. (1988). *Introduction to the principles of ceramic processing*. New York: Wiley. 227-249

[35] Krieger, I.M., Dougherty, T.J. (1959). trans. Soc. Rheol. **3**, 137

[36] Mehos, G., Clement, S. (2008). *Prevent caking and unintended agglomeration*. Chemical Engineering. **Vol 155**. Issue 8. 55-62

[37] Fayed, M.E., Otten, L. (1997). *Handbook of powder science and technology*. 2nd ed. 206-226

[38] Wildman, R., Blackburn, S., Gee, M. (?). *A comparison of Agglomerate strength testing techniques*. IRC in Materials for High Performance Applications and School of Chemical Engineering. 149-156

[39] Kawakita, K., Lüdde, K.H. (1969). *Some considerations on powder compression equations*. Powder Technology. **4**. 61-68

[40] Yap, S.F., Adams, M.J., Seville, J.P.K, Zhang, Z. (2008). *Single and bulk compression of pharmaceutical excipients: Evaluation of mechanical properties*. Powder Technology. **185**. 1-10

[41] Cai, M., Kaiser, P.K. (2004). *Numerical simulation of the Brazilian test and the tensile strength of anisotropic rocks and rocks with pre-existing cracks*. Int. J. Rock Mech. Min, Sci. **Vol 41**. 1-6

[42] Brinker, J.C., Scherer, G.W. (1990). *Sol-gel science: the physics and chemistry of sol-gel processing*. Gulf Professional Publishing. 5th ed. 453-477

[43] Mujumda, A.S. (1980). *Advances in drying*. New York: Hemisphere. **Vol 1**. 288-292

[44] Chaubal, M.V., Popescu, C. (2008). *Conversion of nanosuspensions into dry powders by spray drying: a case study*. Pharmaceutical Research. **Vol 25**. 2302-2308

[45] BüCHI Labortechnik AG. (2002). *Training Papers: Spray Drying*. 1-19

[46] Dusanter, A., Saleh, K., Guigon, P., (2008). *Formulation of Highly Concentrated Suspensions for Spray Drying in a Fluidized Bed*. KONA Powder and Particle Journal. **No.26**. 215-226

[47] BüCHI. (2009). *Mini Spray Dryer B-290*. 1-8

[48] Adelwahed, W., Degobert, G., Stainmesse, S., Fessi, H. (2006). *Freeze-drying of nanoparticles: formulation, process and storage considerations*. Advanced drug delivery reviews. **58**. 1688-1713

[49] INRA Press Service. (2006). *Improving the freeze drying process for pharmaceutical proteins*. Available: http://www.international.inra.fr/research/some_examples/improving_the_freeze_drying_process. Last accessed 18 July 2009

[50] Freezedry Specialties. (2009). *How freeze drying works*. Available: http://www.freezedry.com/fl_tips.htm. Last accessed 18 July 2009

[51] Purdue University. (2006). *Scanning Electron Microscope*. Available: http://www.purdue.edu/REM/rs/sem.htm. Last accessed 15 January 2009

[52] Klesel, J. (2008). Scanning Electron Microscopy. Available: http://mse.iastate.edu/microscopy/home.html. Last accessed 17 January 2009

[53] University of Groningen. (2006). *Measurement Techniques*. Chapter 3, 24-26.

[54] ElectroScan Corporation. (1996). *Environmental Scanning Electron Microscopy*. Robert Johnson Associates. 5-30

[55] Philips Electron Optics. (1996). *An Introduction to ESEM*. Available: http://www.cb.uu.se/~ewert/SEM.pdf . Last accessed 23 January 2009

[56] Gibaud, A., Harza, S. (2000). *X-ray reflectivity and diffuse scattering*, Current Science. **Vol. 78**. 12

[57] Lowell, S., Shield, J.E. (1991). Powder *Surface Area and Porosity*. 3rd ed. Chapman & Hall. 14-27

[58] TA Instruments. (2000). *AR 500/1000 Rheometers Hardware Manual*. A Subsidiary of Waters Corporation. **6**

[59] Deer, W.A., Howie, R.A., Zussman, J. (1962). *Rock Forming Minerals*. **Vol 5**. Longmans

[60] Todor, D.N. (1976). *Thermal Analysis of Minerals*. Abacus Press. 159-160

[61] Zhaodong, N., Xiangna, C., Quianqian, Y., *et al*. (2008). *Structure transition from aragonite to vaterite and calcite by the assistance of SDBS*. Journal of Colliod and Interface Science. **325**, 331-336.

[62] Hacker, B.R., Kirby, S.H. and Bohlen, S.R. (1992). *Time and Metamorphic Petrology: calcite to aragonite Experiments*. Science. **Vol 258**, 110-112

[63] Bergström, L. (1998). *Shear thinning and shear thickening of concentrated ceramic suspensions*. Colloids and Surfaces A: Physicochemical and Engineering Aspects. **133**, 151-155

[64] Barnes, H.A., Fletcher, J.H. and Walters, K. (1989). *An introduction to rheology*. 7th ed. Elsevier. 115-133